Assessing dose-response of antibiotics and monitoring degradation of RNA aptamer biosensor on microfluidic devices

by

Jing Dai

A dissertation submitted to the Graduate Faculty of
Auburn University
in partial fulfillment of the
requirements for the Degree of
Doctor of Philosophy

Auburn, Alabama
December 14, 2013

Keywords: Microfluidics, Antibiotics, Dose-response,
RNA aptamer biosensor, Degradation characterization

Approved by

Jong Wook Hong, Chair, Associate Professor, Materials Research and Education Center, Mechanical Engineering
Jeffery W. Fergus, Professor, Materials Research and Education Center, Mechanical Engineering
Zhongyang Cheng, Professor, Materials Research and Education Center, Mechanical Engineering
Sang-Jin Suh, Associate Professor, Biological Sciences

Abstract

In the last century, the technologies developed to miniaturize transistors and manufacture microprocessors have enabled the miniaturization and integration of tools in biology, chemistry, biotechnology and medical fields. These tools have low reagent consumption, display high levels of integration, parallelization and automation, can carry out fast reactions, and are portable. The miniaturized and integrated microfluidic platforms are capable of integrating multiple analysis steps: sample preparation, reaction, and detection onto a single chip, termed as "Lab-on-chip" or μTAS (micro total analysis system). This technology has altered and influenced the way various questions are addressed in biology, chemistry, and biotechnology.

In this dissertation, we investigated the concentration- and time-dependent response of cell (bacteria) or molecule (RNA aptamer-based biosensor) to reagents (antibiotics or degrading agents) by using microfluidic systems. We obtained useful information for evaluating the attenuated inhibitory effect of antibiotics by bacteria's resistance and differentiating degrading agents through monitoring the degrading profiles of RNA biosensor. Two microfluidic systems were used in this study. The first microfluidic system has multiplex reactors, and the second microfluidic system integrates a concentration gradient generator, reagent mixing and reaction sections. Both systems enable simultaneous, parallel and independent reactions, requiring nanoliter amount of reagents, unlike the conventional test tube or microtiter method. Our microfluidic tools are potential alternative to replace conventional batch culture methods. In addition, they have a great potential for screening drug molecules, determining drug's potency as

well as replacing conventional monitoring methods in transcriptomics. So, these devices are highly potential to benefit the process of lead identification and optimization during drug discovery as well as promote the transcriptomic researches.

Acknowledgement

"To strive, to seek, to find, and not to yield."
- Ulysses by Afred, Lord Tennyson, 1842

At first, I would like to sincerely thank my advisor Dr. Jong Wook Hong for his guidance and support. I am very grateful for Dr. Hong's help to open the door to an amazing research area for me. With Dr. Hong's mentoring during my Ph.D study, I developed both critical and logical thinking which are essential for academic success.

I am also grateful to my committee members, Dr. Jeffery W. Fergus, Dr. Zhongyang Cheng, and Dr. Sang-Jin Suh for their valuable suggestions and expertise. I want to thank Dr. Jacek Wower for being an external reader.

I want to thank Dr. Jae Young Yun, Dr. Sachin Jambovane, and Dr. Morgan Hamon for their valuable suggestions and generous help during my research, specially thank Dr. Hamon for providing valuable suggestions during preparation of this dissertation. I want to thank Ms. Hye Young Sim, Mr. Hoon Suk Rho, Ms. Kirn Cramer, Ms. Ting Chen, Ms. Lauren Bradley, and Mr. Austin Adamson for their collegiality, friendship and help.

I want to thank Dr. Lingzhao Kong, a great friend and faithful brother, Dr. Min Shen, Dr. Jiawei Zhang, Dr. Qing Dai, Dr. Xiaoyun Yang, Dr. Dan Liu, Dr. Lin Zhang, Dr. Yingjia Liu, Ms. ZhiZhi Shen, Mr. Honglong Wang, Ms. Jing Zou, Ms. Wei Wang, Dr. Yu Zhao, Mr. Yang Xu, Dr. Shiyu Wang for their support and help.

I also want to express thanks to my friends and relatives: Mr. Le Mu, Ms. Lei Lei, Ms. Qingjun Miao, Mr. Yunfei Yan, Mr. Wenxin Shi, Mr. Jiapei He, Ms. Miao Li, Mr. Xinjun He, Ms. Ping Shi, Mr. Mingang Shi, and Ms. Shudi Shi.

Finally, I have to thank my parents, Qin Shi and Yongming Dai, the most important and beloved persons in my life. They devoted their unconditional love to me. Their love motivated me an endless strength to overcome the hardest times in my life.

This research was supported by U.S. National Institute of Health, USDA Nanotechnology Program, and National Science Foundation. We also acknowledge 21st Century Frontier R&D Program of Microbial Genomics and Applications Center, Republic of Korea.

Table of Contents

List of Tables

List of Figures

List of Abbreviations

RNA	Ribonucleic acid
RNase	Ribonuclease
DNA	Deoxyribonucleic acid
PDMS	Polydimethlysiloxane
SAV	Surface area to volume ratio
EPS	Extracellular polymeric substance
CFU	Colony forming unit
IC_{50}	Half maximal inhibitory concentration
DFHBI	3,5-difluoro-4-hydroxybenzylidene imidazoline

Chapter 1

INTRODUCTION

1 .1 Introduction

In this chapter, I first review the basis of bacteria, bacterial growth phenotype, pathogenic bacteria, antibiotics, dose-response analysis in drug discovery and development, RNA and RNase, and aptamer. The fundamental concepts of microfluidics, fabrication method, and key components are described. Finally, the objectives and outline of this dissertation are presented.

1.2 Background and Motivation

1.2.1 Bacteria

Bacteria have been living on our planet for about 3.8 billions of years [1]. They are prokaryotic microorganisms with micrometer sizes and have a wide range of shapes including spheres, rods and spirals [2]. *Escherichia coli*, for example, is a rod-shaped bacterium (**Figure 1.1**). Bacteria are highly diverse and widely spread on Earth including inside of human bodies. As of 2011, it is estimated that there here are >10 million species [3] and approximately 5×10^{30} bacteria living on Earth [4].

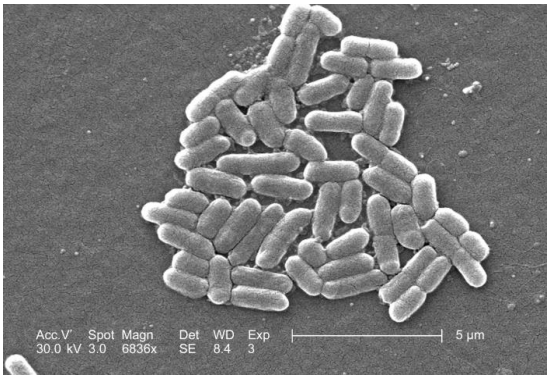

Figure 1.1 Scanning electron micrograph of *Escherichia coli* [5].

Bacterial growth phenotypes

Phenotypes are observable characteristics of an organism. They are shaped by gene expression and modified by environments or by both [6]. Bacterial phenotypes include any bacterial cell property, such as, shape, color of colonies, formation of biofilms or spores, mechanisms of cell-to-cell interactions, as well as growth patterns [7]. Bacterial growth phenotypes define whether or how fast bacteria grow under particular conditions. Typical bacterial growth in batch cultures under laboratory conditions experiences four different phases: lag phase, log phase, stationary phase, and death phase, as shown in **Figure 1.2**. Growth phenotypes in batch cultures can be easily observed and quantified without an expensive and sophisticated technology. In addition, growth curves can provide information about nutrient utilization profiles and growth kinetics required for genetic analysis. This information is also used to measure the impact of environmental and genetic perturbations [7, 8].

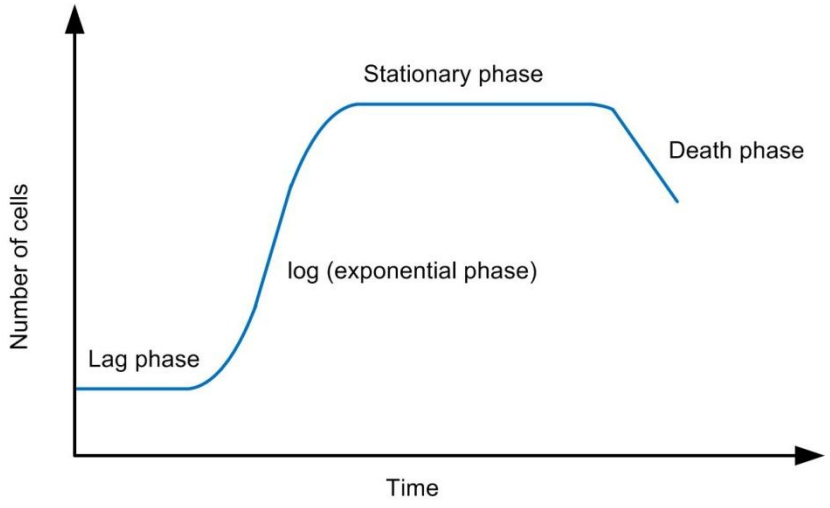

Figure 1.2 A typical growth curve of bacteria in a batch culture [9].

Pathogenic bacteria

Most bacteria are harmless or beneficial; only a small fraction of them are capable of causing disease in plants, animals and humans. Notable pathogenic bacteria, such as

Streptococcus spp., *Pseudomonas spp.*, *Mycobacteria spp.*, *Escherichia coli*, and *Salmonella servovars,* can cause pneumonia (by *Streptococcus* and *Pseudomonas*), tuberculosis (by *Mycobacteria*), and foodborne illnesses (by *Escherichia coli* and *Salmonella*). Infectious diseases caused by pathogenic bacteria have played a significant role in shaping human history and development. For example, *Yersinia pestis,* a bacterium carried by rat flea, has been responsible for the Black Death that decimated almost 50 % of the European population during the Middle Ages [10].

1.2.2 Antibiotics

In 1877, Pasteur and Robert Koch observed that an airborne bacillus could inhibit the growth of *Bacillus anthracis*. This phenomenon, later called antibiosis by Pasteur's pupil Paul Vuillemin, is a cornerstone in the discovery of antibacterial agents. The most celebrated antibiosis effect led to the discovery of penicillin by Alexander Fleming in 1929 who observed that the growth of staphylococci colonies was inhibited by the mold *Penicillium notatum* [11]. In 1939, the success of purification and stabilization of penicillin enabled its therapeutic potential. In the later stages of World War II, the mass-produced penicillin saved the lives of millions of wounded soldiers who would otherwise have succumbed to bacterial infections. In the following decades, enormous efforts were devoted to the discovery of new antibacterial agents, which renamed antibiotics by the American microbiologist Selman Waksman in 1942. Since then, thousands of antibiotic molecules were screened and isolated. Nowadays, over 100 different antibiotics are commercially available. Antibiotics are classified as bactericidal if they kill bacteria or bacteriostatic if they prevent bacterial growth [12]. In addition, most antibiotics used to treat bacterial infections can be classified according to their principal mechanism of action

[13]. Five major classes of mechanism of action are categorized: (1) interference with cell wall synthesis, (2) inhibition of protein synthesis, (3) interference with nucleic acid synthesis, (4) disruption of bacterial membrane structure, and (5) inhibition of metabolic pathway as summarized in the **Table 1.1**.

Table 1.1 Mechanism of action of antibiotics (from reference [14])

	Mechanism of action	Antibiotics
1	Interference with cell wall synthesis	β-Lactam, Glycopeptide
2	Inhibition of protein synthesis	Macrolide, Chloramphenicol, Clindamycin, Quinupristim-dalfopristin, Linezolid, Aminoglycoside, Tetracycline, Mupirocin
3	Interference with nucleic acid synthesis	Fluoroquinonlne, Rifampin
4	Disruption of bacterial membrane structure	Polymyxin, Daptomycin
5	Inhibition of metabolic pathway	Sulfonamide, Folic acid analogue

1.2.3 Bacterial resistance to antibiotics

The inappropriate and excessive use of antibiotics has led to the emergence of pathogenic bacteria that are resistant to currently available antibiotics [14-17]. Bacteria achieve active resistance to antibiotics through three major mechanisms: (1) efflux of antibiotics from cells, (2) enzymatic degradation and modification of antibiotics, and (3) target site alteration [13]. First, bacteria have efflux pumps that extrude the antibiotic from cells before the drug reaches its target sites and exerts its effect. Second, bacteria may acquire genes encoding enzymes that are able to destroy the antibacterial agent before it can have an effect. Third, bacteria may acquire several genes to reprogram biosynthetic pathways which produce altered bacterial cell walls that no longer contain the binding site for antibacterial agents or even through mutation that limits the access of antibacterial agents to the intracellular target sites. Some bacteria species have passive resistance to antibiotics. For example, Gram-negative bacteria have outer membrane to serve as a

significant barrier to penetration of antibiotics, restricting the rate of penetration of molecules [13].

1.2.4 Dose-response analysis in drug discovery and development

Generating a new drug is an expensive and time-consuming process. On average, 10~15 years and $ 800 million to 1 billion are required. This process includes thousands of failures: for every 5,000~10,000 compounds that enter into the research and development pipeline, ultimately only one receives governmental approval [18].

The process of generating new drugs consists of two main stages: drug discovery and drug development, as shown in the **Figure 1.3.** The drug discovery stage includes target selection, lead identification and optimization, and preclinical studies, while the drug development stage includes clinical trials, manufacturing and product management. The first step in drug discovery is to identify a drug target that can interact with a drug candidate. Once successful compounds (hits) are identified, the molecules, now called "lead", will be optimized. The lead will be tested in progressively more complex systems including cells and model animals. Only a few candidates out of thousands can enter into the drug development stage. In the process of lead optimization, establishing a dose-response relationship is of critical important step. It involves a so-called secondary screen. In the secondary screen, a range of drug concentration prepared by serial dilution is tested to assess the dose dependence of the assay's readout. It is essential to quantitatively characterize the inhibitory potency of potential drug candidates to determine the best candidate [19].

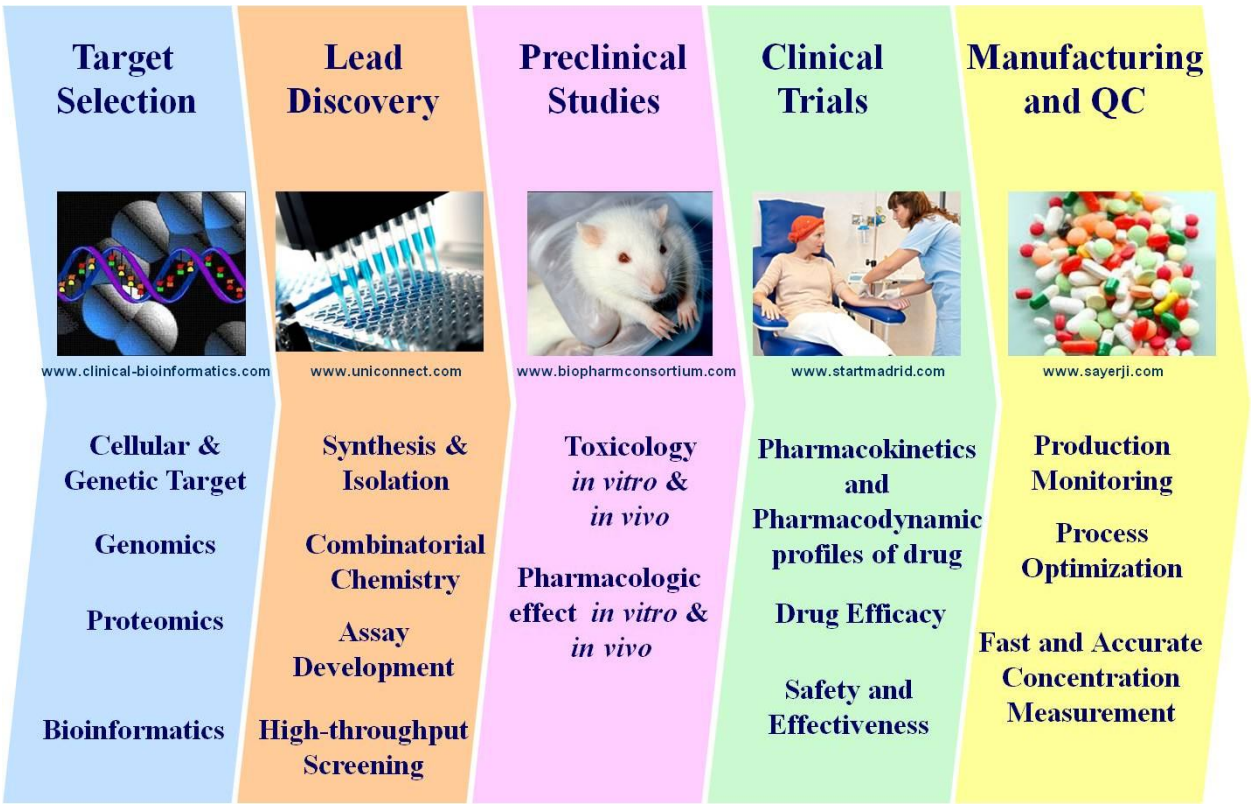

Figure 1.3 Drug discovery and development process [20].

In a medical definition, the dose-response relationship describes the pattern of physiological response to varied dosage (as of a drug or radiation) after certain exposure time. Response to dose follows a sigmodial curve increasing rapidly over a relative small change in dose, and eventually reaching a plateau level. **Figure 1.4** shows a typical dose-response curve. EC_{50}, half maximal effective concentration referring to the concentration of a compound where 50% of its maximal effect is observed, can be determined from a dose-response curve. It is commonly used as a measure of agonist drug's potency [21]. EC_{50} value can be determined through curve–fitting of the four-parameter nonlinear-logistic-regression model based on obtained inhibition data. The four-parameter model is shown below:

$$I = I_{min} + \frac{I_{max} - I_{min}}{1 + 10^{(log(EC_{50}) - [I])h}} \tag{1.1}$$

where I represents inhibiting potency (%), I_{Max} and I_{Min} is the maximum and minimum inhibiting potency, [I] represents concentration of inhibitor, and h is hill slope.

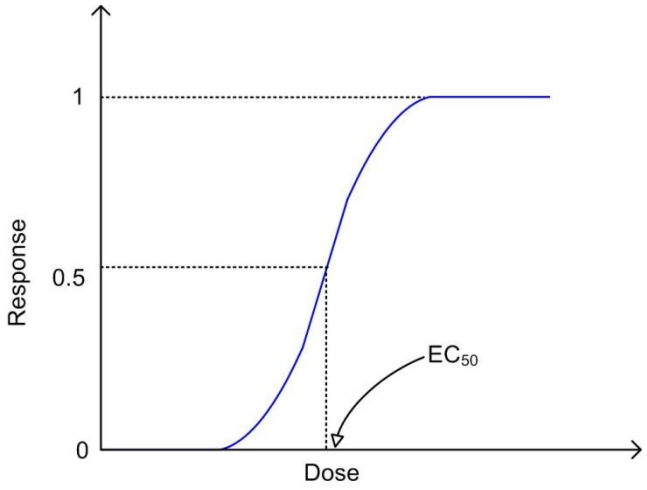

Figure 1.4 A typical dose-response curve.

1.2.5 RNA and RNase

Ribonucleic acid (RNA) is a polymeric molecule made up of one or more kinds of nucleotides. A strand of RNA is a chain with a ribonucleotide at each chain link. Each ribonucleotide is made up of a base (adenine (A), cytosine (C), guanine (G), and uracil (U)), a ribose sugar, and a phosphate [22]. **Figure 1.5** shows a diagram of a single-stranded RNA. RNA plays a central role in the information transfer from DNA to proteins, known as the "Central Dogma" of molecular biology [23]. There are 4 main classes of RNA species: (1) Messenger RNA (mRNA), (2) Transfer RNA (tRNA), (3) Ribosomal RNA (rRNA), and (4) Regulatory RNA.

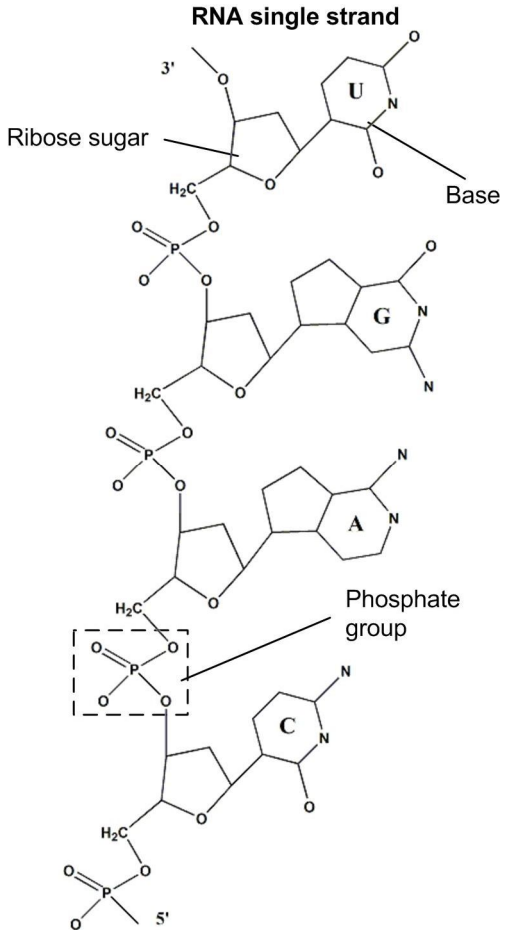

Figure 1.5 A single-stranded RNA.

Ribonucleases (RNases) are small and compact proteins that cleave phosphodiester bonds that link ribonucleotides. They play important roles in catalyzing degradation of RNA during nucleic acid metabolism. RNases are found in both prokaryotic and eukaryotic cells. They can be divided into 2 classes: (1) endoribonucleases and (2) exoribonucleases [22]. RNase contamination in laboratory selections will compromise results of RNA-based experiments [24, 25]. Therefore, RNase contamination is of great concern for researchers at both academic research laboratories and biotechnology corporations.

1.2.6 Aptamer

Aptamers are short synthetic oligonucleic acid or peptide molecules that display high selective affinity to specific targets such as small molecules, proteins, nucleic acids, metal ions, viruses and cells [26]. **Figure 1.6** shows the secondary structure of a RNA aptamer. Besides comparable target binding affinity/selectivity to antibodies, aptamers also offer advantages such as easier engineering and synthesis, lower batch-to-batch variability, better thermal stability, smaller size, lower immunogenicity, and more versatile chemistry among others [27]. Aptamers have become increasingly important molecular tools for diagnostics and therapeutics [28-30]. Aptamer-based biosensors have been applied for accurate and rapid detection of a diverse set target proteins [31], small molecules [32], metal ions [33], and many others.

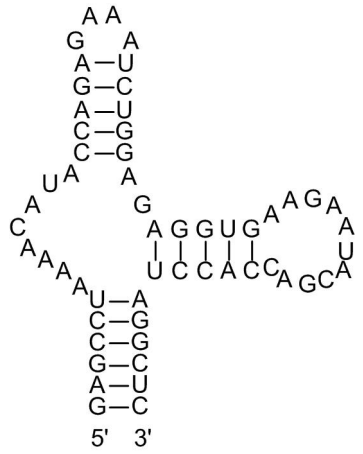

Figure 1.6 The sequence of a RNA aptamer [34].

1.2.7 Microfluidics

Microfluidics is a interdisciplinary field of physics, chemistry, biotechnology, engineering and microtechnology. Microfluidics is using a small platform consisting of channel systems with dimensions of 10~100 micrometers to precisely control and manipulate small (10^{-9} to 10^{-18} liters) amounts of fluids that are dominated by surface tension and laminar effects [35].

Microfluidics offers many advantages that make it a great potential for chemistry and biotechnology [20, 36]. The micrometer-scale channels facilitate the handling nanoliter to femtoliter volumes and significantly reduce sample and reagent consumption. Moreover, microfluidics offers many significant improvements over traditional methods with respect to fast speed of analysis, precise temporal- and spatial- control of environmental conditions, capability of manipulating and detecting single cell and single molecule at a high resolution and sensitivity, and a simultaneous detection and capability to handle parallel and high-throughput analyses [37-40]. However, microfluidics is still in its infancy. Therefore, a great amount of work is required to fully demonstrate its application in fields other than academic researches [35].

Microfluidic systems originated from the development of microanalytical methods, biodefense, molecular biology, and microelectronics [35]. The integration of multiple analysis steps (sample preparation, reaction, and detection) onto a microfluidic system suitable for the advanced applications in the field of biology, biochemistry, chemistry, and pharmaceutical science [41]. Highly developed microfluidic systems are used for manipulating stem cell cultures [42, 43], monitoring bacterial growth at different conditions [44-46], detection of pathogenic bacteria [47], separation and manipulation of single cells [48] or single molecules [49], extraction and amplification of DNA [50, 51], digital PCR [52], protein crystallization [53, 54], determination of enzyme kinetic parameters [55], dose-response analysis [56, 57], and high-throughput drug screening [58, 59].

The earliest microfluidic systems were made of silicon and glass. Because silicon is opaque to visible and ultraviolet light, these systems were not optimal when using conventional optical detection methods. Neither glass nor silicon has the property of gas permeability required to grow live mammalian cells. In addition, it is difficult to fabricate microfluidic components

such as pumps and valves in rigid materials. Nowadays, a polymer-polydimethysiloxane (PDMS) has been widely used to fabricate microfluidic devices with its superior characteristics, such as optical transparence, softness, and biocompatibility [35]. The unique properties of PDMS make multilayer soft lithography technique possible to fabricate microfluidic components such as pneumatic valves, peristaltic pumps, and mixers [60].

1.2.8 Basic concepts of microfluidics

Surface area to volume ratio

One characteristic of microfluidic device is the high surface area to volume ratio (SAV). SAV increases several orders of magnitude when dimension decreases from macroscale to microscale. Large SAV can make surface forces (such as surface tension) the dominant forces to drive flow by capillary effects, enhance heat and mass transfer, and create a large free surface for macromolecule absorption [61]. However, this unique feature elevates the rate of evaporation and presents a challenge for maintaining cell culture [62].

Laminar flow

Fluid flow is categorized into two flow regimes: laminar and turbulent (**Figure 1.7a**). Laminar flow is a smooth and constant fluid flow where the motion of the particles of fluid is very orderly with all particles moving in straight lines parallel to the pipe walls. Turbulent flow is the fluid flow which undergoes irregular fluctuations. The value of Reynolds number (Re) is used to determine the type of fluid flow. Reynolds number is the ratio of inertial forces to viscous forces. Thus, at low Reynolds number ($Re<2300$), laminar flow dominates. In microfluidic systems, Re is typically smaller than 100 and flow is considered to be laminar [63].

Mixing

Mixing is a result of molecular diffusion. At macroscale, mixing is generally achieved by turbulent flow which segregates fluid into small domains, causing an increase in contact surface and a decrease in diffusion path. In microfluidic systems, the absence of turbulent flow makes diffusion difficult to occur, leading to slow mixing. To overcome this problem, two groups of micromixers, passive and active mixers, have been described. Passive micromixers contain no moving parts and require no energy input except for the pressure that drives the fluid flow at a constant rate. Mixing in passive micromixers relies mainly on chaotic advection effects realized by manipulating the laminar flow within the microchannels or by enhancing the molecular diffusion through increasing the contact area and contact time between the different mixing reagents. The examples of passive micromixers are T- or Y- shaped micromixers and chaotic advection micromixers [63, 64]. Active micromixers use external energy source to stir or agitate the fluid flow. Active mixers use many techniques including acoustic/ultrasonic, dielectrophoretic and electrokinetic techniques to enhance mixing performance [63, 64].

Wetting

Wetting is an interfacial phenomenon describing how a liquid maintains contact with a solid surface. It occurs at three interfaces: solid/gas, liquid/solid and liquid/gas. Between each of these interfaces, there is an associated surface energy γ_{sg}, γ_{sl}, and γ_{lg}, respectively. Young's equation: $\gamma_{sg} = \gamma_{sl} + \gamma_{lg} cos\theta$, relates these three surface energy and contact angle θ which determines hydrophilicity ($0° < \theta < 90°$) or hydrophobicity ($90° \leq \theta < 180°$) of the surface (**Figure 1.7b**). Wetting effect is crucial at microscale as the surface forces become dominant over body forces. It plays an important role in digital and droplet microfluidics [65].

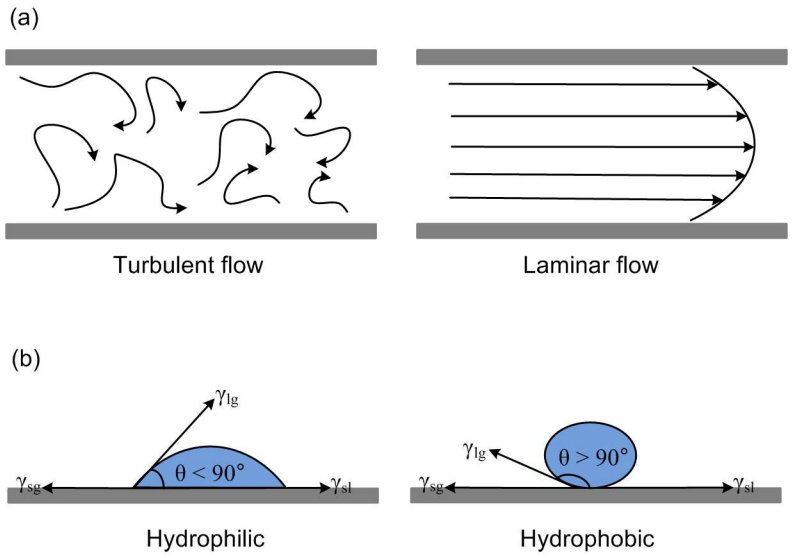

Figure 1.7 Basis of microfluidics. (a) Turbulent and laminar flow. (b) Wetting on hydrophilic surface and hydrophobic surface [66].

1.2.9 Fabrication of microfluidic systems

In order to fulfill the needs of different disciplines, a microfluidic system should employ a series of functional components for introducing reagents, moving fluids inside channels, mixing fluids, and integrating various other devices. The development of fabricating prototype device by soft lithography [67] and the development of fabricating pneumatic valves and mixers [60] on the basis of multilayer soft lithography techniques, have enabled the design of complicated devices and opened new areas of applications.

Soft lithography

Soft lithography was first developed by Whitesides and colleagues [68] as a cheaper and more biocompatible alternative to photolithography. This method refers to a collection of techniques for creating microstructures and nanostructures based on printing, moulding and embossing. This technique is termed ‘soft lithography’ since it is based on using a patterned

elastomeric polymer as a mask, stamp or mould, to pattern 'soft materials' (polymers, gels and organic monolayers). Soft lithography techniques use polydimethylsiloxane (PDMS) (**Figure 1.8**) as the major component. PDMS is a silicon rubber (Momentive Performance Materials RTV 615) consisting of two components: A and B. Part "A" contains polydimethlysiloxane bearing vinyl groups and a platinum catalyst; Part "B" contains a cross-linker with silicon hydride (Si-H) groups to form a covalent bond with vinyl groups of part "A" after applying external thermal energy. The excellent properties of PDMS make it become a widely used material for the application of soft lithography in microbiology and biology; it is durable, biocompatible, permeable to gases and only moderately permeable to water, optically transparent, flexible, unreactive, and suitable for chemical surface treatment [69]. The prepolymer of PDMS is commercially available, inexpensive, and easy to prepare.

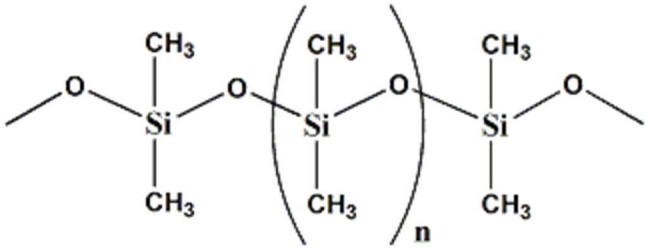

Figure 1.8 Structure of polydimethylsiloxane (PDMS).

Multilayer soft lithography

Multilayer soft lithography was developed by Quake's group, this technique uses soft lithography to fabricate patterned elastomer layers that are then bonded together [60]. **Figure 1.9** shows the process flow of multiplayer soft lithography. The two component silicone rubber (PDMS) is used to fabricate patterned layers. The composition of each layer is designed to contain an excess of specific components (bottom layer has an excess of A, while the upper layer has an excess of B), this composition difference makes the reactive molecule remain at the

interface between the layers to form the irreversible bonding. The simplicity of producing multilayers makes it possible to fabricate multiple layers of fluidics, a difficult task using conventional microfabrication method. Interlayer adhesion failure and thermal stress problems can be avoided because layers are monolithic (all layers are made of same material) [60]. This technique has become one of the most popular in microfluidics for applications in biotechnology.

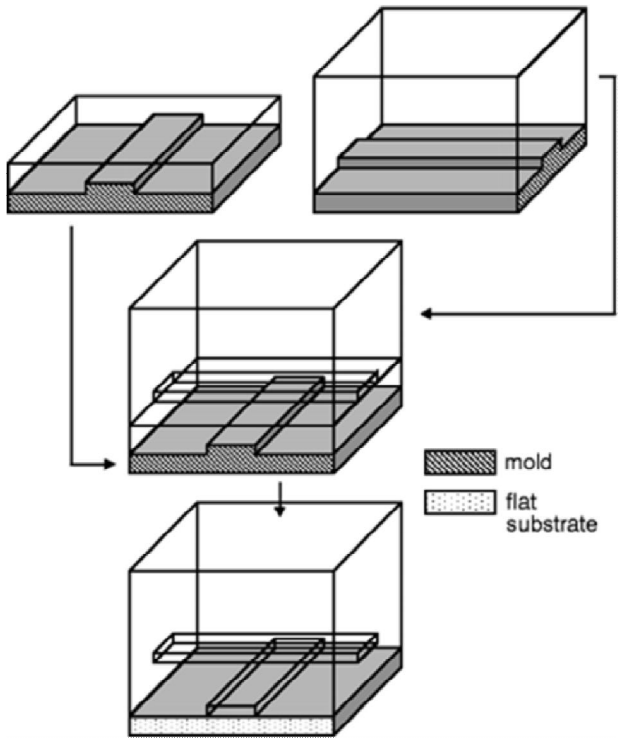

Figure 1.9 Process flow of multiplayer soft lithography [60].

Pneumatic valve

Valve is the basic unit for fluid-handling and controlling the movement of cells and particles in microfluidic channels. Quake's group developed a monolithic pneumatic valves by using multilayer soft lithography [60]. The monolithic valves are based on two PDMS layers produced by replica molding from two masters and sealing the layers together as shown in **Figure 1.10**. Two separate layers are produced: one for the control channels and one for the flow

channels. Typically, the channels are 100 µm wide by 10 µm high to make active area of the valve 100 µm by 100 µm. These two layers are bonded together to form a thin layer of PDMS membrane (10 µm~30 µm thick) where the control channel and flow channel intersect orthogonally. When pressure (usually nitrogen coming from an external source such as pressurized gas tank) is applied to the control channel, the membrane deflects upward to close flow channel. The flow channel must have a rounded profile to enable the valve to close completely.

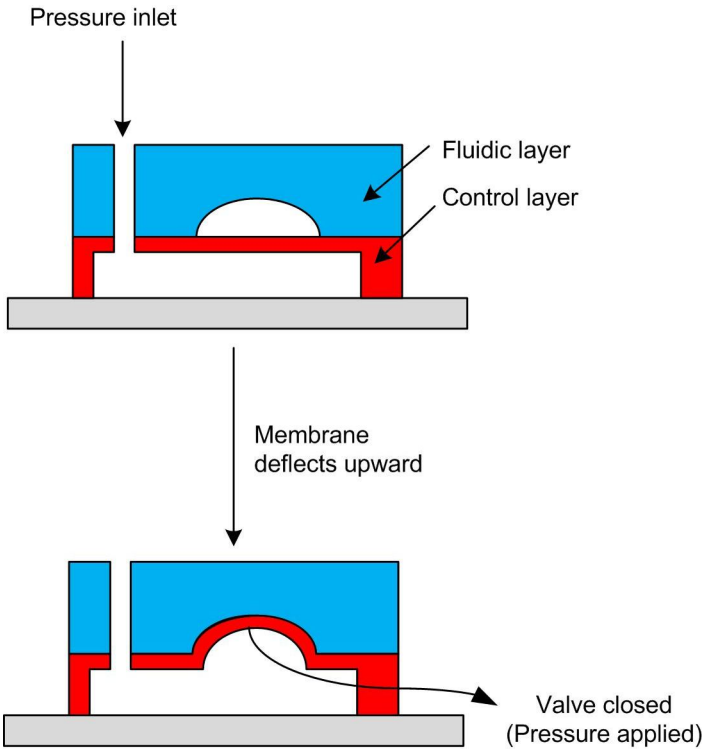

Figure 1.10 A two-layer PDMS valve. An elastomeric membrane is formed where a control channels lies orthogonal to and below fluidic channel. When pressurizing the control channel, the membrane will deflect upward, thus cutting off the flow in fluidic channel.

Peristaltic pump

A peristaltic pump contains an array of valves actuated in a sequence (**Figure 1.11a**). Three valves are placed in a series and the peristaltic pumping occurs when three valves are actuated in a 6-sequence pattern shown in **Table 1.2**. In this case, the control channels are filled with air and the valve actuation frequency is limited by the maximum frequency of the off-chip solenoid control pumps. Because of the sequential motion of the valves, a fluid flow in the flow channel can be generated. When this peristaltic pump operates in a loop, as shown in the **Figure 1.11b**, a fluid can be circulated within the loop to achieve the efficient mixing of reagents by rapidly stretching the interface between fluids to reduce the diffusion distance for mixing [70].

Table1.2 Sequence of valve operation to create a sequential fluid motion in a micromixer

	Sequence 1	Sequence 2	Sequence 3	Sequence 4	Sequence 5	Sequence 6
Valve 1	×	×	×	O	O	×
Valve 2	O	O	×	×	×	O
Valve 3	×	O	O	O	×	×

O : Valve open × Valve closed

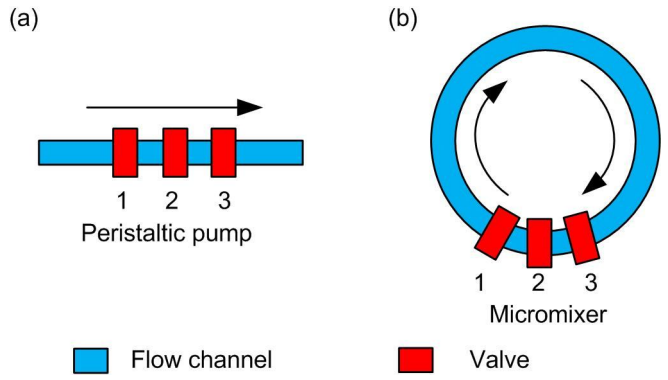

Figure 1.11 (a) A peristaltic pump using three valves in a series. (b) A circular micromixer using a peristaltic pump [60].

1.3 Objectives and organization of dissertation

1.3.1 Objectives

Studying responses of cells (bacteria) or molecule (RNA aptamer-based biosensor) to reagents (antibiotics or degrading agents) in a concentration- and time-dependent manner can provide useful information for pharmaceutical drug discovery and development of biological detection systems.

The rapidly growing resistance of pathogenic bacteria to antibiotics resulted in a demand for new antibiotics. The discovery of new antibiotics requires understanding of bacteria's responses to antibiotics, for example, dose-response relation of bacterial growth to antibiotics and bacteria's resistance to antibiotics. Our microfluidic systems can overcome the limitations when using conventional methods and other microfluidic systems.

The rapid and effective detection of RNase contamination is important in RNA related experiments and analyses. The application of RNA aptamer-based biosensors for detecting RNase contamination requires the understanding of its concentration- and time-dependent degradation behavior by the degrading agents, such as, RNases and metal ions. The development of our RNA aptamer-based biosensor can contribute to stimulating transcriptomic researches to easily detect RNase contaminations in lab environment. The integration of our biosensor and our microfluidic systems can serve as a detection device for rapid detection of RNase contaminations. The objectives of this dissertation are as follows:

1) Investigate the dose-response of bacterial growth to bactericidal antibiotics in a time-course manner. Through monitoring EC_{50} value over time, the attenuated inhibitory effect as a result of bacteria's resistance to antibiotics during their growth can be evaluated.

2) Monitor the concentration- and time-dependent degradation of a novel RNA aptamer-based biosensor. By characterizing degradation of RNA biosensor, its degradation profiles can be obtained to differentiate degrading agents.

To achieve these goals, two microfluidic platforms were used:

1) A multiplex nanoliter reactor array chip was developed to validate the response of cells (bacteria) or molecule (RNA aptamer-based biosensor) to the specifically defined conditions (e.g. growth nutrients/antibiotics or degrading agents) in microenvironments. This device has several unique features including simple architecture that requires no complicated active mixing components, ease to operate without requiring continuous flow of reagents, and simple evaporation suppression component. The detailed work is presented in Chapters 3 and 5.

2) An integrated microfluidic chip was used to investigate the response of cells (bacteria) or molecule (RNA aptamer-based biosensor) to different concentrations of reagents (e.g. bactericidal antibiotics or degrading agents) in a time-dependent manner. These devices is capable of simultaneously generating a wide range of concentrations without requiring continuous flow and growing bacteria in a zero-flow environment. The detailed work is presented in Chapters 4 and 5.

1.3.2 Organization

This dissertation is composed of six chapters. They are organized in the following order:

Chapter 1 introduces fundamental concepts of pathogenic bacteria, antibiotics, bacterial phenotypes, dose-response analysis, RNA and RNase, and aptamer. In addition, the fundamental concepts of microfluidics, fabrication method, and key components are described. Finally, the objectives of this dissertation are presented.

Chapter 2 presents the literature survey of conventional methods and microfluidic devices reported for accessing inhibitory effects of antibiotics on bacterial growth and monitoring RNA degradation.

Chapter 3 describes monitoring of the bacterial response to culture conditions such as growth nutrients and antibiotics on a multiplex nanoliter reactor array chip. Both the diaxuic growth and inhibited growth of bacteria were observed in microenvironments.

Chapter 4 investigates the response of bacteria to various concentrations of bactericidal antibiotics at a time-course manner on an integrated microfluidic chip. The dose-response relation of bacterial growth to bactericidal antibiotics was obtained and bacteria's resistance to antibiotics was discussed.

Chapter 5 reports the monitoring of concentration- and time-dependent degradation of a novel RNA aptamer-based biosensor on microfluidic chips. The detection of biosensor in micoenvironments was validated on the multiplex nanoliter reactor array chip. The concentration- and time-dependent degradation profiles of biosensor by degrading agents were characterized on the integrated microfluidic chip.

Chapter 6 summarizes the key research achievements, and provides the perspectives for their future applications.

Chapter 2

LITERATURE REVIEW

2.1 Introduction

This chapter provides a brief review of methods currently used for assessing inhibitory effects of antibiotics on bacterial growth and for monitoring RNA degradation. The working principle as well as advantages and limitations of these methods are discussed.

2.2 Conventional methods to assess activity of antibiotics

The activity of antibiotics depends on their ability to inhibit bacterial growth. Several techniques have been described to quantitatively determine the activity of antibiotics. One classical method involves agar diffusion assays in which filter paper disks soaked with an antibiotic are placed on the surface of an agar plate that has been inoculated with the test bacterium. During the incubation, the antibiotic diffuses to create a concentration gradient that produces a zone of bacterial growth inhibition [13] (**Figure 2.1**). The disadvantages of the agar diffusion test are the lack of mechanization or automation of the test. Another classical method is the macrobroth or tube dilution test in which a serially diluted solutions of an antibiotic is added to the liquid bacteria culture. After incubation, the bacterial growth is measured by means of turbidity or by determining the viable cell numbers. Because bacterial cultures absorb some of the light, the higher the cell concentration is, the higher the turbidity [71] (**Figure 2.2**). In the early 1970s, automated systems of macrobroth dilution test were developed for the assay of bacterial antibiotic susceptibility [72]. The major disadvantages of the macrodilution method are the tedious tasks when prepared manually, possibility of errors in preparation of the antibiotic solutions, and the relatively large amount of reagents and space required for each test. The

miniaturization of broth dilution test by using small, disposable, plastic "microdilution" plates has made this test popular and practical. A standard plate contains 96 wells, each well accommodating a volume of 100 microliter, allowing 12 antibiotics to be tested in a range of 8 two-fold dilutions [46]. Microdilution is prepared using dispensing instruments such as a pizeo dispenser [73] or a focused acoustic dispenser [74], that are able to dispense small aliquots of diluted antibiotics into individual wells of the plate. Hundreds of identical plates can be prepared from the same master set of solutions in a relatively short period of time. Several automated systems with microdilution method have been developed to rapidly generate results of susceptibility test [75]. The MicroScan WalkAway® plus system (Siemens Healthcare Diagnostics, **Figure 2.3**) is a large self-contained incubator/reader device that can incubate and analyze 40~96 plates at a time. This system uses standard size microdilution plates that are hydrated and inoculated in the instrument. The instrument incubates plates and periodically examines them with either a photometer or a fluorometer to measure growth [76]. However, uncontrolled evaporation of dispensed liquid remains challenging for these systems.

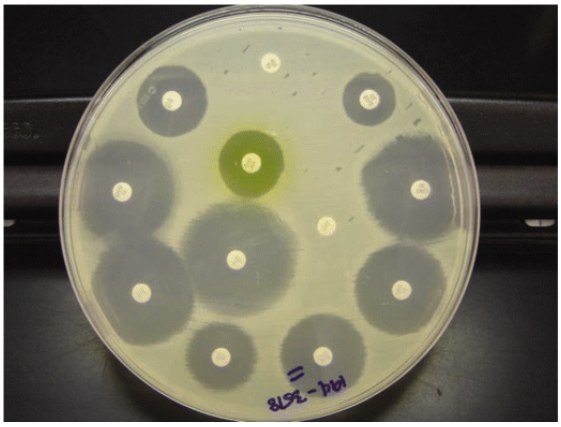

Figure 2.1 A disk diffusion test with an isolate of *Escherichia coli* from a urine culture. The diameters of all zones of inhibition are measured [76].

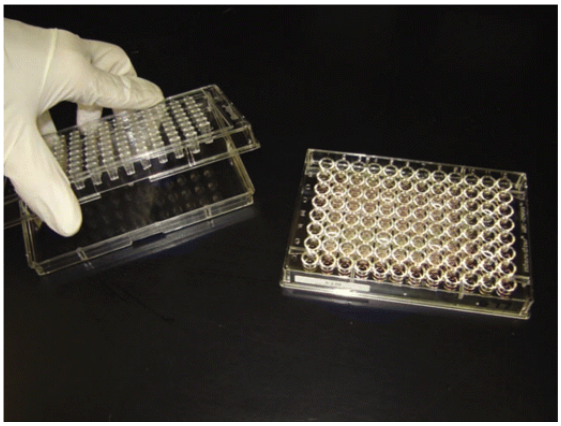

Figure 2.2 A broth microdilution susceptibility plate containing 96 wells [76].

Figure 2.3 The MicroScan WalkAway® plus system [77].

2.3 Microfluidic systems to assess activity of antibiotics

Microchannel based microfluidic systems have been used for assessing the inhibitory effect of antibiotics on bacteria [78-80]. Sun et al [78] described a nanoliter-scale reactor array used for bacterial growth under antibiotic treatments as shown in **Figure 2.4**. In this study, fresh nutrients or antibiotics are continuously supplied via diffusion to bacterial culture reactors. However, the continuous flow of reagent that is supplied outside chip is more likely to cause cross-contamination. Other microfluidic systems have been developed to investigate antibiotic

susceptibility of bacterial biofilms [79, 80]. In these systems, rather than preparing antibiotic concentrations outside chip, antibiotic concentration gradient is generated by networks of microchannels [81] within the microfluidic chip, as shown in **Figure 2.5**. However, these flow-based microfluidic devices require a continuous flow to generate and maintain constant concentration gradient, and additional efforts are needed to calibrate concentration gradient profiles.

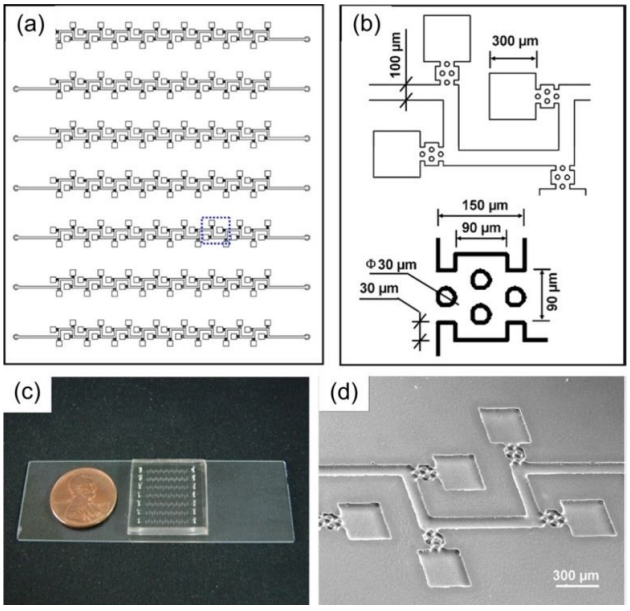

Figure 2.4 Design and picture of the microfluidic device. (a) Schematic representation of the functional circuit used for long-term bacterial colony monitoring and antibiotic testing. (b) Enlarged functional microstructure of the microfluidic device corresponding to the dotted-line square in (a). (c) Optical image of the actual device. A one cent coin was employed to show the size of the device. (d) SEM image of the functional microstructure [78].

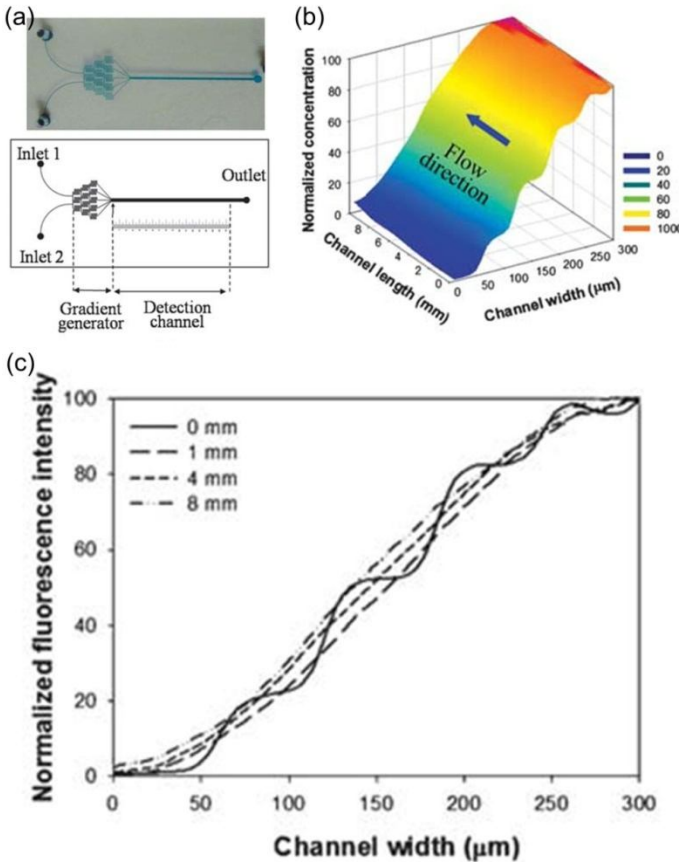

Figure 2.5 The microfluidic device for assessing antibiotic susceptibility of biofilms. (a) Schematic diagram and optical image of the microfluidic device. The microfluidic device consists of gradient generator and main detection microchannel. (b) A 3-D plot of the fluorescence image obtained from 0 mm to 8 mm position in the detection microchannel. (c) Profiles of cross section at each representative position. A flow rate of 0.1 ml min^{-1} is used in the experiment [79].

Microfluidic platforms that use a constant inflow of immiscible liquids into junctions, (e.g. flow-focusing [82, 83] or T-junction[84, 85]) can produce monodispersed droplets. Droplet-based microfluidic systems have been developed for antibiotic susceptibility screening of bacteria [39, 86]. Boedicker et al. [39] utilized reagent-loaded cartridges and a T-junction flow to generate droplets containing bacteria and various concentrations of antibiotics. In **Figure 2.6**, various concentration of drug trails and spacer plugs were pre-stored in a capillary (reagent

loaded cartridge). Then, drug trails and spacer plugs were flowed to microfluidic channels where they were merged with bacteria in a droplet. However, the preparation of a cartridge requires elaborate steps [87] such as dispensing nanoliter of reagents and aspirating reagents into a capillary. In addition, a gas segment must be applied to separate two reagents to prevent cross-contamination. Churski et al. [86] employed four microfluidic T-junctions to create microdroplets for antibiotic screening shown in **Figure 2.7**. Droplets containing bacteria, antibiotics, and culture medium are finally merged and incubated. By varying the droplet volume of antibiotic and culture media, a concentration range of antibiotics is generated. The volume of droplet is controlled by the opening time of external solenoid valves [88] in which longer opening time leads to more dispensed volume. Consequently, volumes vary from several hundred nanoliters to several microliters. However, the typical volume of droplets generated by other types of valves is from several picoliters up to several nanoliters [89-91].

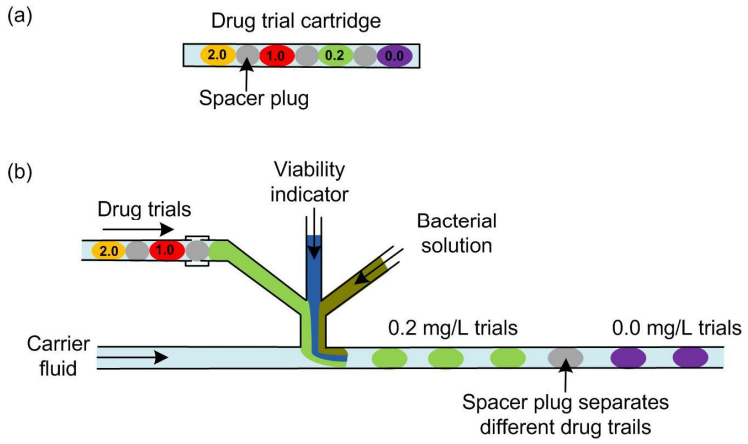

Figure 2.6 Schematic drawing illustrates the formation of droplets containing bacteria, viability indicator, and an antibiotic at varying concentrations. (a) A capillary cartridge loaded with drug trails and gas space plug. (b) A drug trial cartridge is connected to a microfluidic channel, and then drug trials are flowed to merge with viability indicator and bacterial solution. Thus, droplets containing various drug trials are generated at T-junction [39].

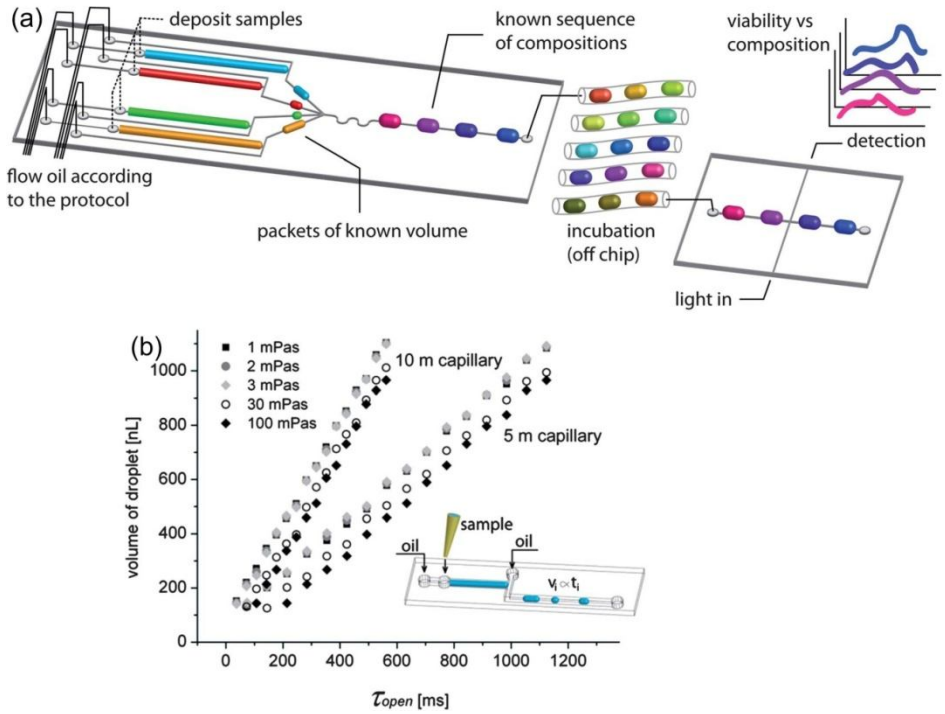

Figure 2.7 A schematic drawing demonstrates the operation of the microfluidic system. (a) Four T-junctions generate packets of microdroplets and merged them to create microdroplets with a defined composition. The sequence of microdroplets formed in the device was incubated off-chip. After incubation, the microdroplets were loaded into a microchannel and the intensity of bacterial viability indicator was detected. (b) A linear relationship of volumes of droplets and valve opening time (τ_{open}) is obtained for fluids with different viscosities (1, 2, 3, 30, 100 mPas) in two capillaries (5 m and 10 m in length) [86].

2.4 Conventional methods for monitoring RNA degradation

The most common method for monitoring RNA degradation is to incubate an RNA substrate with a degrading agent and then check for degradation of the RNA by ethidium bromide stained agarose gel electrophoresis. **Figure 2.8** shows the results of gel-electrophoresis. This test has very low sensitivity and requires a subjective judgment [92]. Other more sensitive tests require a radio-actively RNA substrate or a fluorescence polarization instrument. Both tests are time-consuming, costly, and require large amount of reagents [93].

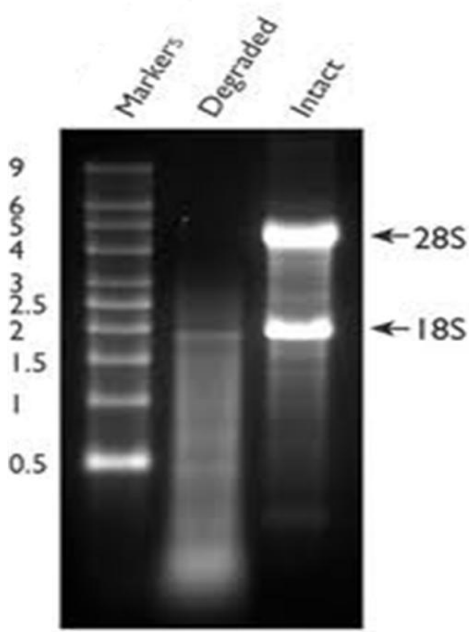

Figure 2.8 Degraded and intact total RNA were run beside RNA markers on a 1.5 % denaturing agarose gel. The 18S and 28S ribosomal RNA bands are clearly visible in the intact RNA sample while no bands are visible in degraded RNA [94].

2.5 Microfluidic methods for monitoring RNA degradation

To date, the application of microfluidic devices as a platform for monitoring RNA degradation has not been reported yet.

Chapter 3

CHARTING MICROBIAL PHENOTYPES IN MULTIPLEX NANOLITER BATCH BIOREACTORS

3.1 Introduction

One of the most fundamental challenges in biology is to understand the relationship between a DNA sequence (genotype) and the engendering observable cellular trait (phenotype) of an individual cell [95]. Recent advances in high-throughput DNA sequencing technology and molecular measurement techniques allow "omics"-scale analysis of genetic information flow from genome to transcriptome to proteome to metabolome of a microorganism [96-99]. Traditionally, phenotypes have been referred to as characteristics related to cell growth, shape, color of the colonies, formation of biofilms or spores, cell-to-cell interactions, as well as growth patterns [7]. Growth phenotypes are the expression of genotypes and reflect microbial physiology and metabolism. For example, the growth curve experiments, which are mostly performed in batch cultures, generate primary information such as nutrient utilization profiles and growth kinetics data required for genetic analysis. This information is also used in systems biology to measure the impact of environmental and genetic perturbations on complex cellular or organismal networks [8, 96, 100, 101]. Consequently, a great deal of effort has been recently directed toward the development of novel high-throughput quantitative techniques for microbial growth assessment [102-105].

Conventional batch culture techniques for studying cell physiology and developing bioproducts remain unchanged for many decades and are still in use in many academic laboratories and by the biotechnology industry. They require a large number of test tubes,

Erlenmeyer flasks, or agar plates, consume large amounts of media and apply laborious manual procedures for optical density measurements or microscopic observations. To overcome these challenges, a commercial system has been developed to test microbial strains on 96-well plates, which require an expensive instrumentation. Indeed, it is not ideal for automation and miniaturization [7, 96, 106]. Consequently, efforts have been directed toward the application of microtiter plates to scale-down (submilliliter) bioreactors for batch and fed-batch cultivations, and to improve the control over culture parameters such as temperature, dissolved oxygen, pH, and medium composition [102, 107-109].

Recent developments in microfluidics provide highly multiplex and quantitative measurements of individual cells, which replace the conventional liquid culture methods with economical and versatile miniaturized devices [36, 78, 110-114]. The application of soft lithography technology, using elastomers such as polydimethylsiloxane (PDMS) in microfluidics, has enabled fabrication of micro- or nanostructures such as valves, pumps, chambers, and channels in microfluidic cell culture systems [36, 60, 111, 115]. The microfluidics-based bioreactors offer several advantages over flask cultures or multi-well plates, including precise control of growth conditions and manipulation of nano- or picoliter volumes of culture media, capacity to integrate real-time growth and image measurements, ease of automation, ability to perform a large number of growth experiments under different conditions at the same time, and cultivation at the single-cell level.

Most of the microfluidic cell culture systems reported to date operate in semicontinuous [44] or continuous culture modes [45, 78, 109, 114, 116], the so-called microchemostat, where a continuous exchange of fresh medium with the same component occurs through a multitude of growth chambers. However, practically, the functionality of any proposed microchemostat

differs in cells cultured in a batch process. In addition to the presence of a high risk of contamination due to intermittent cleaning of the reactor surfaces, the microchemostat devices often utilize a single growth medium, which is insufficient for testing multiple growth environments. Besides, in most of the laboratories, a large number of cell culture processes are operated in batch mode as it generates important growth kinetics data required for genetic-phenotypic analysis, and systems modeling purposes. This necessitates the development of a multiplex microfluidic culture system that is able to simulate macro-cultures, which have been previously performed in flasks, tubes, or microtiter plates.

Despite its importance in genetic-phenotypic analysis and systems biology, a batch culture process on the nanoliter scale has rarely been realized. This is primarily because PDMS is permeable to water vapor and the culture medium inside a PDMS nanoliter reactor easily evaporates, leading to complete drying over time [111, 117]. Also, implementation of on-chip mixing requires more operational steps, further complicating the system. Recently, a microfluidic batch chip was developed to have 120 culture reactors (50 nL each) in which cell suspension was circulated and the whole chip was put in a water bath for temperature and humidity control [113]. However, the active mixing by circulation of the cell suspension mimicked the previous microchemostats, which makes the platform difficult to test multiple culture conditions without changing the reactor design.

3.2 Objective

In the present study, we devised a multiplex microfluidic batch culture chip that enables microbial growth in 24 sets of discrete bioreactors (1 nL each), while simultaneously allowing the assessment of eight different culture conditions in parallel. The flow channels and culture reactors were designed to maintain a uniform distribution of cells in each reactor and to conduct

experiments in triplicates in a single run. The evaporation of the cell culture medium present in each batch reactor was overcome by placing the chip in a humidified incubator and incorporating anti-evaporation channels around the reactor within the chip. Further, we demonstrated the utility of our system in characterizing microbial growth phenotypes by monitoring the growth of *Escherichia coli* with different carbon sources, obtained by both chip and tube cultures. We also demonstrated that the system could be successfully integrated with a fluorescence detection device for real-time observation of cell growth via online monitoring of fluorescent reporters of the opportunistic pathogen *Pseudomonas aeruginosa* incubated under different antibiotic concentrations.

3.3 Materials and methods

Chip fabrication

The platform employed in the present study was fabricated by standard multilayer soft lithography [55, 60, 89]. The mask was designed using AutoCAD software (AutoDesk Inc., San Rafael, CA, USA), which was printed on a transparent film at 20,000 dpi (CAD/Art Services, Inc., Bandon, OR, USA). Molds for the two layers, fluidic and control layers, were prepared by a photolithographic technique using a positive photoresistor (AZ P4620; AZ electronic materials, Branchburg, NJ, USA) onto a 4-inch silicon wafer. This was followed by UV exposure and development. To facilitate reliable opening and closing of the valves, the photoresistor for fluidic layer was rounded by heating the mold at 130 °C for 2 min. We fabricated the top thick fluidic layer of the chip by pouring uncured PDMS (RTV615; Momentive Performance Materials, Waterford, NY, USA; elastomer/crosslinker=10:1) onto the fluidic layer mold to achieve a thickness of 5 mm. Then, the bottom control layer of the chip was fabricated by spin-coating

uncured PDMS (elastomer/crosslinker=20:1) onto the control layer mold at 3,000 rpm for 1 min. Subsequently, the fluidic layer and control layer were cured at 80 °C for 1 h and 45 min, respectively. Thereafter, the fluidic layer was peeled off from the mold, and holes for inlet and outlet ports to flow channels through the thick layer were created using a 19-gauge punch (Technical Innovations, Inc., Brazoria, TX, USA). The fluidic and control layers were aligned and bonded by baking at 80 °C for 80 min, followed by punching holes for inlets to the control channels. The resulting PDMS chip was placed on a pre-cleaned glass slide (Fisher Scientific, Pittsburgh, PA, USA) and cured by incubating in an oven at 80 °C for 18 h. The chip fabrication process is schematically illustrated in **Figure 3.1**.

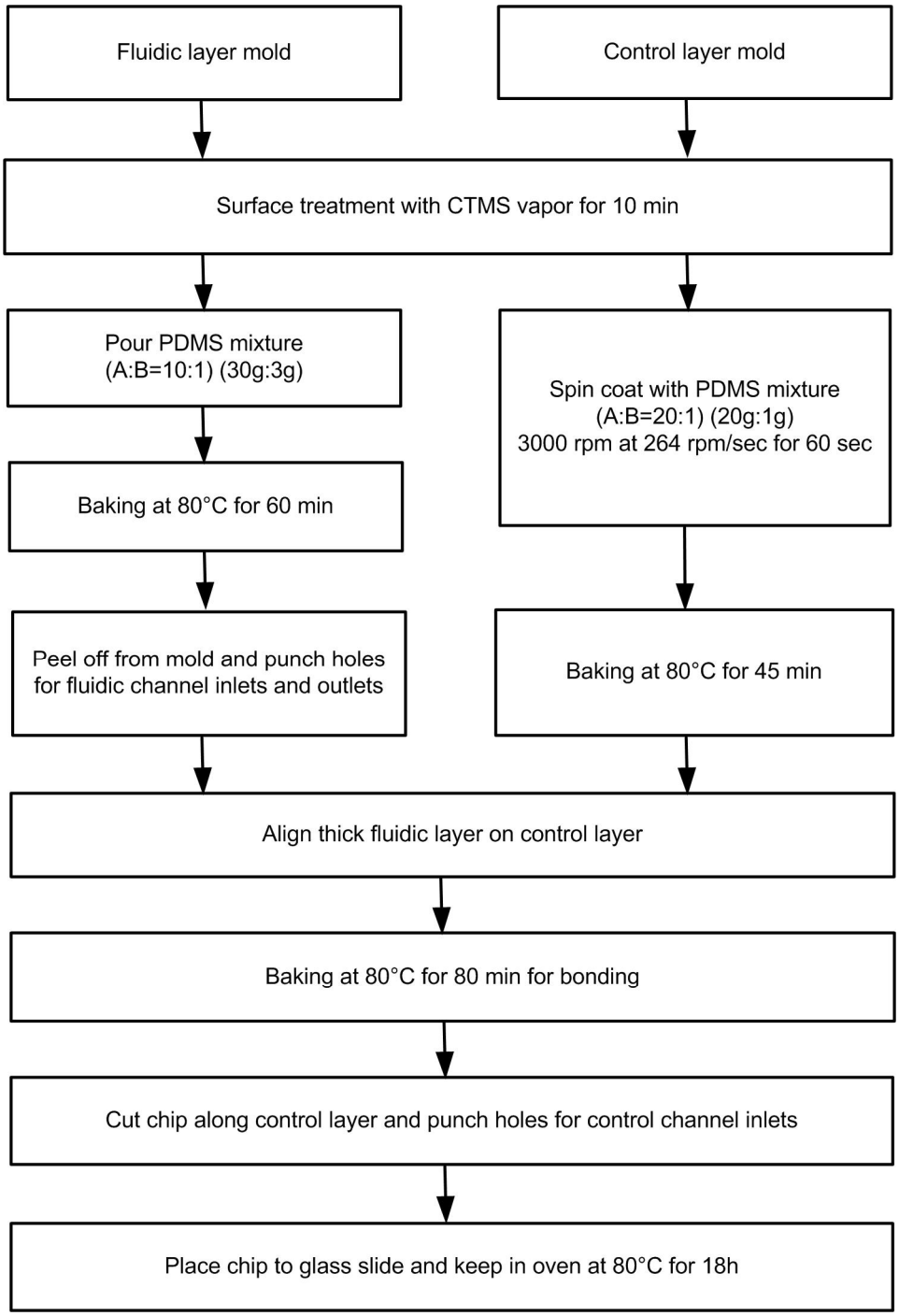

Figure 3.1 Flow chart of chip fabrication using multiplayer soft lithography.

Loading of fluorescent beads or bacterial cells in nanoliter reactors

Fluorescent beads (diameter: 2.0 μm; concentration, 2.84×10^8 particles/mL) or bacterial cells were loaded through "cell in" channels by applying 5 psi loading pressure. By opening C1 and C3 control channel (**Figure 3.3a**), beads or cells were loaded into 12 nanoliter reactors. After maintaining the loading pressure for 1 min, the C1 and C3 channels were closed to retain beads or cells in the nanoliter reactors.

Bacterial strains

E. coli K12 (ATCC 25404) and its lactose non-fermenting (*lac*$^-$) mutant (AB3568, F-, *Δ(cod-lacI)6*, *rpsL60*(strR)) [118] were purchased from the American Type Culture Collection (Manassas, VA, USA) and The Coli Genetic Stock Center (New Haven, CT, USA), respectively. *P. aeruginosa* PT5 was a gift from Dr. Thilo Köhler from University of Geneva, Switzerland. The pE21-EGFP vector having a GFP mutant gene was donated by Dr. Moonil Kim from Tuskegee University, USA. The EGFP, which is a red-shift mutation of the wild type GFP, has an excitation wavelength of 488 nm and an emission wavelength of 507 nm. pE21-EGFP was transformed into PT5 cells to construct the PT5-EGFP strain, using the standard transformation protocol [75].

Cultivation of *E. coli* in tubes and nanoliter reactors

A seed culture was prepared by growing cells in a 14-mL test tube containing 4 mL of LB medium in a shaking incubator with 160 rpm at 37 °C overnight (1.0~1.4 at OD_{600}). For cell growth in a tube, the seed culture was diluted with a fresh LB medium to obtain an OD_{600} of 0.01. A volume of 4 mL of the cell inoculum was aerobically grown in a 14-mL tube at 37 °C with

shaking at 160 rpm. As for *lac*$^-$ mutant, the LB medium was supplemented with 40 μg/mL streptomycin (Sigma-Aldrich, St. Louis, MO, USA). For cell growth in a nanoliter reactor with LB medium, the seed culture was diluted with a fresh LB medium to obtain an OD_{600} of 0.1, and was subsequently introduced into a reactor. For cell growth in a reactor with M9 medium, cells from the seed culture were harvested by centrifugation at 7,711*g* for 1 min, washed 3 times with M9 medium, and then suspended in M9 medium to obtain an OD_{600} of 0.1. Thereafter, they were introduced into each of the nanoliter reactors containing M9 medium with different carbon source(s): no carbon source, glucose (0.4 % wt/vol), lactose (0.4 %), and lactose (0.4 %) plus glucose (0.08 %). Finally, the chip was incubated at 37 °C in a humidity control system developed in our laboratory.

Cultivation of *P. aeruginosa* harboring pEGFP in tubes and nanoliter reactors

A seed culture was prepared by growing cells in a 14-mL test tube containing 4 mL of M9 medium supplemented with Casamino Acids (0.5 % wt/vol), $MgSO_4$ (1.0 mM), glucose (11.1 mM), and 100 μg/mL of ampicillin overnight (1.7~1.8 at OD_{600}). Subsequently, the cells were harvested by centrifugation at 1,600g for 10 min, washed once with 2×M9 medium, and then suspended in 2×M9 medium to obtain an OD_{600} of 0.2. Various concentrations of gentamicin (Sigma-Aldrich, St. Louis, MO, USA) (0, 0.2, 0.4, 0.8, 1.6, 3.2, 6.4, and 12.8 mg/L) were prepared by diluting 100 μg/mL of gentamicin stock solution in water. A volume of 2 mL gentamicin solution was added to 2 mL of the cell inoculum in a 14-mL tube, and the cells were allowed to grow aerobically at 37 °C with shaking at 160 rpm. For cell growth in a nanoliter reactor, the cell inoculum along with a different concentration of gentamicin was introduced into

the reactor. Finally, the chip was incubated at 37 °C in a humidity control system developed in our laboratory.

Chip control and operation

Figure 3.2 shows the schematics of experimental setup for chip control and imaging. A pneumatic control was used to operate the chip. A pressure of 15 psi was applied to control valves for closing control channels, and 5 psi was applied to introduce reagent to fluidic channels. The pneumatic control setup consists of eight-channel manifolds (Fluidigm, South San Francisco, CA, USA) controlled by a BOB3 control board (Fluidigm, South San Francisco, CA, USA). A digital I/O card (National Instruments, Austin, TX, USA) was mounted into the computer to control the switching of each channel of manifolds through the BOB3 control board. A LabVIEW (National Instruments, Austin, TX, USA) program developed by our group was used for automatic control of each control valve.

Chip image acquisition and analysis

The microfluidic chip was imaged using an inverted optical microscope (Axiovert 40 CFL; Carl Zeiss, Munich, Germany) equipped with a CCD camera (Moticam 1000; Motic, Inc., Richmond, BC, Canada). Bright-field images were captured at 40× magnifications every 2 h and digitized using Motic Images Plus 2.0 software (Motic, Inc., Richmond, BC, Canada). For cell culture in nanoliter reactors, the fluorescence image was obtained using a modified ArrayWoRx® biochip scanner (Applied Precision, Issaquah, WA, USA) with 480±15 nm of excitation and 530±20 nm of emission. All captured images were in 16-bit grayscale; the resolution was 7,800 pixels per inch (PPI), and the pixel size was 3.25 μm. The whole image (5.0

mm×3.8 mm) of 24 reactors was acquired by accumulating sequential image (1.25 mm×3.8 mm) four times (2.75 s/scan). ArrayWoRx® 2.5 software suits (Applied Precision, Issaquah, WA) built into the workstation automatically converted the images to an integrated image. The total scanning time of the integrated image (5.0 mm×3.8 mm) was approximately 11 s and exposure time was 0.01 s. The fluorescence images were digitized using ImageJ software (NIH, Bethesda, MD, USA).

For tube culture of PT5-EGFP, the fluorescence intensity was obtained using Hitachi F-7000 fluorescence spectrophotometer (Pleasanton, CA, USA) with 488±10 nm of excitation and 507±10 nm of emission. The fluorescence intensity of 150 µL of PT5-EGFP cells in a 1,000-µL cuvette was measured.

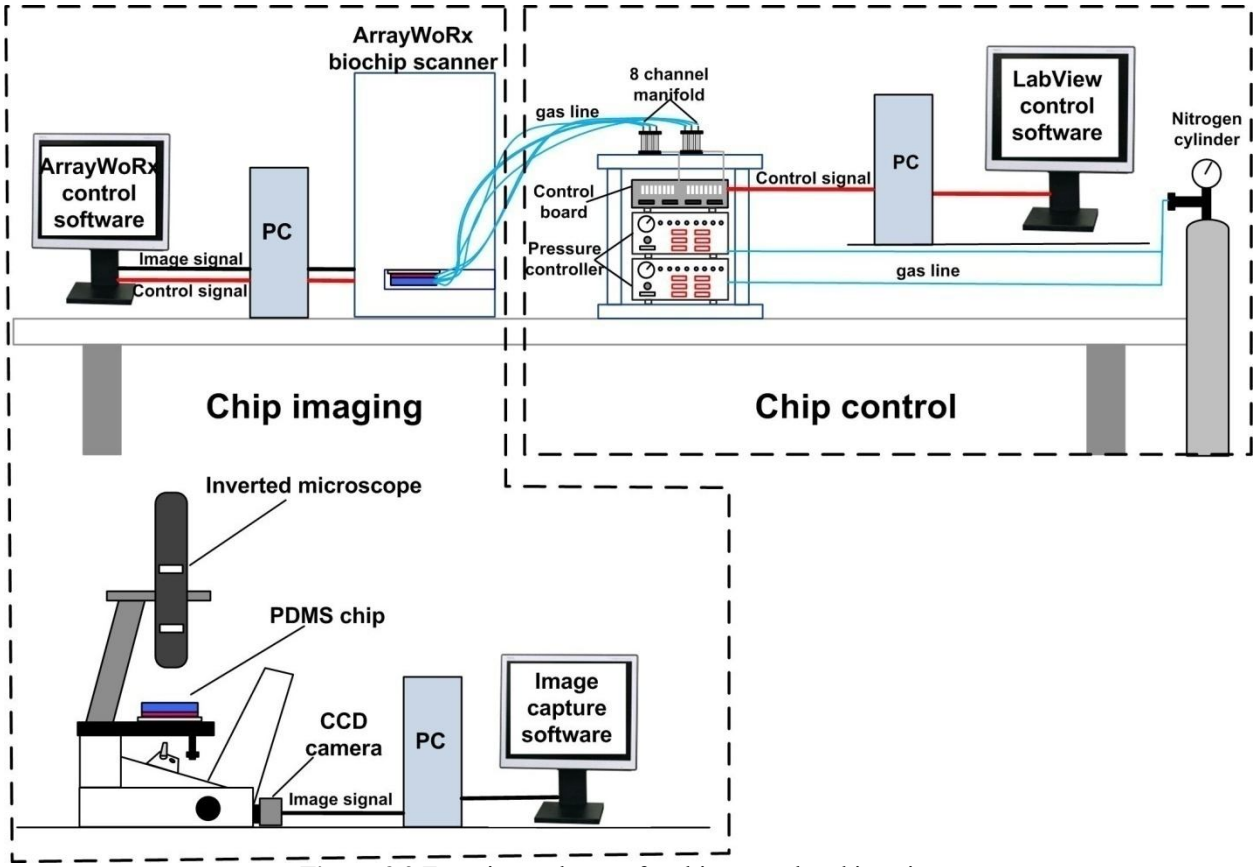

Figure 3.2 Experimental setup for chip control and imaging.

Mixing efficiency of the reagents inside the nanoliter reactors

We captured the mixing phenomena by using an inverted microscope (Axiovert 40 CFL; Carl Zeiss, Munich, Germany) equipped with a CCD camera (Moticam 1000, Motic, Inc., Richmond, BC, Canada). Time series analyzer of ImageJ software was employed for digitizing the captured images and obtaining the gray value of each reactor. When mixing was complete, the value remained constant. To quantify the mixing efficiency based on the average gray value, we used the following equation:

$$I(\%) = \frac{G_i - G}{G_i - G_f} \times 100\ \% \qquad (3.1)$$

where I is the mixing efficiency; and G_i, G, and G_f are the average gray values of initial time, given time, and final time, respectively.

Statistical analyses

The ANOVA test was used to determine the statistical significance of distribution of beads loaded per bioreactor. Normality and constant variance assumption were checked by using Anderson-Darling and Levene's tests, respectively (MINITAB 14, Minitab Inc., State College, PA, USA). The bootstrapping method in the R statistical package was used to assess the significance of the correlation between cell densities and log-transformed antibiotic concentrations.

3.4 Results and Discussion

Design and operation of the multiplex microfluidic nanoliter device

The PDMS device features a 20-μm thin control layer that is overlaid with a 5-mm thick fluidic layer, which is placed on a glass slide (**Figure A1** in Appendix A). The fluidic layer has two parallel rows of 12 culture reactors, each with a volume of 1 nL (**Figure A1b** in Appendix A). Each row is connected to a single-cell suspension channel and four different medium channels, where each of them correspond to three culture reactors. This design enables simultaneous triplicate experiments for each of the eight culture environments in a single run.

Cell suspension and fresh medium were loaded into three reactors present as a single unit, by opening two control channels located at the ends of the reactors (C1 and C3 in **Figure 3.3a**) and closing a control channel at the middle of the reactors (C2). Once they were filled into each half of the reactor, the modes of the channels were switched to open C2 and to close C1 and C3, causing diffusive mixing of the cells and the medium. The diffusion efficiency was determined by monitoring the mixing of green and red dyes (ESCO Foods, Inc., San Francisco, CA, USA) dissolved in M9 medium, Luria–Bertani (LB) complex medium, or 5 % polyethylene glycol (PEG) solution (**Figure 3.3b,c**; **Video A1** in Appendix A). When the temperature was increased from 22 to 37 °C, we observed an approximately 33-55 % increase in the mixing efficiency due to increased energy for diffusion. The difference among mixing efficiency for all tested reagents is due to the different viscosity of reagents (viscosity: M9<LB<5 % PEG). Because the temperature-dependent viscosity is different for three tested reagents [119], all tested regents showed different level of increased mixing efficiency at 37 °C. Three mixing efficiency values are around 102 % for LB at 37 °C, we attributed these values to the fluctuations of light source intensity during video capture. All the tested media showed complete mixing in approximately 9

min, which is negligible when compared to the time taken for the generation of microbial cells in growth curve experiments (for example, at least 12 h for the fast-growing *E. coli*).

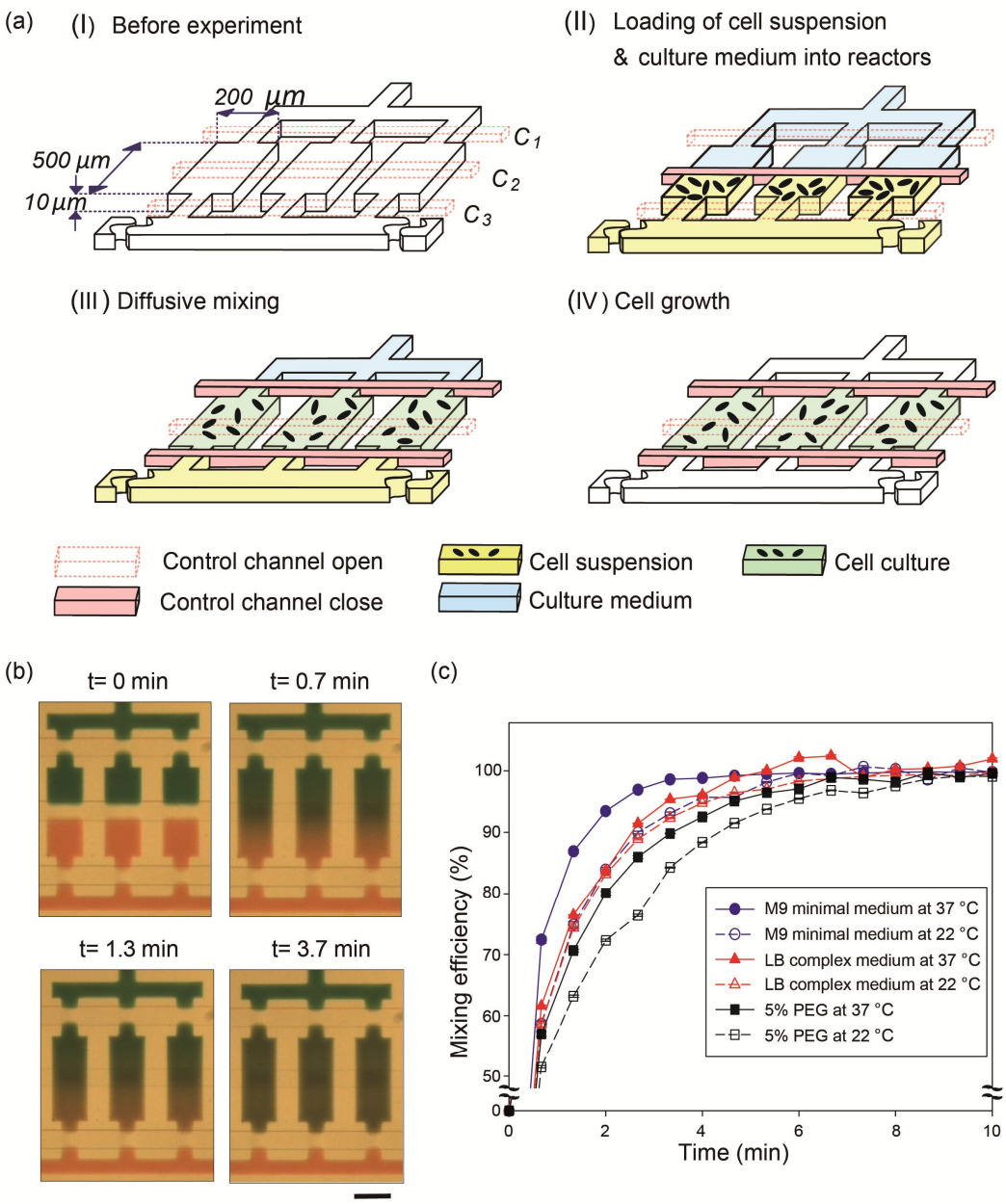

Figure 3.3 Operation of the device. (a) Schematic drawing of the entrapment of cells into three replicate cultivation reactors (I). The middle control channel C2 is closed to load cell suspension (shown in yellow) and culture media (shown in light blue) into the reactors (II). Cells and the medium are mixed by opening C1 and closing both C1 and

C3 (III). The cell cultures are sequestered from the fluid channels and the cells start to grow (IV). Simultaneous triplicate experiments for testing a culture condition can be performed in a single run. Note that control channels and flow channels are at different layers (see **Figure A1** in Appendix A for details) (b) Time-lapse micrographs showing the mixing of green and red dyes in M9 medium at 37 °C. The process of diffusion was initiated by opening C2, and was almost completed in 4 min. Scale bar, 200 μm. (c) A graph representing the time profiles of mixing efficiency of 2 dyes dissolved in M9 minimal medium, LB complex medium, and 5 % PEG solution at 22 °C or 37 °C. Error bar denotes the standard error of the mean from three replicate reactors.

Uniform distribution of particles loaded per bioreactor

The flow of cell-suspension channel perpendicular to the reactors caused the fluid to be pumped tangentially along the entrance of each of the reactors (**Figure 3.4a**). Distribution of particles confined in the reactors was analyzed using 2.0-μm fluorescent polystyrene beads (Polysciences, Inc., Warrington, PA, USA). An applied pressure of 5 psi to the suspension flow forced a portion of the fluid into the reactors. No build-up of the beads was observed at the entrances of the reactors, and hence, closing of the entrances led to the retention of the particles in the reactors, which thus resulted in the uniform distribution of beads trapped in the reactors (29±2 beads per reactor, *P*-value=0.713) (**Figure 3.4b**). Thus, loading of a nearly constant number of cells into each of the reactors allows direct and unbiased comparison of growth phenotypes from the reactors.

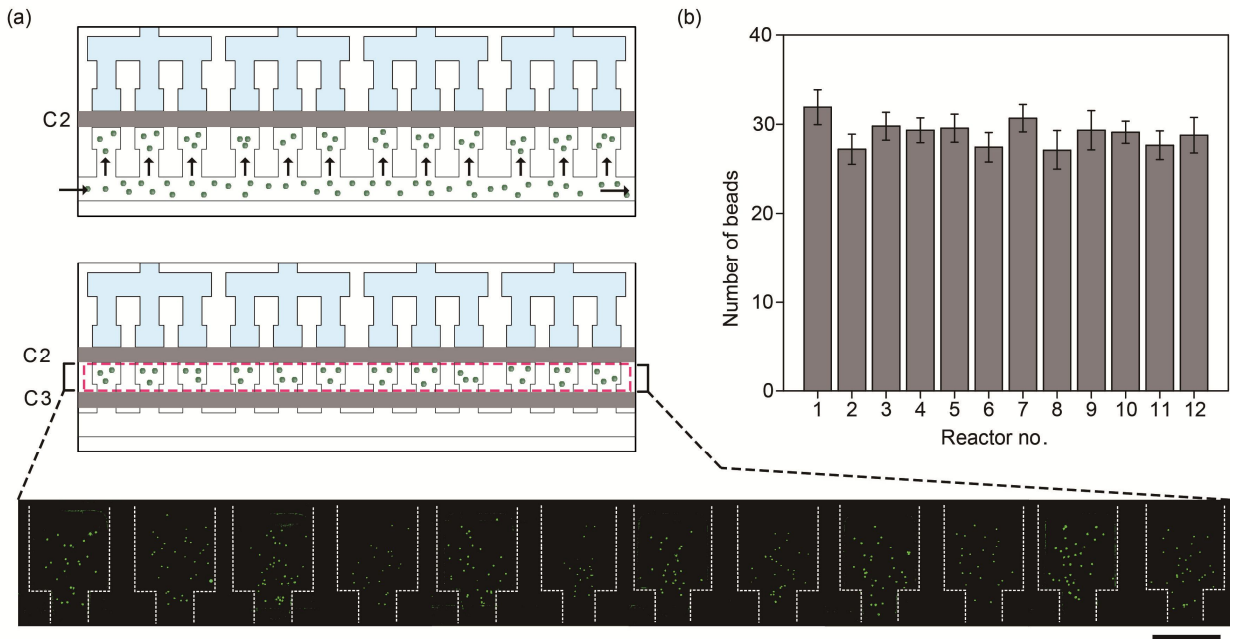

Figure 3.4 Loading of a uniform number of particles into the reactors. (a) Fluorescent beads (2.0 μm) are loaded into each of the 12 reactors by opening C3 control channel, followed by the closing of C3 channel, which retains the beads. Arrows denote the direction of bead suspension flow. Scale bar, 200 μm. (b) Number of beads loaded into each of the reactors. Error bar denotes the standard error of the mean from nine separate experiments.

Evaporation-free batch cultivation

A major challenge in employing microfluidic PDMS devices for cell cultivation at the nanoliter scale is that PDMS, being permeable to water vapor, allowing a rapid evaporation of the culture medium inside the microfluidic chambers [111, 117]. Evaporation is a matter of great concern in a batch cultivation, where the initially supplied liquid medium is not sufficient to support cell growth in a long-term culture. In contrast, this issue can be avoided by the use of fed-batch [44] or continuous [45, 109, 116] cultures through continuous renewal of the medium. In this study, we resolved this problem by placing the whole device in a humidified incubator and incorporating water-filled anti-evaporation channels around the nanoliter reactors within the device (**Figure A1b** in Appendix A). Water-filled channels installed around or above reactors

can suppress evaporation by letting water to saturate surrounding PDMS [120, 121]. The use of water jackets for long term cultivation could raise a concern of different salt concentrations as the culture chambers. However, as long as the medium in each chamber is retained to be constant during the culture, the variation in the medium concentration should be negligible.

To determine the effects of anti-evaporation channels and humidified incubator on the degree of evaporation of the media inside the reactors, we measured the amount of green dye that was retained in the reactors at 37 °C after 24 h (**Figure 3.5**; **Figure A2** in Appendix A). Notably, during the initial stage, when the anti-evaporation channels and the humidified incubator were not operated, evaporation of the medium was observed, which resulted in 7 % of volume loss in 4 h to ~26 % in 12 h. We observed the shrinkage of reactors and a dark green oval in the middle of reactors. It is likely that the rapid and elevated water diffusion occurred through a thin membrane (~10 μm thick) between control channel (C2) and the middle of the reactors, causing the concentrated dye molecules (**Figure A2** in Appendix A). Operating anti-evaporation channels under a pressure of 15 psi retarded evaporation for 8 h. The intensive drying was also observed in the middle of the reactors, possibly due to water diffusion from reactors to control channel (C2). We assumed that the upward deflection of the thin membrane separated the reactor into two parts (**Figure A2** in Appendix A). Furthermore, it was noted that placing the device in a humidity-saturated incubator led to approximately 2 % volume loss in 24 h. That loss seems to be negligible and to be caused by the diffusion through thin membrane between a reactor chamber and a control channel. However, even relatively small shifts in the osmolality of culture media by evaporation through PDMS can drastically affect sensitive mammalian cell behavior [122]. In addition, when the system is applied to slowly growing cells such as myxobacteria (e.g., *Sorangium cellulosum* with doubling time of 16 h) [123], the advserse effect caused by the

volume change can be profound. Strikingly, by operating anti-evaporation channels along with use of the humidified incubator, virtually 100 % of the initial volume in the reactors was maintained throughout incubation. Therefore, our finding highlights the importance of conditioning microfluidic devices in humidified environment in preventing evaporation and further demonstrates that a continuous supply of water molecules from the anti-evaporation channels contributes to the saturation of PDMS backbone-pores around the reactors.

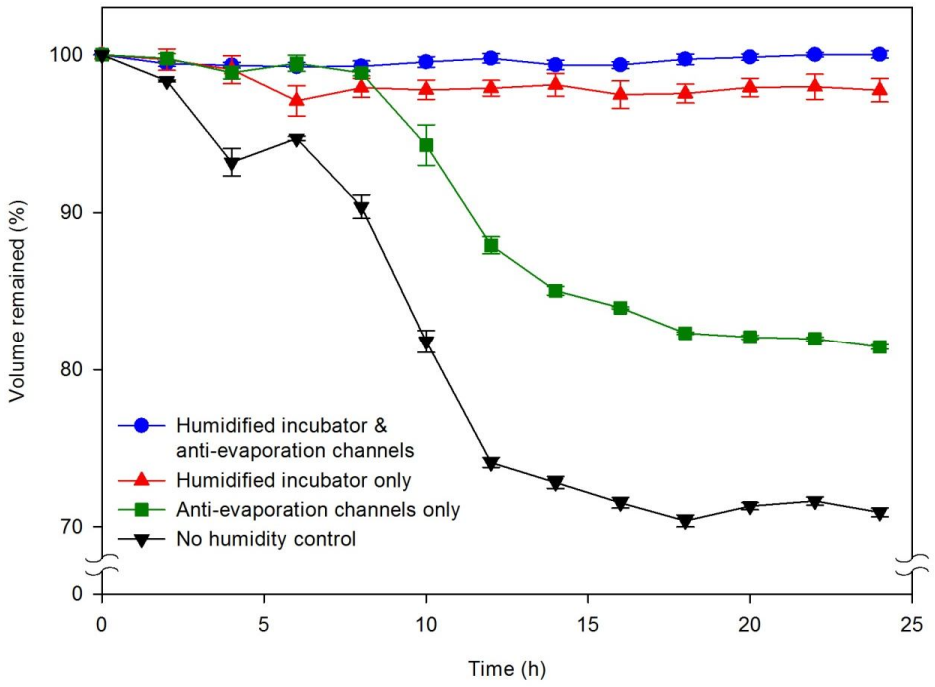

Figure 3.5 Effect of humidity controls on volume changes of the medium inside the reactors. The graph represents the volume changes of the initial medium over a period of time (24 h duration) based on the presence and/or absence of humidity control and/or anti-evaporation channels: in the absence of humidified incubator (denoted with a black line), in the presence of operation of anti-evaporation channels (green line), in the presence of a humidified incubator (red line), and in the presence of both humidified incubator and the operation of anti-evaporation channels (blue line). Error bar denotes the standard error of the mean, obtained from three replicate reactors.

Application of the device to measure bacterial growth phenotypes

As denoted above, we succeeded in developing a novel microfluidic batch culture system that enables uniform distribution of cells in each bioreactor and aids evaporation-free long term cultivation, which have been the major challenge in the development of PDMS-based microculture devices for batch cultivation. A cultivation-associated physiological environment can be easily changed when the reactor volume changes from macro- to microscale [111, 124]. Therefore, we investigated whether the designed system would allow sensitive and accurate measurements of bacterial growth phenotypes that are equivalent to the traditional methods, by performing growth curve experiments with *E. coli* and microbiological assays of antibiotics against the opportunistic pathogen *P. aeruginosa*.

Growth curve experiments

We demonstrated the utility of the developed device to replace the traditional methods by performing batch cultivation using one of the most commonly used laboratory strains of *E. coli* K-12. We obtained micrographs of the cells grown in the LB medium every 2 h after inoculation and counted the number of cells (**Figure 3.6a**). The growth curves were compared with the results obtained from the batch cultures of *E. coli* grown in 14-mL tubes, each containing 4 mL of LB medium (**Figure 3.6b**). The growth profiles derived from both methods reflected the typical batch growth curve of *E. coli*, and were highly similar to each other as shown in **Figure 3.6a**. When grown in M9 minimal medium with glucose (0.04 % wt/vol) and lactose (0.2 %) as carbon sources, nanoliter reactors reproduced the diauxic growth curve [125] that is characterized by two exponential phases separated by a lag period during which cells produce enzymes required for metabolizing the less-preferred carbon source (**Figure 3.6c**). *E. coli* prefer metabolize glucose over lactose because glucose transportation can block of inducer of the *lac*

operon which is responsible for transport and metabolism of lactose [126]. The short lag period may be a result of lower glucose concentration in mixed carbon source as it takes short time for enzymes responsible for metabolizing lactose to build up after glucose is exhausted. Furthermore, in order to determine the ability of the device in accurately characterizing mutant phenotypes, we assessed the growth patterns of a known mutant with different carbon sources (**Figure A3** in Appendix A). Notably, lactose nonfermenting (*lac*$^-$) mutant of *E. coli* K12 [118] failed to grow on lactose as a sole carbon source, and did not show the diauxic growth pattern when grown on glucose and lactose as it lacked the lactose-metabolizing capability.

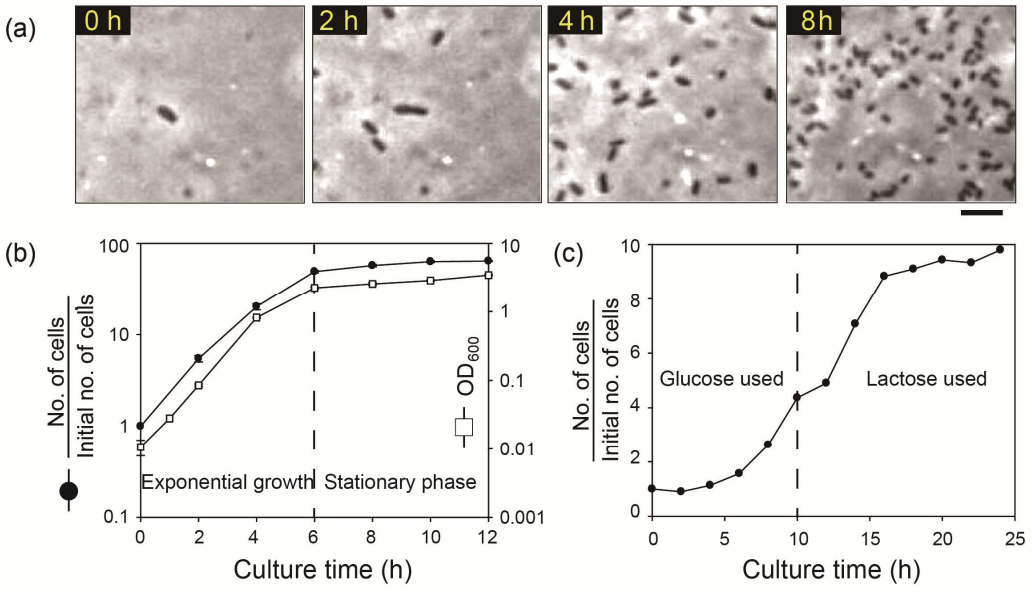

Figure 3.6 Growth of *E. coli* cells during the batch culture in a nanoliter reactor. (a) Micrographs showing time-lapse cell growth on the LB complex medium in a nanoliter reactor. Scale bar, 10 μm. (b) A graph showing the comparison of cell growth on LB medium in the nanoliter reactor (represented by ●) with that in a 14-mL test tube containing 4 mL of LB medium (□). The cell numbers in the reactors were counted every 2 h after inoculation and were normalized to the initial number of cells. The cell density in a tube culture was measured in OD_{600}. Values in *Y* axes are in log scale. Error bar denotes the standard error of the mean from 3 replicate reactors or test tubes. (c) A

graph showing the diauxic growth on M9 minimal medium with glucose (0.04% wt/vol) and lactose (0.2%) in a nanoliter reactor.

Microbiological assay for antibiotics

We validated the capability of the device for determining the concentration-dependent antibacterial activity of gentamicin against the opportunistic pathogen *P. aeruginosa,* which is responsible for nosocomial infections such as severe ventilator-associated pneumonia and bacteremia [127]. For real-time measurement of the cell growth, we employed a fluorescence-based scanner to capture and quantified fluorescence intensity of the growing cells. For this purpose, we employed *P. aeruginosa* that constitutively expressed plasmid-encoded enhanced green fluorescent protein (pEGFP) . Fluorescence intensity and the cell number in the bioreactors were measured by employing a modified biochip scanner, following visual inspection using an optical microscope. We observed that there was a significant linear correlation (R^2=0.986) between the fluorescence signal and the cell density (**Figure A4** in Appendix A). Strikingly, in such a small culture volume (1 nL), cells were diffusively mixed and reached reasonably homogeneous growth (**Figure A5** in Appendix A; see **Figure 3.6a** for *E. coli* cultivation). Most of microbioreactor systems reported to date use active mixing components for microbial culture to ensure homogenous growth conditions [44, 113, 128, 129], which requires delicate and complicated steps for the fabrication and operation of such devices. In this regard, homogenous conditions achieved by diffusive mixing in our system can contribute to the development of high-throughput microfluidic devices for phenotypic analysis.

Further, we measured and compared the concentration-dependent inhibitory effects of gentamicin on *P. aeruginosa* harboring the EGFP plasmid in the cultures obtained from both

nanoliter reactors and test tubes (**Figure 3.7**; **Figure A5** in Appendix A). In the case of test tube cultures, at 24 h following the inoculation, the cell density was found to be inversely correlated significantly with log-transformed antibiotic concentration (r=-0.98, P-value≈0), which is in accordance with previous observations [130, 131]. Remarkably, similar results were obtained using cultures from nanoliter reactors (r=-0.87, P-value<0.007), indicating that our system could be employed for microbiological assay of antibiotics. In addition, significant inhibitory effects were observed for the concentration above 1.6 mg/L in microfluidic cultures. We assumed that bacteria were rapidly killed by high concentration of gentamicin due to the small number of cells introduced at the beginning. The slight different inhibitory effects in the microfluidic cultures from those in the 14-mL test tube cultures might be a result of diffusion-dependent cell behavior in microenvironments [124, 132, 133].

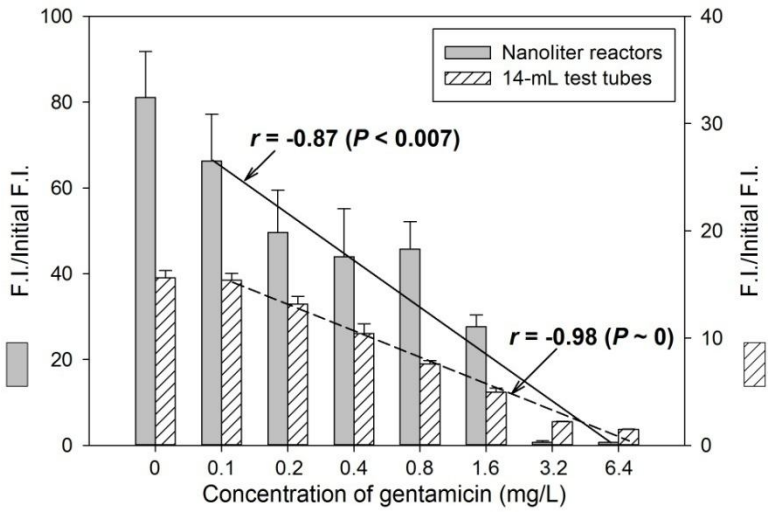

Figure 3.7 Microbiological assay for antibiotics using a nanoliter reactor and a test tube. The graph shows the comparison of antibiotic effects of gentamicin on the growth of *P. aeruginosa* harboring the EGFP plasmid, following 24 h of culture in nanoliter reactors (represented using grey bars, on the left side), with that in the 14-mL test tubes (represented using hatched bars, on the right side). The *X* axis denotes concentration of gentamicin in log scale, and the *Y* axis denotes the fluorescence intensity (F.I.) normalized to the initial intensity of the cell culture,

immediately following inoculation. The error bar represents the standard error of the mean from three replicate reactors or test tubes

3.5 Conclusion

We demonstrated the utility of the device in charting phenotypic changes of *E. coli* by assessing the growth patterns with different carbon sources and also of *P. aeruginosa* cells in response to growth inhibitors with various concentrations of antibiotics through fluorescence-based growth measurement. Our system was designed to conduct experiments in triplicate in a single run and ensure uniform distribution of cells in nanoliter reactors at the inoculation stage, which enabled direct comparison of the results from eight different culture environments. Importantly, virtually complete prevention of evaporation of the cell culture media was achieved by placing the device in a humidified incubator and installing water-filled anti-evaporation channels around the nanoliter reactors within the device. The present device has a simple architecture, ease of operation, and ability to precisely control multiple culture conditions while the batch culture format simulates a conventional microbial assay. This could further be exploited for investigating host-microbe interactions, and applied to a variety of cell types, not limited only to bacteria. In addition, by increasing the number of reactors and adding a concentration gradient generator at the inlets of the reactors, the device could be used to screen a multitude of metabolites, peptides, and proteins, thereby significantly reducing time and expenditure involved in drug-screening processes. Collectively, our study confirmed that high-throughput growth phenotyping using multiplex nanoliter batch reactors, in combination with real-time growth and image measurements, will be able to meet the increasing demand for genome-wide studies, single cell analyses and drug discovery.

Chapter 4

DETERMINATION OF EC_{50} OF BACTERICIDAL ANTIBIOTICS AT TIME-COURSE ON A MICROFLUIDIC CHIP

4.1 Introduction

In antimicrobial drug discovery and clinical practice, the knowledge of antimicrobial pharmacodynamics (PD) is useful for developing new antimicrobial drugs and establishing guidelines for therapy of infections. PD focuses on the relationship between drug concentrations and their antimicrobial effects [134]. The dose-response relationship is used to determine EC_{50}, the antibiotic concentration that induces 50 % maximal inhibitory effect. EC_{50} is an important parameter to quantitatively characterize the inhibitory potency of antibiotics. Generally, the dose-response data are obtained from end-point readout of inhibitory effect after certain period of antibiotic treatment [65], thereby, a EC_{50} value is determined. Two classes of antibiotics (bactericidal and bacteriostatic antibiotics) are primarily used in antimicrobial therapy. Bactericidal antibiotics kill bacteria while bacteriostatic antibiotics prevent the growth of bacteria [12]. For most infections, bactericidal and bacteriostatic antibiotics function to prevent the spread of bacteria and permit the body's defense mechanisms to eradicate infectious agents. However, bactericidal antibiotics are preferred for severe or difficult-to-treat bacterial infections (e.g. endocarditis or meningitis) [81] and may be required when the immune defenses are not effective or in chronic conditions [12].

Eliminating bacteria by antibiotics is a complicated process involving transportation of the drug to appropriate sites and its interactions with targets [63]. The transportation of bactericidal antibiotics, such as aminoglycosides and quinolones, requires the penetration through cell wall to reach the target sites [43]. Metabolic activities of bacteria provide the

essential energy for uptake of antibiotics. For example, the aerobic catabolism of carbon source by *Pseudomonas aeruginosa* provides energy for aminoglycoside transportation and interaction with targets [135]. Bacteria resist antibiotics by employing three mechanisms: efflux of antibiotics from cells, enzymatic degradation and/or modification of antibiotics, and target site alteration [64]. The efflux pump is an energy-dependent mechanism by which the cell can become resistant to antibiotics, including aminoglycosides and quinolones, by preventing drug entry into the cytosol. It is an important property of *P. aeruginosa* and many other bacteria that have broad resistance to for antibiotics [43]. Because efflux systems typically require energy expenditure by the cell, metabolic activity of the bacterial cell is important for its effectiveness. Thus, determining EC50 by conventional end-point analysis in the dose-response data is insufficient to demonstrate the attenuation effect caused by restricting antibiotic uptake. In contrast, determining EC50 values from time-course readouts allows correlating the inhibitory effect with bacterial growth and resistance.

Currently, effect of antibiotics is determined by the inhibition of bacterial growth in test tubes, microtiter plates and on solid medium using disk diffusion method [61]. Although effective, these traditional methods require a large volume of reagents. This is an important consideration when the availability of antibiotics to be tested is limited. The sophisticated concentration gradient preparation through dilution also can cause high possibility of errors. The automated high-throughput screening (HTS) method has been used for measuring dose-response of antibiotic molecules [136]. However, this method is also limited due uncontrolled evaporation of dispensed liquid at nanoliter or picoliter scales [137]. Microfluidic methods that can precisely manipulate small volume of reagent and generate concentration gradient are reported to be effective in study of antibiotic susceptibility of bacterial biofilms [79, 80] and effects of drug

concentration on bacterial chemotaxis [138-140]. However, these microfluidic devices require continuous flow to generate and maintain concentration gradient. Thus, cross-contamination of reagents is more likely to happen.

4.2 Objetive

At present, the investigation of time-course EC_{50} values from dose-responses of antibiotics on a microfluidic platform has not been reported yet. In this study, we determined EC_{50} for two bactericidal antibiotics on a microfluidic system device we previously reported [56]. Our data clearly demonstrate the feasibility of this microfluidic device for maintaining bacterial growth and assessing dose-response of bactericidal antibiotics (gentamicin and ciprofloxacin) against growth of *P. aeruginosa*. In addition, we demonstrate that the EC_{50} values acquired from the microfluidic device are comparable to those obtained from conventional test tube cultures. Furthermore, we demonstrate our microfluidic device for detecting attenuation of bactericidal activity of antibiotics as a function of bacterial growth and metabolism. Thus, our microfluidic device is a viable alternative to the conventional methods for effective determination of EC_{50} while offering advantages including generation of a wide concentration range and conservation of precious reagents.

4.3 Materials and methods

Chip design and concentration generation

The microfluidic device used in this work was previously reported by our laboratroy [56]. We fabricated microfluidic device by using standard multilayer soft lithography [60], the microfluidic device is composed of two polydimethylsiloxane (PDMS) layers. This microfluidic

chip has 14 parallel processors for generating 14 concentrations and bacterial cell culture. (**Figure B1 in** Appendix B) shows the step-by-step operation of generating 14 concentrations. Antibiotic solution and dilution buffer are introduced to metering channels. By varying the length ratio of metering channels, 14 different antibiotic concentrations ranging from 0 to 1000× are generated. Then, diluted antibiotics are mixed with bacterial cells by accelerated diffusion through fluid circulation [70].

Antibiotics and bacteria

Gentamicin was purchased from Sigma-Aldrich (St. Louis, MO, USA). Ciprofloxacin was purchased from Santa Cruz Biotechnology (Dallas, TX, USA). Stock solutions of antibiotics were prepared for use. *P. aeruginosa* (PT5-EGFP) was constructed by transforming a pE21-EGFP vector containing a GFP mutant gene into a wild type *P.aeruginosa* PT5 by following the standard transformation protocol [75]. The EGFP, which is a red-shift mutation of the wild GFP, has an excitation wavelength of 488 nm and emission wavelength of 507 nm.

Bacterial cell culture and suspension preparation for on chip and test tube culture

An overnight cell culture was prepared by growing a single colony in a 45-mL test tube containing 19 mL of M9 medium supplemented with Casamino Acids (0.5 % wt/vol), $MgSO_4$ (1.0 mM), glucose (11.1 mM), and 100 μg/mL of ampicillin (1.3~1.5 at OD_{600}). Subsequently, the cells were harvested by centrifugation at 1,600× g for 10 min, washed once with 2×M9 medium, and then suspended in 2×M9 medium to obtain a cell density of $3\sim4\times10^8$ CFU/mL for subsequent experiments. Cell density was determined using a normal plate count method. 14 concentrations of antibiotics were prepared by diluting stock solution in water. For test tube

culture, 1.5 mL of antibiotic solutions was added to 1.5 mL of cells in a 14-mL tube, and they were grown aerobically at 37 °C with shaking at 160 rpm. For on chip culture, cells were loaded into 14 reactors through "cell in" channels by applying 5 psi pressure. After maintaining the loading pressure for 1min, separation valves around reactors were closed to trap cells in reactors. Then, cells are mixed with various concentrations of antibiotics with three sequential peristaltic pumps for 10 mins. Three sequential valves were filled with water and kept pressurized at 2 psi throughout experiment. The chip was placed at 37 °C in a humidity control system developed in our laboratory [46].

Measuring number of cells in reactors

The number of cells was visually counted under an inverted optical microscope (Axiovert 40 CFL; Carl Zeiss, Munich, Germany) at 40× magnifications.

Fluorescent signal acquisition and analysis

For test tube culture, the fluorescence intensity was obtained using Hitachi F-7000 fluorescence spectrophotometer (Pleasanton, CA, USA) with 488±10 nm of excitation and 507±10 nm of emission. The fluorescence intensity of 150 μL of PT5-EGFP cells in a 1000-μL cuvette was measured. For on chip culture, the fluorescence image was obtained using a modified ArrayWoRx® biochip scanner (Applied Precision, Issaquah, WA, USA) with 480±15 nm of excitation and 530±20 nm of emission. All captured image were 16-bit grayscale, the resolution was 7,800 pixels per inch (PPI), and the pixel size was 3.25 μm. The whole image (34.6 mm×4.2 mm) of 14 reactors was obtained by accumulating a sequential image (1.47 mm×4.2 mm) twenty-six times (2.85 s/scan). ArrayWoRx® 2.5 software suites (Applied

Precision, Issaquah, WA, USA) built into the workstation automatically converted the images to an integrated image. The total scanning time of the integrated image (34.6 mm×4.2 mm) was approximately 74 s and exposure time was 0.01 s. The fluorescence images were digitized using ImageJ software (NIH, Bethesda, MD, USA).

Growth quantification, data fitting and statistical analysis

The cell growth was normalized by using the following equation:

$$\text{Normalized growth} = \frac{F.I. - F.I.at\ 0\ h}{Maximum\ of\ (F.I. - F.I.at\ 0\ h)\ for\ 14\ concentrations}$$

The normalized growth points were fitted by using a four parameter nonlinear-logistic-regression model:

$G = G_{min} + \frac{G_{max} - G_{min}}{1+10^{(log(EC_{50}) - [c])h}}$, where G is normalized growth, G_{Max} is maximum normalized growth, G_{Min} is minimum normalized growth, $[c]$ is antibiotic concentration, and h is hill slope. Then, EC_{50} values were determined.

ANOVA test was used to determine the statistical significance of distribution and growth of cells loaded in reactors. Student's T-test was used to determinate the statistical significance of inhibition data between the on chip and test tube culture method. Normality and constant variance assumption were checked by using Anderson-Darling and Levene's tests, respectively (MINITAB 14, Minitab Inc., State College, PA, USA).

4.4 Results and Discussion

Operation of microfluidic device to grow bacteria with antibiotics

A microfluidic device with 14 parallel processors [56] was used to grow bacteria with antibiotics in a zero-flow enviornment. (**Figure 4.1a**) Each processor consists of an 8-nanoliter

rectangle shaped reactor for cell growth and metering channels where antibiotics are diluted. **Figure 4.1b** shows the steps for introducing antibiotics to cell cultures to determine their inhibitory effect on bacterial growth in reactors. First, bacterial culture is introduced through "Cell in" inlet and cells are trapped in the first half of the reactor. Antibiotic solution and dilution buffer are then introduced into the metering channels through "Antibiotics" and "Buffer" inlets. After metering, both antibiotic solution and dilution buffer are pushed into the second half of reactor, separated from the cell solution compartment by separation valves. Each reactor is then isolated from the rest of the device and the separation valves is opened. Three mixing valves are activated sequentially to generate a fluidic flow in each reactor and mix the reagents.

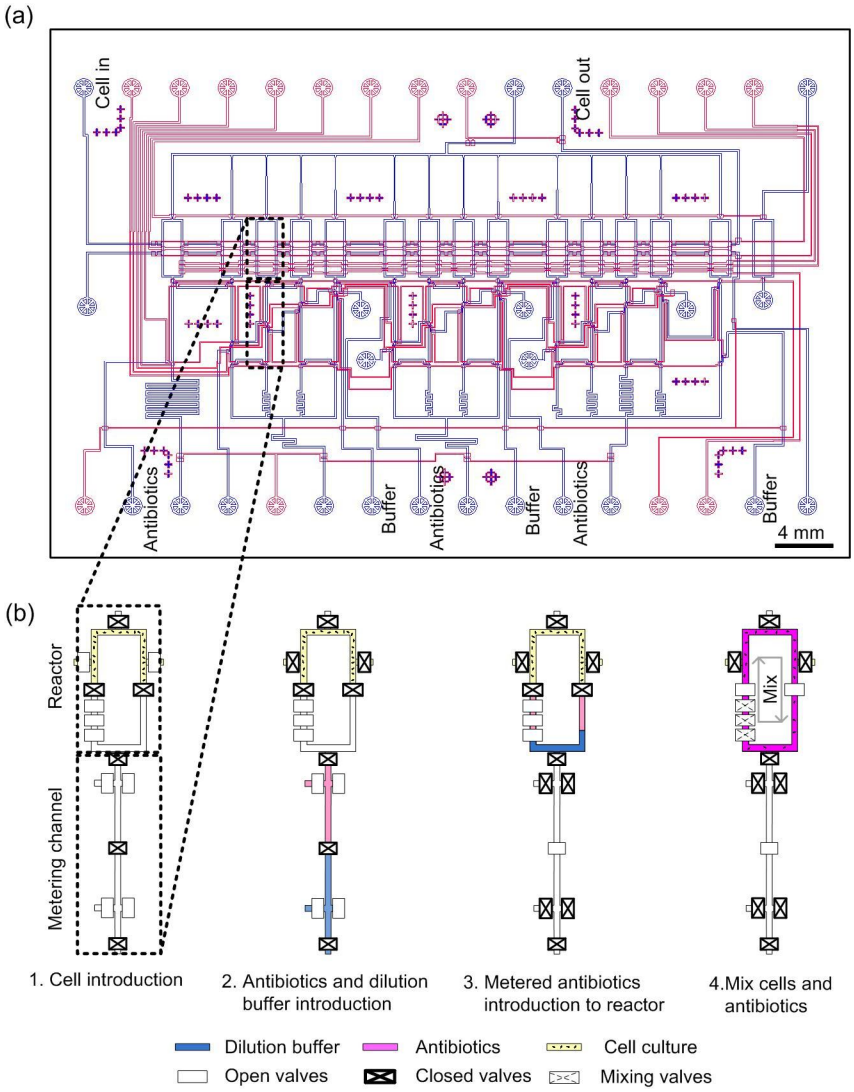

Figure 4.1 The microfluidic chip with 14 processors and operation of one processor. (a) Design of microfluidic chip with 14 processors where bacterial cells grow with 14 concentrations of antibiotics. (b) Operation of one processor. Bacterial cells are introduced into first half of reactors, then, antibiotics and dilution buffer are introduced into metering channels. After introducing metered antibiotics to second half of reactors, cells and antibiotics are mixed by three mixing valves.

Cell introduction and growth in reactors

A wild type *P. aeruginosa* strain that constitutively expresses plasmid-encoded enhanced green fluorescent protein (pEGFP) was used for real-time monitoring of cell growth [46]. A significant linear correlation between fluorescence intensity and cell density was observed (R^2=0.992) (**Figure B2** in Appendix B). Bacterial cell culture was pumped into half of reactors along the cell entrance channel which connects 14 reactors (**Figure 4.2a**). Cells were forced to enter the reactors under a 5 psi driven pressure and trapped by closing separation valves which resulted in the uniform distribution of cells in reactors (184±23 per reactor, p-vale=0.787) (**Figure 4.2b**). Thus, a nearly constant number of cells in reactors allowed unbiased comparison of cell growth. The trapped cells were mixed with water from the second half of reactor. Then, the growth of cells cultured in 1× culture medium was monitored. We further validated the uniformity of culture conditions within this microfluidic device by comparing the cell growth in 14 reactors. By comparing the fluorescence intensity of cells in the reactors after 24 h of growth (**Figure 4.2c**), we observed no significant difference across 14 reactors (p-value=1.000). Therefore, this microfluidic system can maintain consistent growth of bacteria in each reactor to enable multiple antibiotic testing.

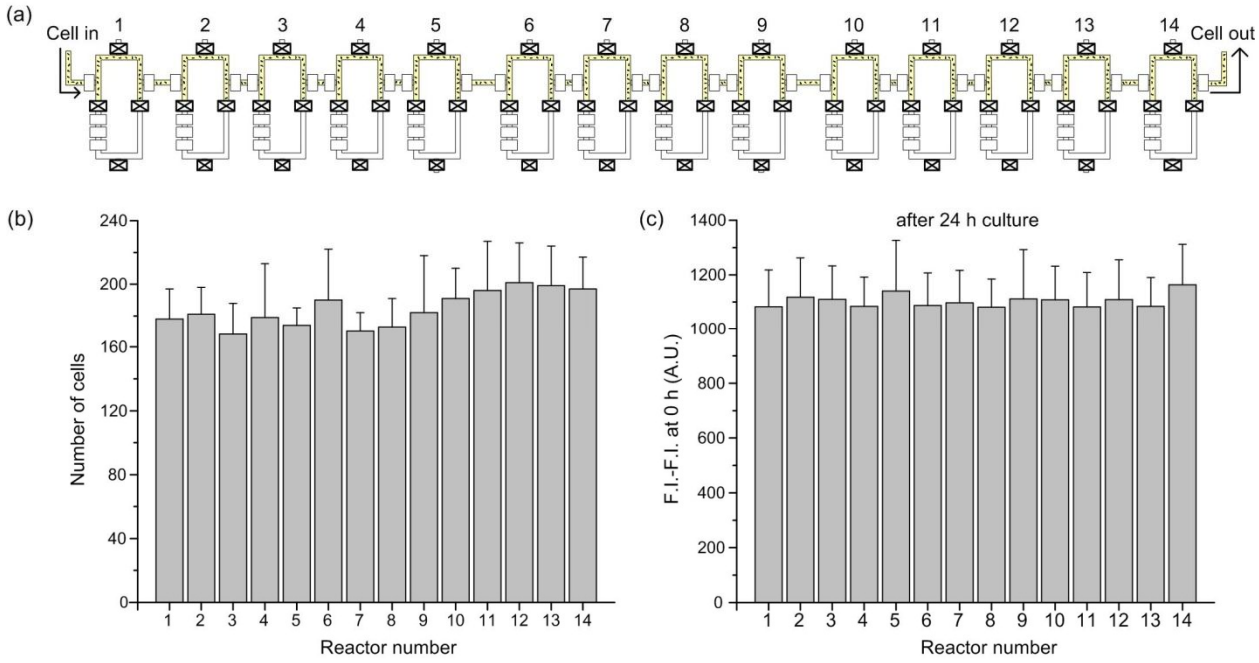

Figure 4.2 Introduction and growth of PT5-EGFP cells in reactors. (a) Cells are loaded into 14 reactors through "cell in" inlet, and cells are trapped in reactors by closing surrounding valves. (b) Number of cells in each reactor after introduction. Data are represented as means ± SD of three independent experiments. There was no significant difference in number of cells in 14 reactors. (c) The fluorescence intensity of cells after 24 h cultivation. Data are represented as means ± SD of three independent experiments. There was no significant difference in cell growth across 14 reactors.

Oxygen supply and consumption in reactors

Oxygen plays an important role for organisms that rely on aerobic respiration including *P. aeruginosa* [9]. Some investigators [141, 142] used oxygenator systems incorporated in the perfusion circuits to provide a sufficient supply of oxygen for tissue and cell culture. The high surface-to-volume (S/V) ratio characteristic of microfluidic devices makes it an effective approach to provide oxygenation inside a microfluidic cell culture system [143]. PDMS-based microfluidic devices have been used for cell culture [74, 82, 87] because PDMS is a polymer with high oxygen diffusivity [84]. In the PDMS reactors on this microflidic device, the

maximum amount of oxygen flux F_{max} by diffusion through PDMS can be estimated by the following equation [82, 85]:

$$F_{max} \approx D_{PDMS}\left(\frac{\Delta C}{\Delta z}\right) \quad (4.1)$$

in which D_{PDMS} denotes the diffusivity of oxygen in PDMS, D_{PDMS}= 4.1×10^{-9} m^2/s [84]; ΔC denotes the difference of oxygen concentration across the PDMS layer, the oxygen concentration in atmosphere is 2.0 mol/m^3 and used to estimate the maximum oxygen difference [82]; Δz denotes the thickness of PDMS layer, the PDMS layer for this microfludic device is 5 mm. Because the height of a reactor (10 μm) is approximately two order of magnitude smaller compared to the length and the width, the oxygen supply is dominated by the top surface. For one reactor, the total surface area is 9.37×10^{-7} m^2, and the maximum oxygen flux can be estimated to be 1.53×10^{-13} mol/s. The oxygen consumption rate of *P. aeruginosa* has been reported to be 5.97×10^{-19} mol/cell/s when cultured in LB medium at 32 °C with agitation at 150 rpm [83]. Based on the correlation of cell density and fluorescence intensity from our published work [46], the bacteria concentration in a 8 nL reactor after 24 h culture under the experimental condition (**Figure 4.2c**) is estimated to be 0.98×10^{9} CFU/mL with the oxygen consumption rate of 4.68×10^{-15} mol/s. Given these conditions, the maximum oxygen supply flux in our system is almost 33 times higher than the oxygen consumption rate. Therefore, this microfluidic device can provide adequate amount of oxygen for sustaining the aerobic growth of bacteria.

Glucose supply and consumption in reactors

Carbon compounds such as glucose are major sources of cellular carbon and energy [9]. The culture medium contains 11.1 mM glucose and, therefore, the total amount of glucose supplied in a reactor is 8.88×10^{-11} mol. It has been reported that the maximum glucose uptake

rate of *P. aeruginosa* is 1.2×10^{-9} mol/min/mg dry cell at 30 °C [144]. Estimating the mass of a dry bacterial cell to be 1.0×10^{-9} mg [9] and bacteria concentration in a reactor to be 0.98×10^{9} CFU/mL after 24 h of growth, the maximum amount of glucose consumption during 24 h culture is 1.35×10^{-11} mol. The amount of supplied glucose is almost 7 times higher than the amount of glucose consumption. So, a sufficient amount of glucose is supplied for maintaining bacterial growth for at least 24 h under experimental conditions.

Dose-responses of *P. aeruginosa* to bactericidal antibiotics on chip and in test tubes

Two bactericidal antibiotics, gentamicin and ciprofloxacin, were used to investigate the inhibitory effect on growth of *P. aeruginosa*. *P. aeruginosa* is a common opportunistic human pathogen that causes various acute and chronic infections [51]. Gentamicin is an aminoglycoside antibiotic that inhibits protein synthesis by interrupting the 30S ribosomal subunit [145]. Ciprofloxacin is a highly active fluoroquinolone antibiotic that interferes with the DNA gyrase and Topoisomerase IV that are involved in uncoiling of the supercoiled DNA during replication and decatenation of the replicated circular DNA [145] .

We first monitored the growth of *P. aeruginosa* under the treatment of gentamicin or ciprofloxacin on chip and in test tubes (**Figure B3** in Appendix B). Then, we assessed the inhibitory effects at three different growth times. We benchmarked the normalized growth of bacteria on chip with those of the test tube grown cultures (**Figure 4.3a and b**). The inhibitory effects of antibiotics on chip were similar to those obtained in test tubes for both antibiotics. Based on the growth inhibition profiles, we determined the EC_{50} value for each antibiotic (**Table 4.1**). Standard antibiotic susceptibility test requires a certain culture time (16~24 h), therefore, the inhibitory effect of antibiotics are generally evaluated within this time frame [65]. In this

study, we evaluated the inhibitory effects of antibiotics at 16, 20, and 24 h, respectively. The average of EC_{50} values obtained on chip is close to that obtained in test tubes for both gentamicin and ciprofloxacin. Therefore, this microfluidic system was validated to be accurate for assessing inhibitory effects of antibiotics on bacterial growth. The EC_{50} values obtained in this study were of the same order of magnitude as IC_{50} values reported previously for *P. aeruginosa*: 1.69 μg/ml for gentamicin [146], 0.06 μg/ml for ciprofloxacin [54].

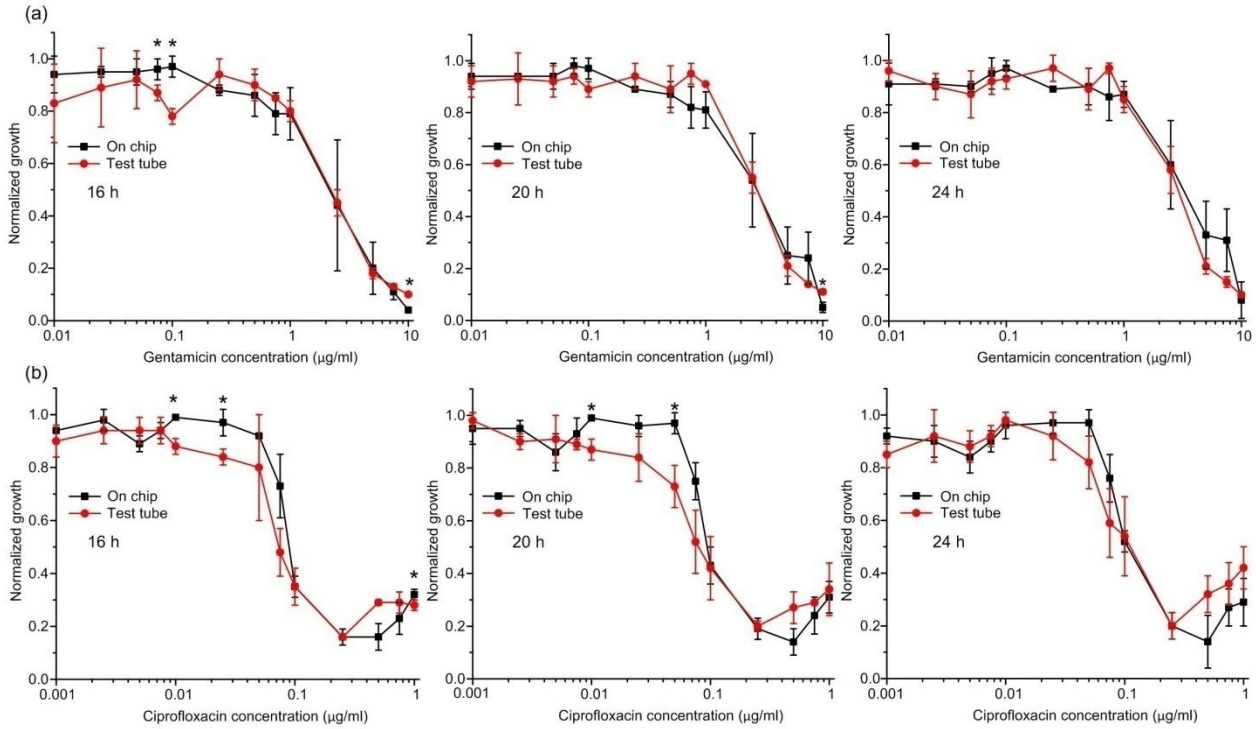

Figure 4.3 Growth inhibition profiles of two bactericidal antibiotics. (a) Gentamicin, and (b) Ciprofloxacin. Bacterial cells were treated with 14 concentrations of antibiotics in a wide concentration range. Cell growth was normalized by the fluorescence intensity. Data are presented as means ± SD of three independent experiments. Asterisks indicate statistical significance compared to test tube culture, $p<0.05$.

Table 4.1 EC_{50} (μg/ml) of gentamicin and ciprofloxacin

Time (h)	Gentamicin		Ciprofloxacin	
	On chip	Test tube	On chip	Test tube
16	1.88 ± 0.38	2.35 ± 0.33	0.083 ± 0.003	0.067 ± 0.012
20	2.39 ± 0.41	2.69 ± 0.29	0.088 ± 0.001	0.066 ± 0.015
24	2.97 ± 0.68	2.81 ± 0.30	0.095 ± 0.001	0.079 ± 0.025

Bacterial resistance to antibiotics

Because transportation of gentamicin through inner bacterial membrane to reach its target site is an oxygen-requiring process [78] and the interaction with target occurs in an energy-dependent step [147], we calculated the supply and consumption of oxygen and glucose during growth of *P. aeruginosa* in reactors as well as in test tubes (data not shown). Since the supply of oxygen and glucose is adequate, we assumed that the effect of limitation of oxygen and glucose on reducing gentamicin uptake was minimal in our system. In contrast to gentamicin, because the uptake of ciprofloxacin is an energy-independent process of passive diffusion [148], we do not believe the ciprofloxacin uptake was affected in our device.

In our study, we observed an increase among average EC50 values of gentamicin for both on chip culture and test tube culture (Table 1). For ciprofloxacin, we observed an increase among average EC50 values only on chip. A possible reason for the difference in bacterial counteracting to these two antibiotics may be due to the effect of the exopolysaccharide alginate on the drugs. Alginate forms a layer of anionic polysaccharide which surrounds cells to serve as a barrier to restrict uptake of aminoglycoside [43]. The binding of gentamicin to alginate may reduce the rate of gentamicin diffusion as the antibiotic-binding sites act as sinks to reduce free concentration of gentamicin [149]. Therefore, the accumulation of alginate layers produced during *P. aeruginosa* growth could be a likely cause to reduce the uptake of gentamicin, leading to increased average EC50 values.

Efflux systems play a key role in bacterial resistance to antibiotics. It is well known that *P. aeruginosa* uses four efflux systems to extrude antibiotics to attenuate inhibitory effect of antibiotics [150] . The efflux pump MexA-MexB-OprM of wild type *P. aeruginosa* is expressed during bacterial growth where it contributes to the intrinsic resistance to quinolones [91]. It has

been reported that the expression of MexA-MexB-OprM efflux gene is regulated by growth phase of *P. aeruginosa* [47]. The expression of MexA-MexB-OprM parallels to cell growth and may be a reflection of increased metabolic activity of cells at log phase. For on chip culture, we observed that the growth of bacteria was at late-log phase within 16~24 h (**Figure B3b** in Appendix B). Therefore, we speculated the inhibitory effect of ciprofloxacin may have been attenuated as a result of the continuous expression of MexA-MexB-OprM efflux genes at late-log phase. The increase of average EC_{50} values for on chip culture (**Table 4.1 and Figure 4.3d)** validated our assumption. However, for test tube culture, the growth of bacteria was at late-log to early stationary phase (**Figure B3b** in Appendix B) during which metabolic rate was decreased, and no increase of average EC_{50} values from 16~20 h was observed (**Table 4.1 and Figure 4.3d**).

Ciprofloxacin is considered to be a concentration-dependent bactericidal antibiotic [151]. However, above 0.5 μg/ml of ciprofloxacin, both on chip and test tube culture showed reduced growth inhibition (**Figure 4.3b**). We attributed this phenomenon to the survival of antibiotic-tolerant persister cells induced by ciprofloxacin [152-154].

Features of our microfluidic device

This microfluidic chip integrates concentration generation components (metering channels) which facilitate the preparation of a wide range of antibiotic concentrations and avoid pipetting errors during antibiotic dilution. The bacterial growth in our microfluidic device mimics batch culture mode where bacteria grow in test tubes or microtiters in most laboratories [76]. The zero-flow culture environment of this device prevents cross-contamination of ragent. Therefore, the unique features of this microfluidic method make it a viable alternative to conventional methods to study dose-responses of antibiotics against bacteria.

4.5 Conclusion

Because metabolic activities and efflux pumps of bacteria can affect the uptake of antibiotics, EC_{50} value may change during bacterial growth. In this study, we investigated dose-responses of bactericidal antibiotics against growth of *P. aeruginosa* and obtained EC_{50} values. Our results are the first efforts to demonstrate the efficacy of using a microfluidic device in the time-course analysis of EC_{50}. Our analysis provided a method to evaluate the inhibitory effect associated with the uptake of gentamicin and ciprofloxacin. The unique features of this microfluidic device make it a viable alternative to conventional methods to study dose-responses of antibiotics against bacteria. We envision this microfluidic tool can be further applied to study the concentration effect of different molecules such as ions, nutrients, or antibiotic degrading enzymes as well as the combinatorial effect of antibiotics on multidrug resistant pathogenic bacteria.

Chapter 5

MONITORING OF RNA DEGRADING AGENTS WITH A NOVEL APTAMER-BASED BIOSENSOR

5.1 Introduction

The transcriptome is the complete set of RNAs in a cell [155], reflecting genes expressed in a specific cell at a specific time. The study of the transcriptome is critical for interpreting the functional elements of the genome, revealing the molecular constituents of cells [156] and tissues [157], and understanding development of organisms [158] and molecular origins of diseases [159-162]. The accuracy of gene expression profiling is influenced by the quantity and quality of starting transcripts. RNA purity and integrity are critical for the successful realization of RNA-based analyses [163, 164] as starting with low quality transcripts may strongly compromise the results of labor-intensive, time-consuming and very expensive experiments [24, 25] (quantitative RT-PCR, micro-arrays, northern blot analysis, RNA mapping, cDNA library construction and any applications where the integrity of RNA should be checked).

The most important factor obstructing the analysis of gene expression in human cells and tissues is the rapid degradation of cellular RNAs [165]. After extraction of a tissue from its normal environment, the relative rates of RNA metabolism change, resulting in changes in the relative proportions of various RNA species within a tissue, and an overall reduction of RNA concentrations, due to degradation by endogenous or exogenous RNases [165, 166]. To reduce the rate RNA catabolism after tissue collection, several approaches have been used. Although RNA degradation from endogenous RNases can be prevented (for review, see Srinivasan et al. (2002) [167]), contamination of samples with exogenous ribonucleases (RNases) remains an important cause of RNA loss. Careful handling during the experimentation can limit RNA

degradation [168] but simple mistakes from inexperienced researcher can easily ruin controlled samples [169]. When RNase contamination is suspected, detection of the contamination source is primordial. However, common electrophoresis-based methods have a very low sensitivity and depend on a subjective judgment [92]. Other tests for RNase require a radio-actively RNA substrate or a fluorescence polarization instrument [93]. Although those assays are very sensitive, they are time-consuming, lab-intensive, and expensive. Consequently, when RNase contamination is suspected in one of the reagents, the simplest solution is to throw away all the solutions and re-start the experiment with fresh reagents.

Aptamers are nucleic acids or peptides that exhibit selective affinity for a target molecule, often higher than antibodies [26], and that have little cross-reactivity to other homologous compounds [26, 170]. They are thus currently considered to be attractive detection and diagnostic tools in various domains from health to food science [26, 170-173] because they are inexpensive to generate and produce, easy to modify and easy to combine with other molecules to fit testing/diagnostic purposes [26], including fluorescent dyes [174, 175] that can be activated or inactivated in the presence of target molecules [176].

5.2 Objetive

In this work, we report a novel RNA aptamer-based biosensor for the detection of RNA degrading agents. Using microfluidic systems, we demonstrated the capability of our biosensor to detect different degrading agents and, for the first time, we observed the degradation profiles of the biosensor as a function of time and concentration of degrading agents, in a single experiment. With the advantages of rapid characterization and small reagent consumption,

microfluidic systems are superior to conventional methods to fully characterize degrading effects of enzymes and metal ions.

5.3 Materials and methods

Chip design and fabrication

In this work, we used a microfluidic device, which was previously reported by our group [56]. This microfluidic chip has 14 processors. Each processor consists of an 8-nanoliter rectangle shaped reactor and a metering channel. We fabricated a polydimethylsiloxane (PDMS) based microfluidic device by using standard multilayer soft lithography [60].

Materials

The DFHBI-binding aptamer used in this study is composed of two RNA strands, denoted as strands A and B. Both strands were synthesized by transcription of duplex synthetic DNA templates with T7 RNA polymerase. DNA template for the strand A was formed by annealing deoxyoligonucleotides:

AATTCCTGCAGTAATACGACTCACTATAGACGCGACTGAATGAAATGGTGAAGGAC

GGGTCCAGGTGCGGCTGC and

GCAGCCGCACCTGGACCCGTCCTTCACCATTTCATTCAGTCGCGTCTATAGTGAGTC

GTATTACTGCAGGAAT. DNA template for strand B was formed by annealing deoxyoligonucleotides:

AATTCCTGCAGTAATACGACTCACTATAGCAGCTGCACCTTGTTGAGTAGAGTGTGA

GCTCCGTAACTAGTCGCGTC and

GACGCGACTAGTTACGGAGCTCACACTCTACTCAACAAGGTGCAGCTGCTATAGTGA

GTCGTATTACTGCAGGAATT. These deoxyoligonucleotides were synthesized by Eurofins

MWG Operon and purified by preparative 20 % polyacrylamide gel electrophoresis. The purified deoxyoligonucleotides were stored in 10 mM Tris-HCl, pH=7.5 at -20 °C. Templates were prepared by heating the two complementary DNA strands to 70 °C for 3 minutes and then cooling the DNA on ice. RNA strands A and B were produced by incubating 0.2~1.0 μM template with T7 RNA polymerase (0.1 mg/mL) together with 4 mM ATP, 4 mM GTP, 4 mM CTP, 4 mM UTP in 40 mM Tris-HCl (pH=8.0), 10 mM $MgCl_2$, 1 mM spermidine, 5 mM dithiothreitol and 0.01 % Triton X-100 for 1 hour at 37 °C. Transcripts were purified by electrophoresis in a 1.5-mm thick 20 % polyacrylamide sequencing gel, located by UV shadowing, eluted by crushing in 0.25 mM ammonium acetate/10 mM Tris-HCl (pH=8)/1 mM EDTA, and concentrated by DEAE–cellulose chromatography and ethanol precipitation as described by Cazenave and Uhlenbeck [177]. RNA was dissolved in sterile water and stored at -20 °C. The DFHBI-binding aptamer was assembled by heating equimolar aliquots of strands A and B in 40 mM HEPES-KOH (pH=7.5) buffer containing 125 mM KCl and 5 mM $MgCl_2$ for 3 min at 65 °C and then incubating them for 1 hour at 37 °C. The DFHBI-binding aptamer was stored at -20 °C. To construct RNA aptamer biosensor, DFHBI was bound to its two-stranded aptamer by combining equal volumes of 1.2 μM RNA and 1.2 μM DFHBI, both were resuspended in 40 mM HEPES-KOH (pH=7.5) buffer containing 125 mM KCl and 5 mM $MgCl_2$ and incubating them at 37 °C for 15 min.

Lead acetate ($Pb(Ac)_2$) is from Sigma-Aldrich (St. Louis, MO, USA), RNase T_1 is from Ambion (Grand Island, NY, USA), and RNase A is from Worthington Biochemical Corp., (Lakewood, NJ, USA). RNase A was diluted in 30 mM Tris-HCl, pH=7.5 buffer, RNase T_1 and lead acetate were diluted in RNase-free water. RNA aptamer biosensor was suspended in 40 mM HEPES-KOH, 125 mM KCl, 5 mM $MgCl_2$, 5 % DMSO, pH=7.5 buffer. All agents are prepared

at room temperature. The final concentrations generated in reactors were: 0, 0.05, 0.125, 0.25, 0.375, 0.5, 1.25, 2.5, 3.75, 5, 12.5, 25, 37.5, 50 mM for lead acetate; 0, 0. 5, 1.25, 2.5, 3.75, 5, 12.5, 25, 37.5, 50, 125, 250, 375, 500 U/μL for RNase T_1; 0, 0.05, 0.125, 0.25, 0.375, 0.5, 1.25, 2.5, 3.75, 5, 12.5, 25, 37.5, 50 U/μL for RNase A.

Image acquisition and analysis

Fluorescence image was obtained using a modified ArrayWoRx® biochip scanner (Applied Precision, Issaquah, WA, USA) with 480±15 nm of excitation and 530±20 nm of emission. All captured image were 16-bit grayscale, the resolution was 7,800 pixels per inch (PPI), and the pixel size was 3.25 μm. The whole image (5.0 mm×3.8 mm) of multiplex reactor array chip was acquired by accumulation sequential image (1.25 mm×3.8 mm) four times (2.75 s/scan). The whole image (34.7 mm×4.5 mm) of integrated chip was obtained by accumulating a sequential image (1.47 mm×4.5 mm) twenty-seven times (2.89 s/scan). ArrayWoRx® 2.5 software suits (Applied Precision, Issaquah, WA, USA) built into the workstation automatically converted the images to an integrated image. The total scanning time of the integrated image (5.0 mm×3.8 mm) and (34.7 mm×4.5 mm) was approximately 11 s and 78 s, respectively, exposure time was 0.01 s. The fluorescence images were digitized using ImageJ software (NIH, Bethesda, MD, USA).

To characterize RNA biosensor degradation, a reference image was captured before mixing reagents. Right after mixing, time-lapse images of reactors are obtained by 12 consecutive image scans. Total incubation time is 60 min. Reagents are circulated within reactors before each scan. The intensity of 12 consecutive images is compared by intensity of the reference image.

5.4 Results and Discussion

Design and working principle of fluorescent RNA aptamer biosensor

The fluorescent RNA aptamer biosensor (S4) is constructed with a RNA aptamer and non-fluorescent 3,5-difluoro-4-hydroxybenzylidene imidazoline (DFHBI) (**Figure 5.1a**). When bounded to the RNA aptamer, DFHBI becomes fluorescent under excitation. The two-stranded design increases sensitivity of this biosensor. In the presence of a RNA degrading agent, RNA aptamer is cleaved and DFHBI is released. As DFHBI is a conditional fluorophore, its free form is not fluorescent (**Figure 5.1b**).

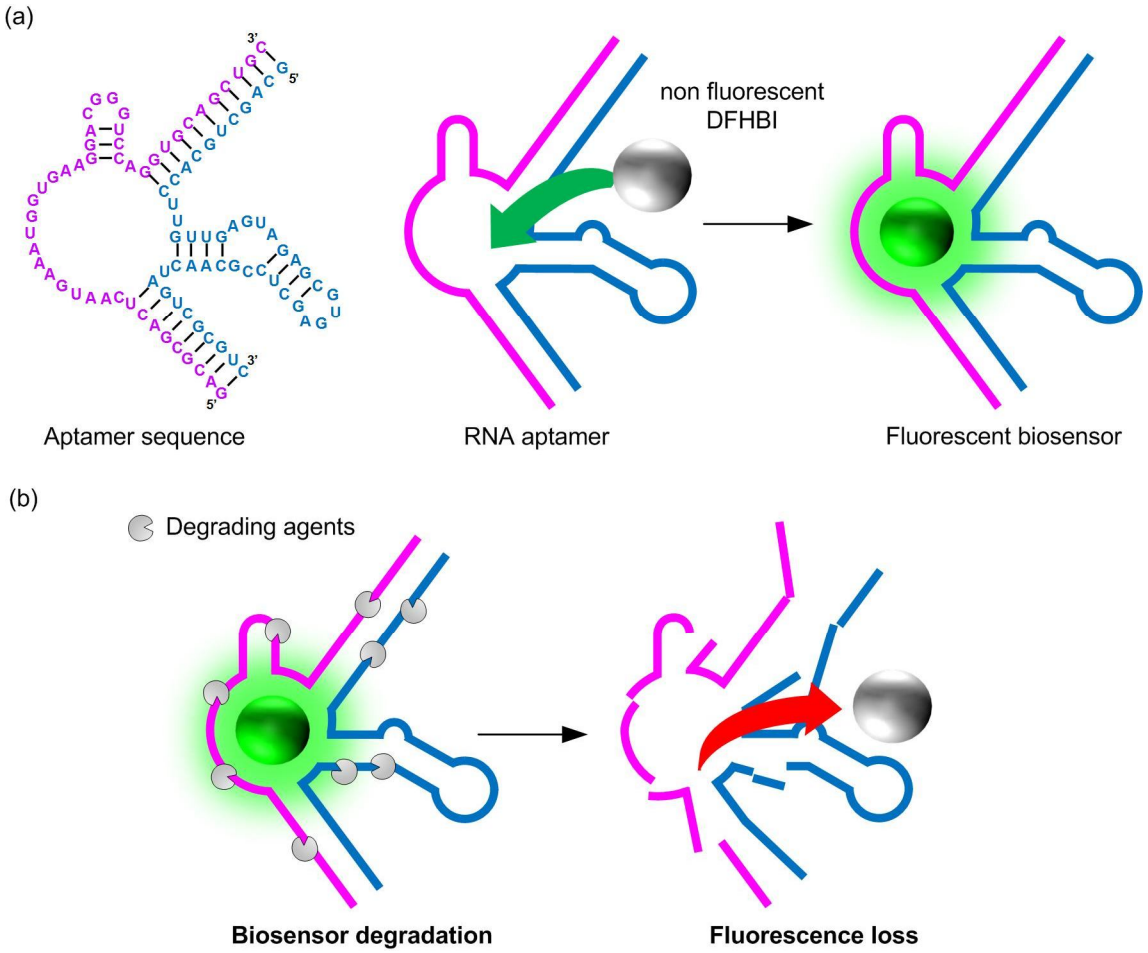

Figure 5.1 Structure and working principle of biosensor. (a) Sequence and structure of biosensor. (b) Working principle of biosensor.

Validation of biosensor in a microfluidic chip

We first demonstrated that our biosensor can detect RNA degrading agents in a microfluidic chip that was described in chapter 1 (**Figure C1** in Appendix C) [46]. The device is composed of two units of 12 reactors. The 12 reactors are divided into 4 sub-units of 3 reactors each, allowing testing 8 different conditions in triplicate in a single experiment. Each reactor is divided into two halves by a central valve. When the valve is closed, two different reagents can be introduced in each half-reactor. When the valve is open the two reagents are mixed by diffusion. In the first unit, we introduced RNase-free water, the RNA aptamer without dye, the dye without aptamer, and the RNA biosensor in triplicate in the 4 sub-units. In the second unit, the central valve was closed and the biosensor was introduced in the first half of the reactors. The second half was then filled with RNase-free water, RNase T_1 (3 U/μL), RNase A (0.5 U/μL), or lead acetate (50 mM). As a control, we introduced RNase-free water, the RNA aptamer, DFHBI, and the biosensor S4, alone, in triplicate, in the 4 sub-units of the second unit. At t=0, the valve was open and fluorescence intensity was measured at fixed time with a modified biochip scanner. When incubated alone or with RNase-free water, fluorescence remained constant in time showing the stability of the RNA aptamer-DFHBI complex and the possibility to detect nanoliter volumes of RNA aptamer biosensors in a microfluidic environment. A significant decrease of fluorescence level was observed when the RNA biosensor was incubated with $Pb(Ac)_2$ and RNase A, suggesting that a single cleavage in the two-stranded RNA aptamer is sufficient to extinguish fluorescence. However, we observed that RNase T_1 did not affect the fluorescence at 3 U/μL concentration, probably due to the low number of unpaired guanosine residues, which are specifically recognized by RNase T_1, in the RNA aptamer [178] (**Figure C1c** in Appendix C).

Characterization of concentration- and time- dependent degradation of biosensor

To determine the minimum detectable concentration of an RNA degrading agent and quantify the concentration- and time-dependant degradation process, we used a microfluidic chip that we previously developed for wide range concentration gradient formation [56] (**Figure 5.2a**). The device has three gradient generators (GGs) with 4 parallel processors each. Every processor contains a metering section and a reactor section, separated by a pneumatic valve. Each reactor integrates a valve-based peristaltic pump for mixing of the reagents in the reactor. A step-by-step process of the chip operation is shown in **Figure 5.2b**. Briefly, a log scale concentration gradient of RNA degrading reagents ($Pb(Ac)_2$, RNase T_1, or RNase A) was generated in the GGs (from 0 to 100 mM, 0 to 1000 U/μL, and 0 to 100 U/μL, respectively) and introduced into the first half of the reactors. Fluorescent RNA biosensor was introduced into the second half of the reactor. Consequently, the concentration of the degrading agent was different for each reactor while the concentration of the RNA biosensor was identical along the chip. Both reagents were 2-fold diluted after mixing inside reactors. The fluorescent intensity inside each reactor was measured with a modified biochip scanner at specific times. A curve of the normalized fluorescence intensity was then plotted for each time point. As a preliminary experiment, we generated a gradient of our RNA aptamer biosensor to determine the minimum fluorescence intensity, and thus the minimum amount of RNA aptamer biosensor, that could be monitor with our system. As shown in **Figure C2** in Appendix C, we could detect as low as 0.84 μM of RNA aptamer biosensor.

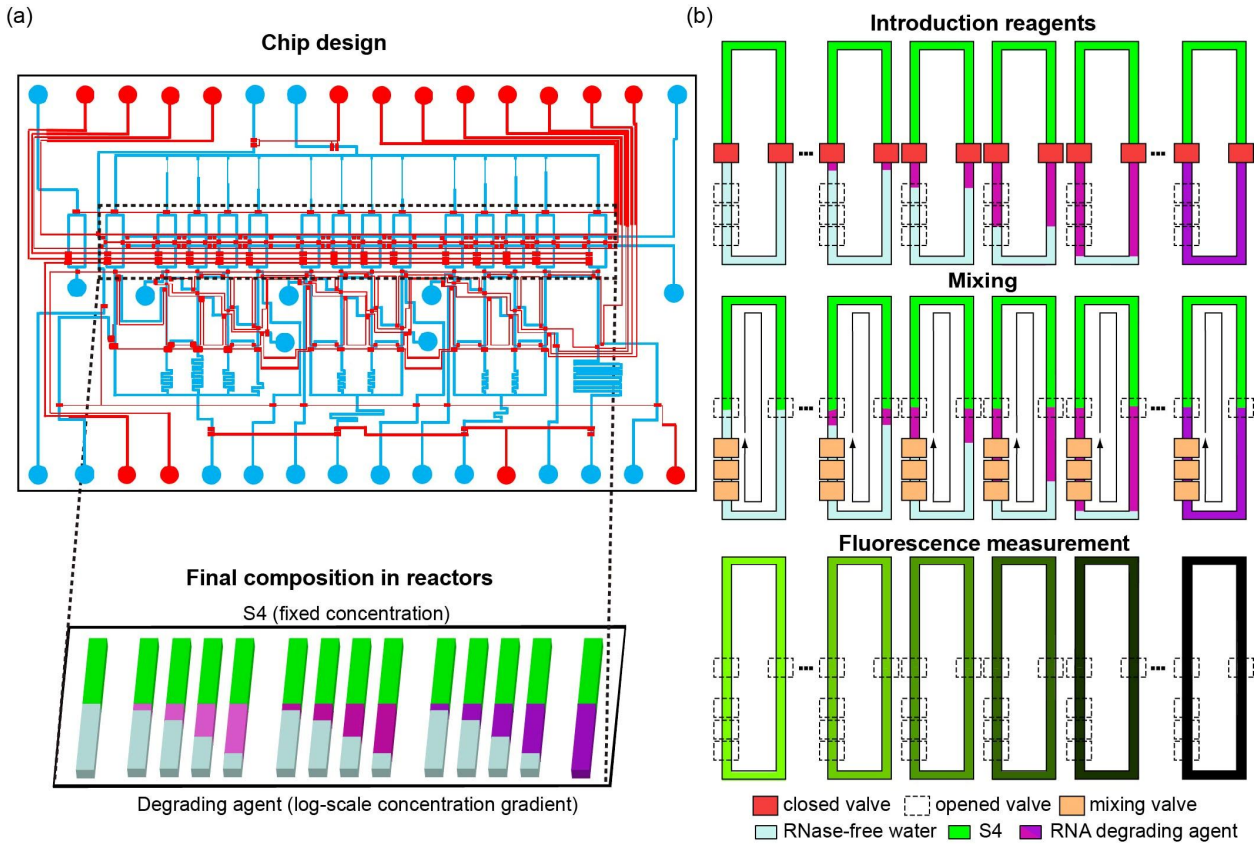

Figure 5.2 Concentration gradient formation of degrading agents on a microfluidic chip. (a) Microfluidic chip with concentration gradient generators, (b) Step-by-step process of concentration gradient formation.

As expected, we observed that the degrading process is a concentration- and time-dependent process **(Figure 5.3)**. For each of the three degrading reagents, we observed a decrease of the fluorescence intensity when the concentration of the degrading agent reached a threshold concentration, 0.375 mM, 37.5 U/µL and 0.375 U/µL for $Pb(Ac)_2$, RNase T_1, and RNase A, respectively. Below the threshold concentrations, the presence degrading agents did not influence the fluorescence intensity, while at high concentration, RNA biosensor was entirely degraded in the first time after mixing (**Figure 5.3**). After 60 min incubation, we were able to detect 0.375 mM of $Pb(Ac)_2$, 37.5 U/µL of RNase T_1 and 0.375 U/µl of RNase A. For $Pb(Ac)_2$, we observed that at concentrations above 3.75 mM, the fluorescence intensity tended to increase

with the concentration. Close observation of the reactors under microscope showed aggregated particles inside the reactors (data not shown). We assumed that DFHBI recombined with random RNA oligomers aggregated by the high concentration of divalent ions (here Pb^{2+}) [179] and recovered its fluorescence.

The differences observed in the degradation pattern of both enzymes are due to the nucleotide composition of the RNA biosensor which has less cleavage target sites for RNase T_1 than RNase A. RNase A is a ubiquitous endoribonuclease that cleaves single-stranded RNA at 3'-ends of unpaired cytosine and uracil residues [180]. In contrast, RNase T_1 is an endonuclease that specifically cleaves RNA at 3'-ends of unpaired guanine residues [178]. Because degradation kinetics is different for RNase A and RNase T_1, our detection system can support which of these two enzymes contaminates analyzed samples. In addition, the integration of microfluidic chip and portable detection system can provide a sensing platform for rapid and cost-effective RNase detection using this RNA biosensor.

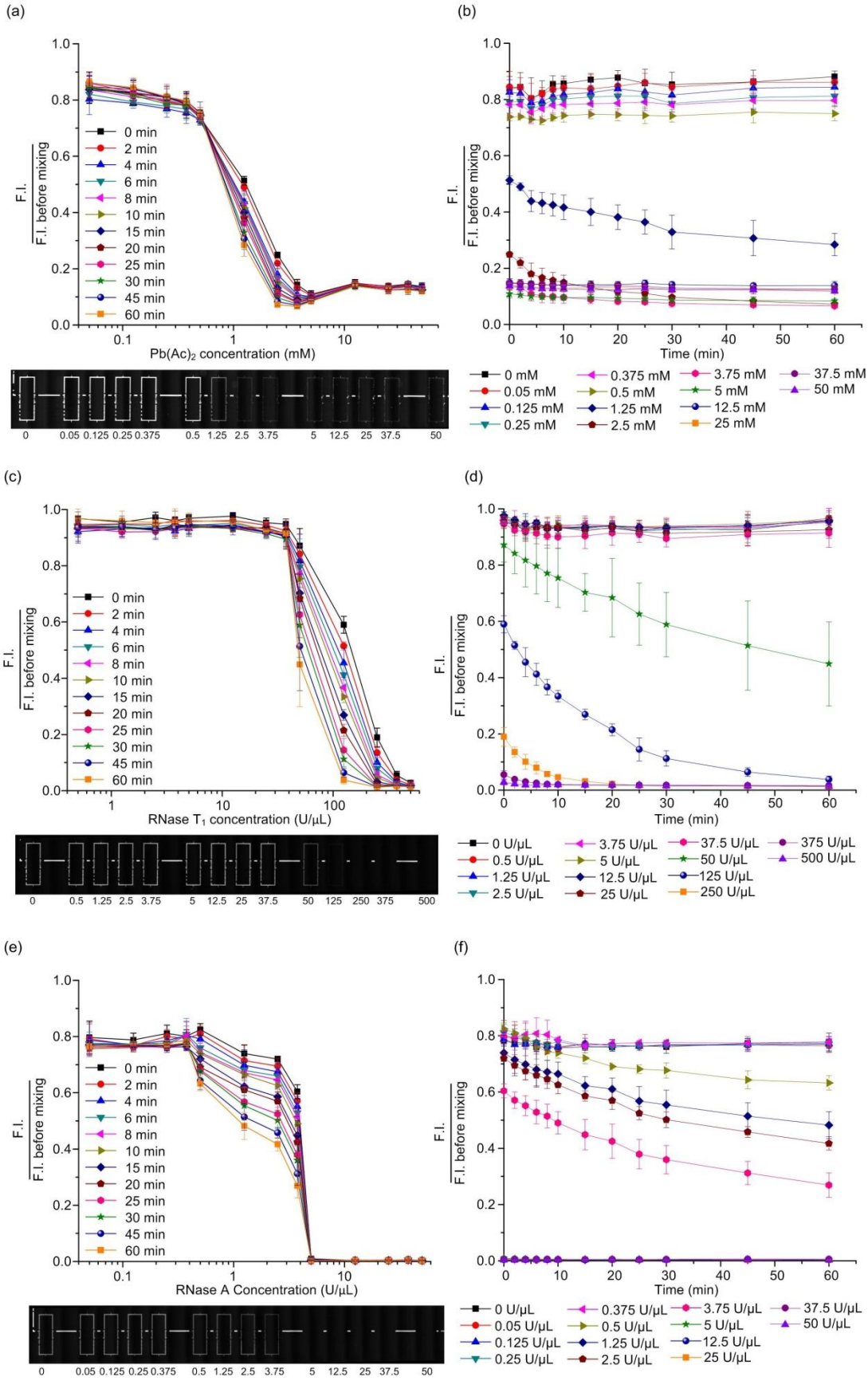
(a)
F.I. / F.I. before mixing
Pb(Ac)2 concentration (mM)
0 min
2 min
4 min
6 min
8 min
10 min
15 min
20 min
25 min
30 min
45 min
60 min
0 0.05 0.125 0.25 0.375 0.5 1.25 2.5 3.75 5 12.5 25 37.5 50
(b)
F.I. / F.I. before mixing
Time (min)
0 mM
0.05 mM
0.125 mM
0.25 mM
0.375 mM
0.5 mM
1.25 mM
2.5 mM
3.75 mM
5 mM
12.5 mM
25 mM
37.5 mM
50 mM
(c)
F.I. / F.I. before mixing
RNase T1 concentration (U/μL)
0 0.5 1.25 2.5 3.75 5 12.5 25 37.5 50 125 250 375 500
(d)
F.I. / F.I. before mixing
Time (min)
0 U/μL
0.5 U/μL
1.25 U/μL
2.5 U/μL
3.75 U/μL
5 U/μL
12.5 U/μL
25 U/μL
37.5 U/μL
50 U/μL
125 U/μL
250 U/μL
375 U/μL
500 U/μL
(e)
F.I. / F.I. before mixing
RNase A Concentration (U/μL)
0 0.05 0.125 0.25 0.375 0.5 1.25 2.5 3.75 5 12.5 25 37.5 50
(f)
F.I. / F.I. before mixing
Time (min)
0 U/μL
0.05 U/μL
0.125 U/μL
0.25 U/μL
0.375 U/μL
0.5 U/μL
1.25 U/μL
2.5 U/μL
3.75 U/μL
5 U/μL
12.5 U/μL
25 U/μL
37.5 U/μL
50 U/μL

Figure 5.3 Characterization of the concentration- and time-dependent degradation of the biosensor. Degradation profile (top) and scanned images (bottom) of the biosensor by different concentration of (a,b) lead acetate, (c,d) RNase T_1, and (e,f) RNase A. Data are presented as means ± SD of three independent experiments.

5.5 Conclusion

The integrity and purity of RNA is essential for the successful RNA-related analyses while RNase contamination can affect the accuracy of these results. To date, aptamer based biosensors have rarely been developed for detection of RNase contamination. In this paper, a novel fluorescent RNA aptamer-based biosensor was reported for the first time. We demonstrated the possibility to detect RNA degrading agents at very low concentration. The concentration- and time-dependent degrading profiles were rapidly obtained using only nanoliter volume of reagents. Our biosensor could detect degrading agent within minutes, while traditional gel electrophoresis-based methods require at least several hours [181]. We believe that our system will stimulate transcriptomic research world-wide, as laboratories lacking experience in RNA research will be able to easily monitor RNase contaminations in solutions and lab equipment. In addition, we demonstrated that microfluidic systems can be used to give alternative and complementary information for the development of molecular tools and, when integrated with a portable detection system, can provide a platform where rapid detection of RNases can be realized with this novel biosensor.

Chapter 6

SUMMARY AND FUTURE PERSPECTIVES

6.1 Summary

In this dissertation, we investigated the concentration- and time-dependent response of cells (bacteria) or molecule (RNA aptamer-based biosensor) to reagents (antibiotics or degrading agents) by using microfluidic systems. We validated the growth of bacterial cells and detection of the RNA aptamer-based biosensor on a multiplex nanoliter reactor array chip. With an integrated microfluidic chip, we further investigated the dose-responses of bacterial growth to bactericidal antibiotics at a time-course manner and monitored the concentration- and time-dependent degradation of the biosensor by RNases and metal ion. This dissertation includes following contributions:

1. We developed a multiplex nanoliter reactor array chip that is capable of cultivating bacteria in a batch culture mode. We validated the bacterial growth phenotypes and quantified the inhibitory effect of antibiotics on bacterial growth in a microfluidic environment. This microfluidic platform is capable of precisely controlling multiple culture conditions with successful evaporation suppression. It is ease of operation without requiring complicated active mixing components and continuous flow of reagents. Our results demonstrated this device can be an alternative to a conventional batch culture assay. Moreover, this device is highly applicable to develop a high-throughput platform for screening potential drug molecules for lead identification in drug discovery.
2. We utilized an integrated microfluidic platform which can generate a wide range of different concentrations and grow bacteria in a zero-flow environment to evaluate dose-response

of bacterial growth to bactericidal antibiotics. This device can prevent cross-contamination of regents and mimic conventional batch culture mode. We determined EC_{50}, an antibiotic concentration which induces 50 % inhibitory effect. Our results are the first effort to demonstrate the efficacy of using microfluidic devices in the time-course analysis of EC_{50}. Our time-course analysis of EC_{50} could provide a method to evaluate the attenuated inhibitory effect as a result of bacteria's resistance to antibiotics during their growth. This device is a potential alternative to replace conventional microtiter plate to determine drug's potency for lead optimization in drug discovery.

3. The degradation profile of a novel RNA aptamer-based biosensor by a gradient of different degrading agent concentrations at specific time intervals can be rapidly obtained with the integrated microfluidic platform. The degradation profiles of RNA biosensors can be used for differentiating degrading agents. Our microfluidic approach is expected to replace costly, time- and labor-intensive conventional methods. This biosensor can contribute to stimulating transcriptomic researches to monitor RNase contaminations. In addition, our microfluidic platform can be integrated with this biosensor to be a detection device for rapid detection of RNase contaminations.

6.2 Future perspectives

Since tremendous efforts have been devoted to the development of microfluidic systems in recent decades, microfluidic systems have brought up a new route for pharmaceutical drug discovery and biochemical analysis. This dissertation focused on assessing the concentration- and time-dependent response of cell (bacteria) or molecule (RNA aptamer-based biosensor) to reagents (antibiotics or degrading agents) by using microfluidic systems. These microfluidic

systems can be further applied to a variety of cell types and molecules, such as, yeast, mammalian cells, proteins, and peptides. By increasing the number of reactors of multiplex reactor chip, high-throughput screening of metabolites, peptides, and proteins can be achieved for drug discovery with reduced time and cost. With the concept of integration of multiplex reactor array chip and biosensors with a portable detection system, a hand-held device for rapid in-field detection of RNases can be developed. Furthermore, these platforms can be applied to investigate concentration-dependent effects of different molecules such as ions, nutrients, or antibiotic degrading enzymes on bacterial growth. In the absence of new pharmaceuticals, multidrug resistance pathogens are frequently treated with combinations of two or more antibiotics. Combination therapy provides a potential means to alleviate the emergence of drug resistance traits as microbial pathogens are less likely to simultaneously develop mutations that have resistance to multiple antibiotics [182]. The effects of antibiotic combinations show either improved (synergistic) or reduced (antagonistic) efficiency compared to each antibiotic applied individually. The effects of antibiotic combinations can be evaluated using our microfluidic systems.

Reference

1. DeLong, E.F. and N.R. Pace, *Environmental diversity of bacteria and archaea.* Syst Biol, 2001. **50**(4): p. 470-478.
2. Lim, D., *Microbiology*. third ed. 2003, Dubuque, Iowa, USA: Kendall/Hunt.
3. Anissimov, M. *How Many Species of Bacteria Are There?* 2013 [cited 2013 10/30].
4. *Biodiversity 2010: the tip of the iceberg.* Nat Rev Micro, 2010. **8**(6): p. 384-384.
5. CDC, *Escherichia coli* Centers for Disease Control and Prevention.
6. Hartl, D.L., *Genetics: analysis of genes and genomes*. 8th ed. 2012, Burlington, MA, USA: Jones & Bartleet learning.
7. Bochner, B.R., *Global phenotypic characterization of bacteria.* FEMS Microbiol. Rev., 2009. **33**(1): p. 191-205.
8. Karr, J.R., et al., *A whole-cell computational model predicts phenotype from genotype.* Cell, 2012. **150**(2): p. 389-401.
9. Shuler, M.L. and F. Kargi, *Bioprocess engineering*. 2nd ed. 2002, Upper Saddle River, NJ, USA: Prentice Hall.
10. Alchon, S.A., *A Pest in the Land: New World Epidemics in a Global Perspective*. 2003, Albuquerque, N.M, USA: University of New Mexico Press.
11. Fleming, A., *On the Antibacterial Action of Cultures of a Penicillium, with Special Reference to their Use in the Isolation of B. influenzæ.* Br J Exp Pathol., 1929. **10**(3): p. 226-236.
12. Lancini, G., F. Parenti, and G.G. Gallo, *Antibiotics A Multidisciplinary Approach*. 1995, New York, USA: Plenum Press.

13. Bauer, A.W., et al., *Antibiotic susceptibility testing by a standardized single disk method.* Am J Clin Pathol, 1966. **45**(4): p. 493-496.

14. Alfonso J, A., *Resistance to Antibiotics: Are We in the Post-Antibiotic Era?* Archives of Medical Research, 2005. **36**(6): p. 697-705.

15. Bax, R., N. Mullan, and J. Verhoef, *The millennium bugs: the need for and development of new antibacterials.* International Journal of Antimicrobial Agents, 2000. **16**(1): p. 51-59.

16. Norrby, S.R., C.E. Nord, and R. Finch, *Lack of development of new antimicrobial drugs: a potential serious threat to public health.* The Lancet Infectious Diseases, 2005. **5**(2): p. 115-119.

17. Silver, L.L. and K.A. Bostian, *Discovery and development of new antibiotics: the problem of antibiotic resistance.* Antimicrob Agents Chemother, 1993. **37**(3): p. 377-83.

18. Tonkens, R., *An Overview of the Drug Development Process*, in *The Physician Executive*. 2005. p. 48-52.

19. Liu, P., et al., *Pharmacokinetic-pharmacodynamic modelling of antibacterial activity of cefpodoxime and cefixime in in vitro kinetic models.* International Journal of Antimicrobial Agents, 2005. **25**(2): p. 120-129.

20. Kang, L., et al., *Microfluidics for drug discovery and development: From target selection to product lifecycle management.* Drug Discovery Today, 2008. **13**(1): p. 1-13.

21. Gupta, S.K., *Drug Discovery and Clinical Research*. 2011, New Delhi, India: Jaypee Brothers Medical Publishers.

22. Clark, D.P. and N.J. Pazdernik, *Molecular Biology*. 2nd ed. 2013, Waltham, MA, USA: Academic Press.

23. Jan Barciszewski, B.F.C.C., *RNA Biochemistry and Biotechnology*. 1998, Netherlands: Kluwer Academic Publishers.

24. Raeymaekers, L., *Quantitative PCR: Theoretical Considerations with Practical Implications.* Analytical Biochemistry, 1993. **214**(2): p. 582-585.

25. Imbeaud, S., et al., *Towards standardization of RNA quality assessment using user-independent classifiers of microcapillary electrophoresis traces.* Nucleic Acids Research, 2005. **33**(6): p. e56-e56.

26. Ellington, A.D. and J.W. Szostak, *In vitro selection of RNA molecules that bind specific ligands.* Nature, 1990. **346**(6287): p. 818-822.

27. Keefe, A.D., S. Pai, and A. Ellington, *Aptamers as therapeutics.* Nature Reviews Drug Discovery, 2010. **9**(7): p. 537-550.

28. Ni, X., et al., *Nucleic acid aptamers: clinical applications and promising new horizons.* Current medicinal chemistry, 2011. **18**(27): p. 4206.

29. Song, S., et al., *Aptamer-based biosensors.* TrAC Trends in Analytical Chemistry, 2008. **27**(2): p. 108-117.

30. Brody, E.N. and L. Gold, *Aptamers as therapeutic and diagnostic agents.* Reviews in Molecular Biotechnology, 2000. **74**(1): p. 5-13.

31. Wang, L., et al., *Fluorescent strip sensor for rapid determination of toxins.* Chem. Commun., 2011. **47**(5): p. 1574-1576.

32. Du, Y., et al., *Microfluidic Electrochemical Aptameric Assay Integrated On-Chip: A Potentially Convenient Sensing Platform for the Amplified and Multiplex Analysis of Small Molecules.* Analytical Chemistry, 2011. **83**(5): p. 1523-1529.

33. Xu, J.-P., et al., *Label-free fluorescence detection of mercury(ii) and glutathione based on Hg2+-DNA complexes stimulating aggregation-induced emission of a tetraphenylethene derivative.* Analyst, 2010. **135**(11): p. 3002-3007.

34. Xiao, H., T.E. Edwards, and A.R. Ferré-D'Amaré, *Structural Basis for Specific, High-Affinity Tetracycline Binding by an In Vitro Evolved Aptamer and Artificial Riboswitch.* Chemistry & Biology, 2008. **15**(10): p. 1125-1137.

35. Whitesides, G.M., *The origins and the future of microfluidics.* Nature, 2006. **442**(7101): p. 368-373.

36. Weibel, D.B., W.R. DiLuzio, and G.M. Whitesides, *Microfabrication meets microbiology.* Nat Rev Micro, 2007. **5**(3): p. 209-218.

37. Saleh-Lakha, S. and J.T. Trevors, *Perspective: Microfluidic applications in microbiology.* Journal of Microbiological Methods, 2010. **82**(1): p. 108-111.

38. Abdelgawad, M. and A.R. Wheeler, *Low-cost, rapid-prototyping of digital microfluidics devices.* Microfluidics and nanofluidics, 2008. **4**(4): p. 349-355.

39. Boedicker, J.Q., et al., *Detecting bacteria and determining their susceptibility to antibiotics by stochastic confinement in nanoliter droplets using plug-based microfluidics.* Lab Chip, 2008. **8**(8): p. 1265-1272.

40. Mariella Jr, R., *Sample preparation: the weak link in microfluidics-based biodetection.* Biomedical microdevices, 2008. **10**(6): p. 777-784.

41. Auroux, P.-A., et al., *Micro total analysis systems. 2. Analytical standard operations and applications.* Analytical Chemistry, 2002. **74**(12): p. 2637-2652.

42. Kim, L., et al., *Microfluidic arrays for logarithmically perfused embryonic stem cell culture.* Lab on a Chip, 2006. **6**(3): p. 394-406.

43. Flanagan, L.A., et al., *Human neural stem cell growth and differentiation in a gradient-generating microfluidic device.* Lab on a Chip, 2005. **5**(4): p. 401-406.

44. Balagadde, F.K., et al., *Long-Term Monitoring of Bacteria Undergoing Programmed Population Control in a Microchemostat.* Science, 2005. **309**(5731): p. 137-140.

45. Groisman, A., et al., *A microfluidic chemostat for experiments with bacterial and yeast cells.* Nat. Methods, 2005. **2**(9): p. 685-689.

46. Institute, C.a.L.S., *Methods for dilution antimicrobial susceptibility testing for bacteria that grew aerobically.Approved Standard M7-A10*. 2009, Clinical and Laboratory Standards Institute: Wayne, PA.

47. Mairhofer, J., K. Roppert, and P. Ertl, *Microfluidic systems for pathogen sensing: a review.* Sensors, 2009. **9**(6): p. 4804-4823.

48. Wheeler, A.R., et al., *Microfluidic device for single-cell analysis.* Analytical chemistry, 2003. **75**(14): p. 3581-3586.

49. Dittrich, P.S. and A. Manz, *Single-molecule fluorescence detection in microfluidic channels—the Holy Grail in μTAS?* Analytical and bioanalytical chemistry, 2005. **382**(8): p. 1771-1782.

50. Hong, J.W., et al., *A nanoliter-scale nucleic acid processor with parallel architecture.* Nat Biotech, 2004. **22**(4): p. 435-439.

51. Yang, M., et al., *An integrated microfluidic device for influenza and other genetic analyses.* Lab on a Chip, 2005. **5**(10): p. 1024-1032.

52. Ottesen, E.A., et al., *Microfluidic Digital PCR Enables Multigene Analysis of Individual Environmental Bacteria.* Science, 2006. **314**(5804): p. 1464-1467.

53. Hansen, C.L., et al., *A robust and scalable microfluidic metering method that allows protein crystal growth by free interface diffusion.* Proceedings of the National Academy of Sciences, 2002. **99**(26): p. 16531-16536.

54. Zheng, B., et al., *A Droplet‐Based, Composite PDMS/Glass Capillary Microfluidic System for Evaluating Protein Crystallization Conditions by Microbatch and Vapor‐Diffusion Methods with On‐Chip X‐Ray Diffraction.* Angewandte chemie international edition, 2004. **43**(19): p. 2508-2511.

55. Jambovane, S., et al., *Determination of kinetic parameters, K_m and k_{cat}, with a single experiment on a chip.* Anal. Chem., 2009. **81**(9): p. 3239-3245.

56. Yun, J.Y., et al., *Log-Scale Dose Response of Inhibitors on a Chip.* Analytical Chemistry, 2011. **83**(16): p. 6148-6153.

57. Hamon, M., et al., *Cell-Based Dose Responses from Open-Well Microchambers.* Analytical Chemistry, 2013. **85**(10): p. 5249-5254.

58. Viravaidya, K., A. Sin, and M.L. Shuler, *Development of a microscale cell culture analog to probe naphthalene toxicity.* Biotechnology progress, 2008. **20**(1): p. 316-323.

59. Pregibon, D.C., M. Toner, and P.S. Doyle, *Multifunctional encoded particles for high-throughput biomolecule analysis.* Science, 2007. **315**(5817): p. 1393-1396.

60. Unger, M.A., et al., *Monolithic microfabricated valves and pumps by multilayer soft lithography.* Science, 2000. **288**(5463): p. 113-116.

61. S. Pennathur, C.D.M., H. T. Soh, *How to exploit the features of microfluidics technology.* Lab on a Chip, 2008. **8**(1): p. 20-22.

62. Heo, Y.S., et al., *Characterization and Resolution of Evaporation-Mediated Osmolality Shifts That Constrain Microfluidic Cell Culture in Poly(dimethylsiloxane) Devices.* Analytical Chemistry, 2006. **79**(3): p. 1126-1134.

63. Capretto, L., et al., *Micromixing within microfluidic devices.* Microfluidics, 2011: p. 27-68.

64. Lee, C.-Y., et al., *Microfluidic mixing: a review.* International Journal of Molecular Sciences, 2011. **12**(5): p. 3263-3287.

65. Berthier, J., *Micro-drops and digitial microfluidics*. 2nd ed. 2013, Oxford, UK: Elsevier.

66. Nguyen, N.-T. and S.T. Wereley, *Fundamentals and Applications of Microfluidics* 2nd ed. 2006, Norwood, USA: ARTECH HOUSE.

67. McDonald, J.C., et al., *Fabrication of microfluidic systems in poly(dimethylsiloxane).* Electrophoresis, 2000. **21**(1): p. 27-40.

68. Xia, Y. and G.M. Whitesides, *Soft Lithography.* Angewandte Chemie International Edition, 1998. **37**(5): p. 550-575.

69. Whitesides, G.M., et al., *Soft lithography in biology and biochemistry.* Annu Rev Biomed Eng, 2001. **3**: p. 335-373.

70. Chou, H.-P., M.A. Unger, and S.R. Quake, *A Microfabricated Rotary Pump.* Biomedical Microdevices, 2001. **3**(4): p. 323-330.

71. Ericsson, H.M. and J.C. Sherris, *Antibiotic sensitivity testing. Report of an international collaborative study.* Acta Pathol Microbiol Scand B Microbiol Immunol, 1971. **217**: p. Suppl 217:1+.

72. Isenberg, H.D., A. Reichler, and D. Wiseman, *Prototype of a fully automated device for determination of bacterial antibiotic susceptibility in the clinical laboratory.* Appl Microbiol, 1971. **22**(6): p. 980-986.

73. Niles, W.D. and P.J. Coassin, *Piezo- and solenoid valve-based liquid dispensing for miniaturized assays.* Assay Drug Dev Technol, 2005. **3**(2): p. 189-202.

74. Ellson, R., et al., *Transfer of low nanoliter volumes between microplates using focused acoustics—automation considerations.* Journal of the Association for Laboratory Automation, 2003. **8**(5): p. 29-34.

75. Patrick R. Murray, E.J.B., James H. Jorgensen, Marie Louise Landry, and Michael A. Pfaller *Manual of Clinical Microbiology*. 9th ed. Susceptibility testing instrumentation and computerized expert systems for data analysis and interpretation, ed. F.M. Richter SS. 2008, Washington, DC: ASM Press.

76. Reller, L.B., et al., *Antimicrobial susceptibility testing: a review of general principles and contemporary practices.* Clinical infectious diseases, 2009. **49**(11): p. 1749-1755.

77. Diagnostics, S.H., *MicroScan WalkAway plus System*. 2008: USA.

78. Sun, P., et al., *High-throughput microfluidic system for long-term bacterial colony monitoring and antibiotic testing in zero-flow environments.* Biosensors and Bioelectronics, 2011. **26**(5): p. 1993-1999.

79. Kim, K.P., et al., *In situ monitoring of antibiotic susceptibility of bacterial biofilms in a microfluidic device.* Lab on a Chip, 2010. **10**(23): p. 3296-3299.

80. Kim, J., et al., *A microfluidic device for high throughput bacterial biofilm studies.* Lab on a Chip, 2012. **12**(6): p. 1157-1163.

81. Dertinger, S.K.W., et al., *Generation of Gradients Having Complex Shapes Using Microfluidic Networks.* Analytical Chemistry, 2001. **73**(6): p. 1240-1246.

82. Anna, S.L., N. Bontoux, and H.A. Stone, *Formation of dispersions using "flow focusing" in microchannels.* Applied physics letters, 2003. **82**(3): p. 364-366.

83. Garstecki, P., et al., *Formation of monodisperse bubbles in a microfluidic flow-focusing device.* Applied Physics Letters, 2004. **85**(13): p. 2649-2651.

84. Thorsen, T., et al., *Dynamic pattern formation in a vesicle-generating microfluidic device.* Physical review letters, 2001. **86**(18): p. 4163-4166.

85. Garstecki, P., et al., *Formation of droplets and bubbles in a microfluidic T-junction—scaling and mechanism of break-up.* Lab on a Chip, 2006. **6**(3): p. 437-446.

86. Churski, K., et al., *Rapid screening of antibiotic toxicity in an automated microdroplet system.* Lab on a Chip, 2012. **12**(9): p. 1629-1637.

87. Chen, D.L. and R.F. Ismagilov, *Microfluidic cartridges preloaded with nanoliter plugs of reagents: an alternative to 96-well plates for screening.* Current Opinion in Chemical Biology, 2006. **10**(3): p. 226-231.

88. Churski, K., P. Korczyk, and P. Garstecki, *High-throughput automated droplet microfluidic system for screening of reaction conditions.* Lab on a Chip, 2010. **10**(7): p. 816-818.

89. Lee, W., et al., *Predictive model on micro droplet generation through mechanical cutting.* Microfluid. Nanofluid., 2009. **7**(3): p. 431-438.

90. Zeng, S., et al., *Microvalve-actuated precise control of individual droplets in microfluidic devices.* Lab on a Chip, 2009. **9**(10): p. 1340-1343.

91. Bo-Chih Lin, Y.-C.S., *Novel on-demand droplet generation for selective fluid sample extraction.* Biomicrofluidics, 2012. **6**(2): p. 024103.

92. Richard Curtis Bird and B.F. Smith, *Genetic Library Construction and Screening: Advanced Techniques and Applications*. 2002, Berlin, Germany: Springer.

93. DiNitto, J.P., L. Wang, and J.C. Wu, *Continuous fluorescence-based method for assessing dicer cleavage efficiency reveals 3'overhang nucleotide preference.* Biotechniques, 2010. **48**(4): p. 303.

94. Invitrogen, *Is Your RNA Intact? Methods to Check RNA Integrity*.

95. Bochner, B.R., *New technologies to assess genotype-phenotype relationships.* Nat. Rev. Genet., 2003. **4**(4): p. 309-314.

96. Yoon, S.H., et al., *Comparative multi-omics systems analysis of Escherichia coli strains B and K-12.* Genome Biol., 2012. **13**(5): p. R37.

97. Schneider, M.V. and S. Orchard, *Omics technologies, data and bioinformatics principles.* Methods Mol. Biol., 2011. **719**: p. 3-30.

98. Lee, S.Y., D.Y. Lee, and T.Y. Kim, *Systems biotechnology for strain improvement.* Trends Biotechnol., 2005. **23**(7): p. 349-358.

99. Buescher, J.M., et al., *Global network reorganization during dynamic adaptations of Bacillus subtilis metabolism.* Science, 2012. **335**(6072): p. 1099-1103.

100. Covert, M.W., et al., *Integrating high-throughput and computational data elucidates bacterial networks.* Nature, 2004. **429**(6987): p. 92-96.

101. Yoon, S.H., et al., *Parallel evolution of transcriptome architecture during genome reorganization.* Genome Res., 2011. **21**(11): p. 1892-1904.

102. Duetz, W.A., *Microtiter plates as mini-bioreactors: miniaturization of fermentation methods.* Trends Microbiol., 2007. **15**(10): p. 469-475.

103. Kumar, S., C. Wittmann, and E. Heinzle, *Minibioreactors.* Biotechnol. Lett., 2004. **26**(1): p. 1-10.

104. Marques, M.P., J.M. Cabral, and P. Fernandes, *High throughput in biotechnology: from shake-flasks to fully instrumented microfermentors.* Recent Pat. Biotechnol., 2009. **3**(2): p. 124-140.

105. Li, N., A. Tourovskaia, and A. Folch, *Biology on a chip: microfabrication for studying the behavior of cultured cells.* Crit. Rev. Biomed. Eng., 2003. **31**(5-6): p. 423-488.

106. Bochner, B.R., P. Gadzinski, and E. Panomitros, *Phenotype microarrays for high-throughput phenotypic testing and assay of gene function*. Genome Res, 2001. **11**(7): p. 1246-55.

107. Funke, M., et al., *Bioprocess control in microscale: scalable fermentations in disposable and user-friendly microfluidic systems.* Microb. Cell. Fact., 2010. **9**: p. 86.

108. Kensy, F., C. Engelbrecht, and J. Buchs, *Scale-up from microtiter plate to laboratory fermenter: evaluation by online monitoring techniques of growth and protein expression in Escherichia coli and Hansenula polymorpha fermentations.* Microb. Cell. Fact., 2009. **8**: p. 68.

109. Zhang, Z., et al., *Microchemostat-microbial continuous culture in a polymer-based, instrumented microbioreactor.* Lab Chip, 2006. **6**(7): p. 906-913.

110. Dai, W., et al., *A prototypic microfluidic platform generating stepwise concentration gradients for real-time study of cell apoptosis.* Biomicrofluidics, 2010. **4**(2): p. 024101.

111. Velve-Casquillas, G., et al., *Microfluidic tools for cell biological research.* Nano Today, 2010. **5**(1): p. 28-47.

112. Yeo, L.Y., et al., *Microfluidic devices for bioapplications.* Small, 2011. **7**(1): p. 12-48.

113. Gan, M., et al., *Massively parallel bacterial and yeast suspension culture on a chip.* Small, 2012. **8**(6): p. 863-867.

114. Günberger, A., et al., *A disposable picolitre bioreactor for cultivation and investigation of industrially relevant bacteria on the single cell level.* Lab Chip, 2012. **12**(11): p. 2060-2068.

115. Vyawahare, S., A.D. Griffiths, and C.A. Merten, *Miniaturization and parallelization of biological and chemical assays in microfluidic devices.* Chem. Biol., 2010. **17**(10): p. 1052-1065.

116. Lecault, V., et al., *High-throughput analysis of single hematopoietic stem cell proliferation in microfluidic cell culture arrays.* Nat. Methods, 2011. **8**(7): p. 581-586.

117. Young, E.W. and D.J. Beebe, *Fundamentals of microfluidic cell culture in controlled microenvironments.* Chem. Soc. Rev., 2010. **39**(3): p. 1036-1048.

118. Cook, A. and J. Lederberg, *Recombination studies of lactose nonfermenting mutants of Escherichia coli K-12.* Genetics, 1962. **47**: p. 1335-1353.

119. Seeton, C., *Viscosity–temperature correlation for liquids.* Tribology Letters, 2006. **22**(1): p. 67-78.

120. Urbanski, J.P., et al., *Digital microfluidics using soft lithography.* Lab Chip, 2006. **6**(1): p. 96-104.

121. Liu, J., C. Hansen, and S.R. Quake, *Solving the "World-to-Chip" Interface Problem with a Microfluidic Matrix.* Anal. Chem., 2003. **75**(18): p. 4718-4723.

122. Heo, Y.S., et al., *Characterization and resolution of evaporation-mediated osmolality shifts that constrain microfluidic cell culture in poly(dimethylsiloxane) devices.* Anal. Chem., 2007. **79**(3): p. 1126-1134.

123. Reichenbach, H., *The ecology of the myxobacteria.* Environ. Microbiol., 1999. **1**(1): p. 15-21.

124. Paguirigan, A.L. and D.J. Beebe, *Microfluidics meet cell biology: bridging the gap by validation and application of microscale techniques for cell biological assays.* BioEssays, 2008. **30**(9): p. 811-821.

125. Monod, J., *The growth of bacterial cultures.* Annu. Rev. Microbiol., 1949. **3**(1): p. 371-394.

126. Gorke, B. and J. Stulke, *Carbon catabolite repression in bacteria: many ways to make the most out of nutrients.* Nat Rev Micro, 2008. **6**(8): p. 613-624.

127. Garau, J. and L. Gomez, *Pseudomonas aeruginosa pneumonia.* Curr. Opin. Infect. Dis., 2003. **16**(2): p. 135-143.

128. Szita, N., et al., *Development of a multiplexed microbioreactor system for high-throughput bioprocessing.* Lab Chip, 2005. **5**(8): p. 819-826.

129. Lee, H.L.T., et al., *Microbioreactor arrays with integrated mixers and fluid injectors for high-throughput experimentation with pH and dissolved oxygen control.* Lab Chip, 2006. **6**(9): p. 1229-1235.

130. Zuluaga, A.F., et al., *Application of microbiological assay to determine pharmaceutical equivalence of generic intravenous antibiotics.* BMC Clin. Pharmacol., 2009. **9**: p. 1.

131. Silva, E., et al., *Comparative in vitro study of the antimicrobial activities of different commercial antibiotic products for intravenous administration.* BMC Clin. Pharmacol., 2010. **10**: p. 3.

132. Raty, S., et al., *Embryonic development in the mouse is enhanced via microchannel culture.* Lab Chip, 2004. **4**(3): p. 186-190.

133. Yu, H., et al., *Diffusion dependent cell behavior in microenvironments.* Lab Chip, 2005. **5**(10): p. 1089-1095.

134. Nayyar, G.M.L., et al., *Poor-quality antimalarial drugs in southeast Asia and sub-Saharan Africa.* The Lancet Infectious Diseases, 2012. **12**(6): p. 488-496.

135. *On-demand micro-encapsulation utilizing on-chip synthesis of semi-permeable alginate-PLL capsules.* Microfluidics and Nanofluidics, 2010.

136. De La Fuente, R., et al., *Small molecules with antimicrobial activity against E. coli and P. aeruginosa identified by high-throughput screening.* British Journal of Pharmacology, 2006. **149**(5): p. 551-559.

137. Huser, J., *High-throughput screening in drug discovery*. 2006, Stuttgart, Germany: Wiley-VCH.

138. Jeong, H.-H., et al., *Microfluidic monitoring of Pseudomonas aeruginosa chemotaxis under the continuous chemical gradient.* Biosensors and Bioelectronics, 2010. **26**(2): p. 351-356.

139. Englert, D.L., M.D. Manson, and A. Jayaraman, *Flow-based microfluidic device for quantifying bacterial chemotaxis in stable, competing gradients.* Appl Environ Microbiol, 2009. **75**(13): p. 4557-4564.

140. Kalinin, Y., et al., *Responses of Escherichia coli bacteria to two opposing chemoattractant gradients depend on the chemoreceptor ratio.* J Bacteriol, 2010. **192**(7): p. 1796-1800.

141. Guo, M.T., et al., *Droplet microfluidics for high-throughput biological assays.* Lab on a Chip, 2012. **12**(12): p. 2146-2155.

142. Maharbiz, M.M., et al., *A microfabricated electrochemical oxygen generator for high-density cell culture arrays.* Microelectromechanical Systems, Journal of, 2003. **12**(5): p. 590-599.

143. Jambovane, S., et al., *Creation of Stepwise Concentration Gradient in Picoliter Droplets for Parallel Reactions of Matrix Metalloproteinase II and IX.* Analytical Chemistry, 2011. **83**(9): p. 3358-3364.

144. Eagon, R.G. and P.V. Phibbs Jr, *Kinetics of Transport of Glucose, Fructose, and Mannitol by Pseudomonas aeruginosa.* Canadian Journal of Biochemistry, 1971. **49**(9): p. 1031-1041.

145. Reyes, D.R., et al., *Micro total analysis systems. 1. Introduction, theory, and technology.* ANALYTICAL CHEMISTRY-WASHINGTON DC-, 2002. **74**(12): p. 2623-2636.

146. Scudamore, R.A. and M. Goldner, *Penetration of the outer membrane of Pseudomonas aeruginosa by synergistic combinations of beta-lactam and aminoglycoside antibiotics.* Antimicrobial agents and chemotherapy, 1982. **21**(6): p. 1007-1010.

147. *A microfluidic platform for on-demand formation and merging of microdroplets using electric control.* Biomicrofluidics, 2011. **5**(1): p. 011101.

148. *High-throughput sample introduction for droplet-based screening with an on-chip integrated sampling probe and slotted-vial array.* Lab on a Chip, 2010. **10**(21): p. 2864.

149. *A gravity-actuated technique for flexible and portable microfluidic droplet manipulation.* Microfluidics and Nanofluidics, 2010.

150. Schweizer, H.P., *Efflux as a mechanism of resistance to antimicrobials in Pseudomonas aeruginosa and related bacteria: unanswered questions.* Genet Mol Res, 2003. **2**(1): p. 48-62.

151. *Temperature-induced droplet coalescence in microchannels.* Biomicrofluidics, 2012. **6**(1): p. 012811.

152. *Production of uniform droplets using membrane, microchannel and microfluidic emulsification devices.* Microfluidics and Nanofluidics, 2012.

153. Yi-Ming, T., W. Jhih-Jhe, and S. Yu-Chuan, *A random-access microarray for programmable droplet storage, retrieval and manipulation.* Journal of Micromechanics and Microengineering, 2012. **22**(4): p. 045005.

154. Ralf, S., et al., *Droplet based microfluidics.* Reports on Progress in Physics, 2012. **75**(1): p. 016601.

155. Bernot, A., *Genome Transcriptome and Proteome Analysis*. 2007, West Sussex, England: Wiley.

156. Velculescu, V.E., et al., *Characterization of the yeast transcriptome.* Cell, 1997. **88**(2): p. 243-251.

157. Wang, E.T., et al., *Alternative isoform regulation in human tissue transcriptomes.* Nature, 2008. **456**(7221): p. 470-476.

158. Baugh, L.R., et al., *Composition and dynamics of the Caenorhabditis elegans early embryonic transcriptome.* Development, 2003. **130**(5): p. 889-900.

159. Anisimov, S.V., E.G. Lakatta, and K.R. Boheler, *Discovering altered genomic expression patterns in heart: transcriptome determination by serial analysis of gene expression.* European journal of heart failure, 2001. **3**(3): p. 271-281.

160. Bakay, M., et al., *A web-accessible complete transcriptome of normal human and DMD muscle.* Neuromuscular Disorders, 2002. **12**: p. S125-S141.

161. Connolly, S.B., et al., *Transcriptome profiling and the pathogenesis of diabetic complications.* Journal of the American Society of Nephrology, 2003. **14**(suppl 3): p. S279-S283.

162. Meyerson, M., S. Gabriel, and G. Getz, *Advances in understanding cancer genomes through second-generation sequencing.* Nature Reviews Genetics, 2010. **11**(10): p. 685-696.

163. Perez-Novo, C.A., et al., *Impact of RNA quality on reference gene expression stability.* Biotechniques, 2005. **39**(1): p. 52-56.

164. Fleige, S. and M.W. Pfaffl, *RNA integrity and the effect on the real-time qRT-PCR performance.* Molecular Aspects of Medicine, 2006. **27**(2–3): p. 126-139.

165. Chirgwin, J.M., et al., *Isolation of biologically active ribonucleic acid from sources enriched in ribonuclease.* Biochemistry, 1979. **18**(24): p. 5294-5299.

166. Ullrich, A., et al., *Rat insulin genes: construction of plasmids containing the coding sequences.* Science, 1977. **196**(4296): p. 1313-1319.

167. Srinivasan, M., D. Sedmak, and S. Jewell, *Effect of fixatives and tissue processing on the content and integrity of nucleic acids.* The American journal of pathology, 2002. **161**(6): p. 1961.

168. Bustin, S.A. and T. Nolan, *Pitfalls of quantitative real-time reverse-transcription polymerase chain reaction.* Journal of biomolecular techniques: JBT, 2004. **15**(3): p. 155-166.

169. Robert E. Farrell, J., *RNA Methodologies: Laboratory Guide for Isolation and Characterization*. 4th ed. 2009, London, UK: Elsevier Science.

170. Ellington, A.D. and J.W. Szostak, *Selection in vitro of single-stranded DNA molecules that fold into specific ligand-binding structures.* Nature, 1992. **355**(6363): p. 850-852.

171. Bock, L.C., et al., *Selection of single-stranded DNA molecules that bind and inhibit human thrombin.* Nature, 1992. **355**(6360): p. 564-566.

172. Breaker, R.R., *DNA enzymes.* Nat Biotech, 1997. **15**(5): p. 427-431.

173. Joshi, R., et al., *Selection, characterization, and application of DNA aptamers for the capture and detection of Salmonella enterica serovars.* Molecular and cellular probes, 2009. **23**(1): p. 20-28.

174. Holeman, L.A., et al., *Isolation and characterization of fluorophore-binding RNA aptamers.* Folding and Design, 1998. **3**(6): p. 423-431.

175. Stojanovic, M.N., P. De Prada, and D.W. Landry, *Aptamer-based folding fluorescent sensor for cocaine.* Journal of the American Chemical Society, 2001. **123**(21): p. 4928-4931.

176. Nutiu, R. and Y. Li, *Structure-switching signaling aptamers.* Journal of the American Chemical Society, 2003. **125**(16): p. 4771-4778.

177. Cazenave, C. and O.C. Uhlenbeck, *RNA template-directed RNA synthesis by T7 RNA polymerase.* Proceedings of the National Academy of Sciences, 1994. **91**(15): p. 6972-6976.

178. Nicholson, A.W., *Ribonucleases, Part A: Functional Roles and Mechanisms of Action, Volume 341 (Methods in Enzymology)*. 2001, San Diego, USA: Academic Press.

179. Vlassov, A., *Assay of random RNA oligomerisation in buffers with high concentrations of divalent metal ions.* Nucleosides Nucleotides Nucleic Acids, 2004. **23**(6-7): p. 999-1001.

180. Rushizky, G.W., C.A. Knight, and H.A. Sober, *Studies on the preferential specificity of pancreatic ribonuclease as deduced from partial digests.* J Biol Chem, 1961. **236**: p. 2732-2737.

181. Donald C. Rio, M.A.J., Gregory J. Hannon, and Timothy W. Nilsen, *RNA: A Laboratory Manual*. 2010, Cold Spring Harbor, NY, USA: CSHL Press.

182. Chait, R., A. Craney, and R. Kishony, *Antibiotic interactions that select against resistance.* Nature, 2007. **446**(7136): p. 668-671.

Appendix A

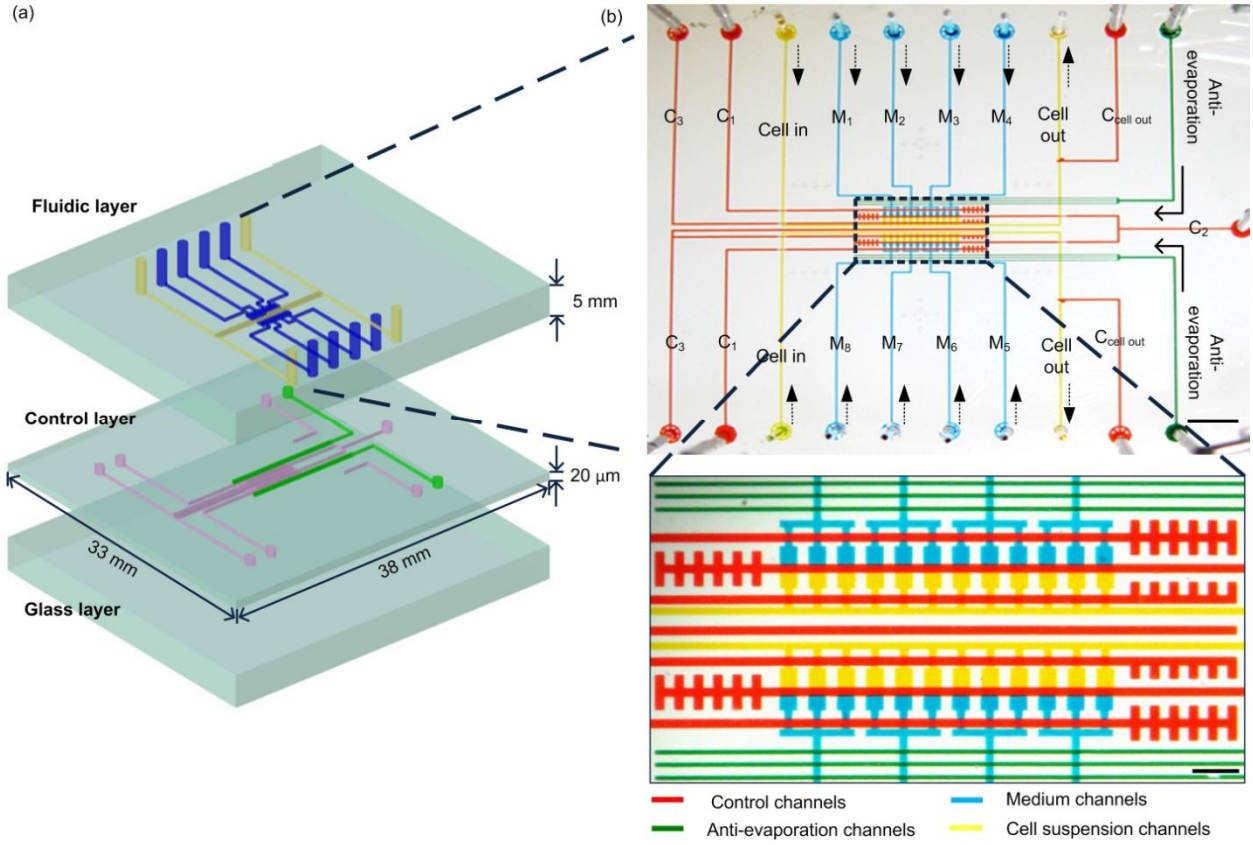

Figure A1. Design of the multiplex microfluidic nanoliter chip. (a) Multi-layered structure of the device. (b) Photographs of the top view of the nanoliter reactor system (scale bar, 2 mm) and the enlarged version of the array comprising 2 × 12 parallel nanoliter culture reactors (scale bar, 500 µm), which are filled with cell suspension (denoted as yellow lines) and culture media (denoted as blue lines, M_1 to M_8). The anti-evaporation and control channels are represented as green and red lines, respectively. In a single unit, an experiment can be performed in triplicates. The arrows denote the direction of flow.

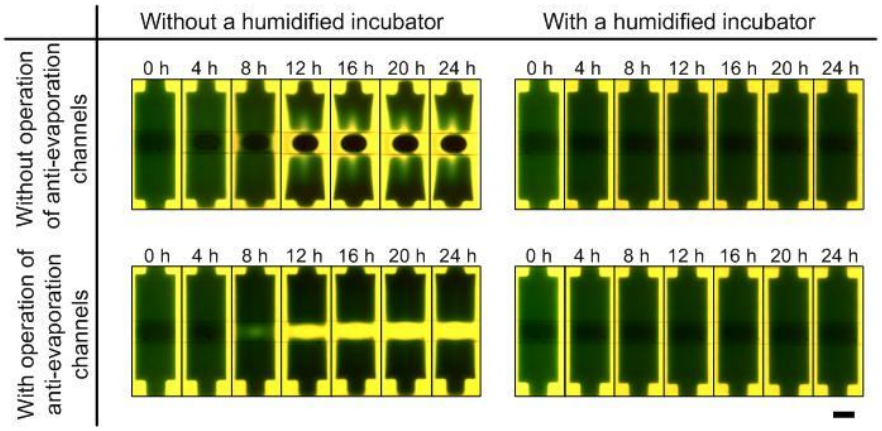

Figure A2. Micrographs showing time profiles (24 h duration) corresponding to the amount of green dye, which was retained in the reactors at 37 °C, based on the presence and/or absence of humidity control and/or anti-evaporation channels—absence of humidity (upper left), in the presence of operation of anti-evaporation channels (lower left), in the presence of a humidified incubator (upper right), and in the presence of both humidified incubator and the operation of anti-evaporation channels (lower right) (scale bar, 100 μm).

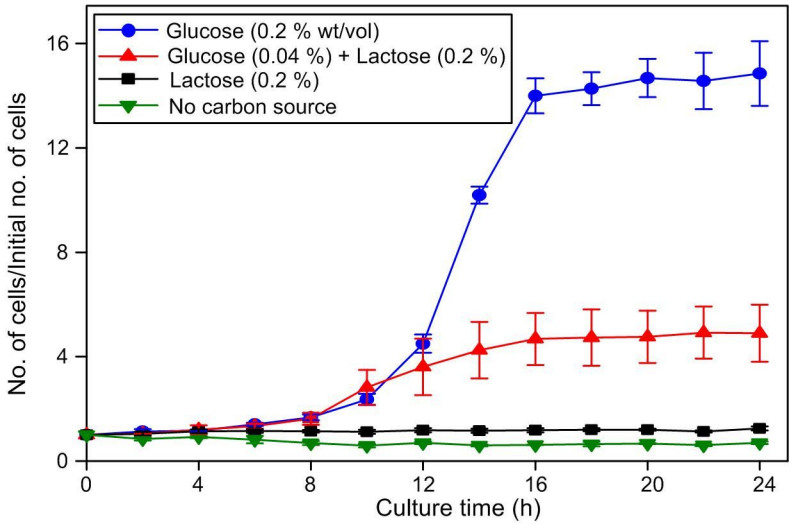

Figure A3. A graph showing the time profile corresponding to the number of *lac*$^{-}$ *E. coli* mutants, which was normalized to the initial number of cells. Cells were loaded into the nanoliter reactors filled with M9 minimal medium along with different carbon sources, namely, glucose (0.2 % wt/vol) (denoted as blue circles), lactose (0.2 %) (red triangles), and glucose (0.04 %), lactose (0.2 %) (black squares), as well as no carbon source (green triangles down). Error bar denotes the standard error of the mean from three replicate reactors.

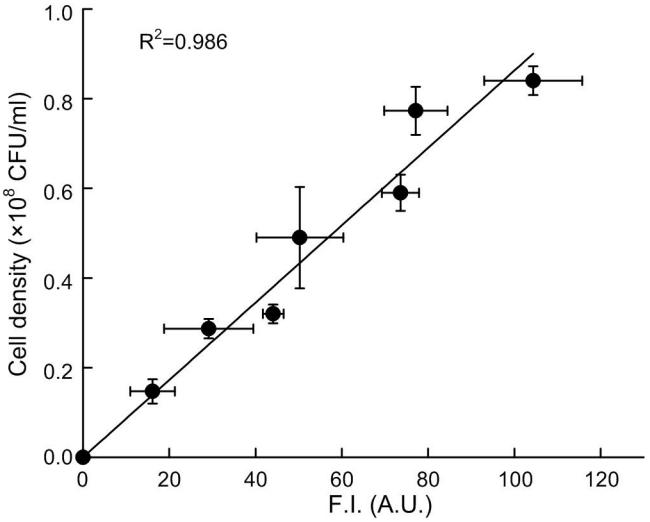

Figure A4. A graph showing the correlation between cell density (×10^8 CFU/mL) and fluorescence intensity (F.I., represented in arbitrary unit (A.U.)) of PT5-EGFP. Error bar denotes the standard error of the mean from three replicate reactors.

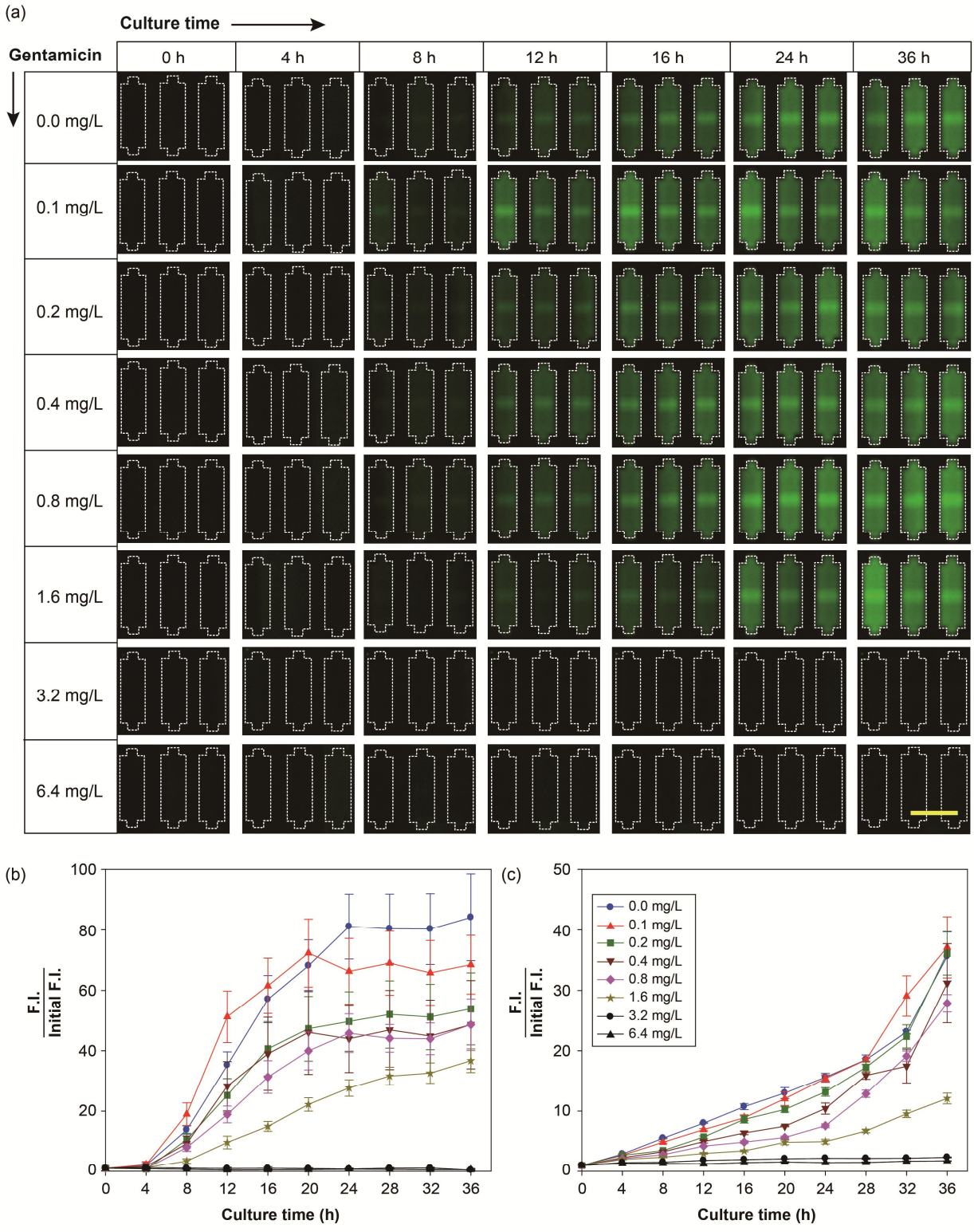

Figure A5. Concentration-dependent inhibitory effect of gentamicin on PT5-EGFP strain. (a) Time-lapse fluorescence images of the 3 replicate nanoliter reactors. Scale bar, 400 μm. Graphs showing the time profiles of cell

density measured as fluorescence signal in (b) nanoliter reactors and (c) 14-mL test tubes. Error bar denotes the standard error of the mean from three replicates.

Appendix B

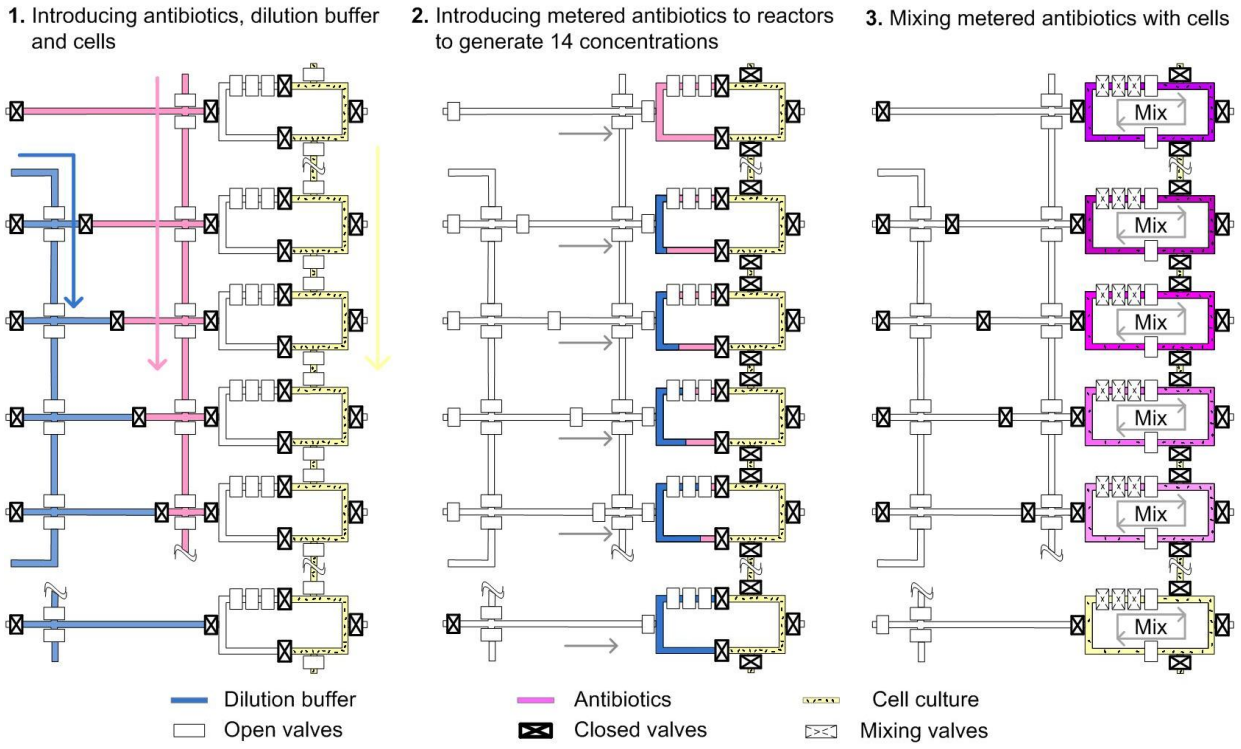

Figure B1. Step-by-step procedure to generate 14 concentrations of antibiotics. First, antibiotics and dilution buffer are introduced to metering channels through “Antibiotics” and ”Buffer” inlets; bacterial cells are introduced into half of reactors through “cell in” inlet. Then, metered antibiotics are introduced to reactors to generate 14 concentrations. Finally, antibiotics are mixed with bacterial cells by operating three mixing valves. (Figure is modified from [56])

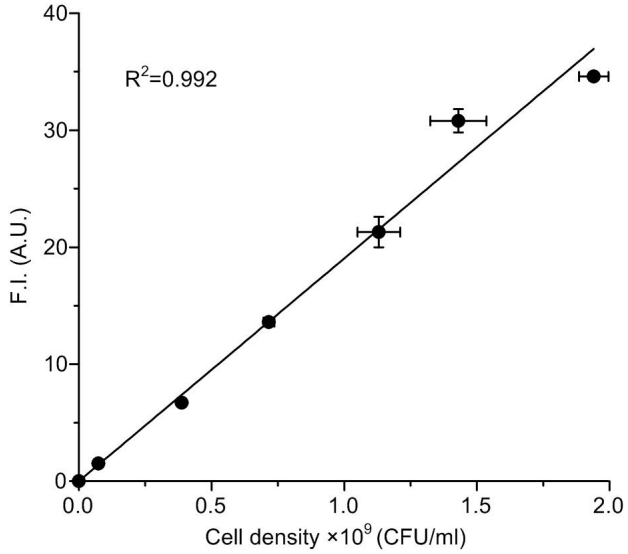

Figure B2. Correlation of cell density and fluorescence intensity. A significant linear correlation was observed. Data are represented as means ± SD of three independent measurements.

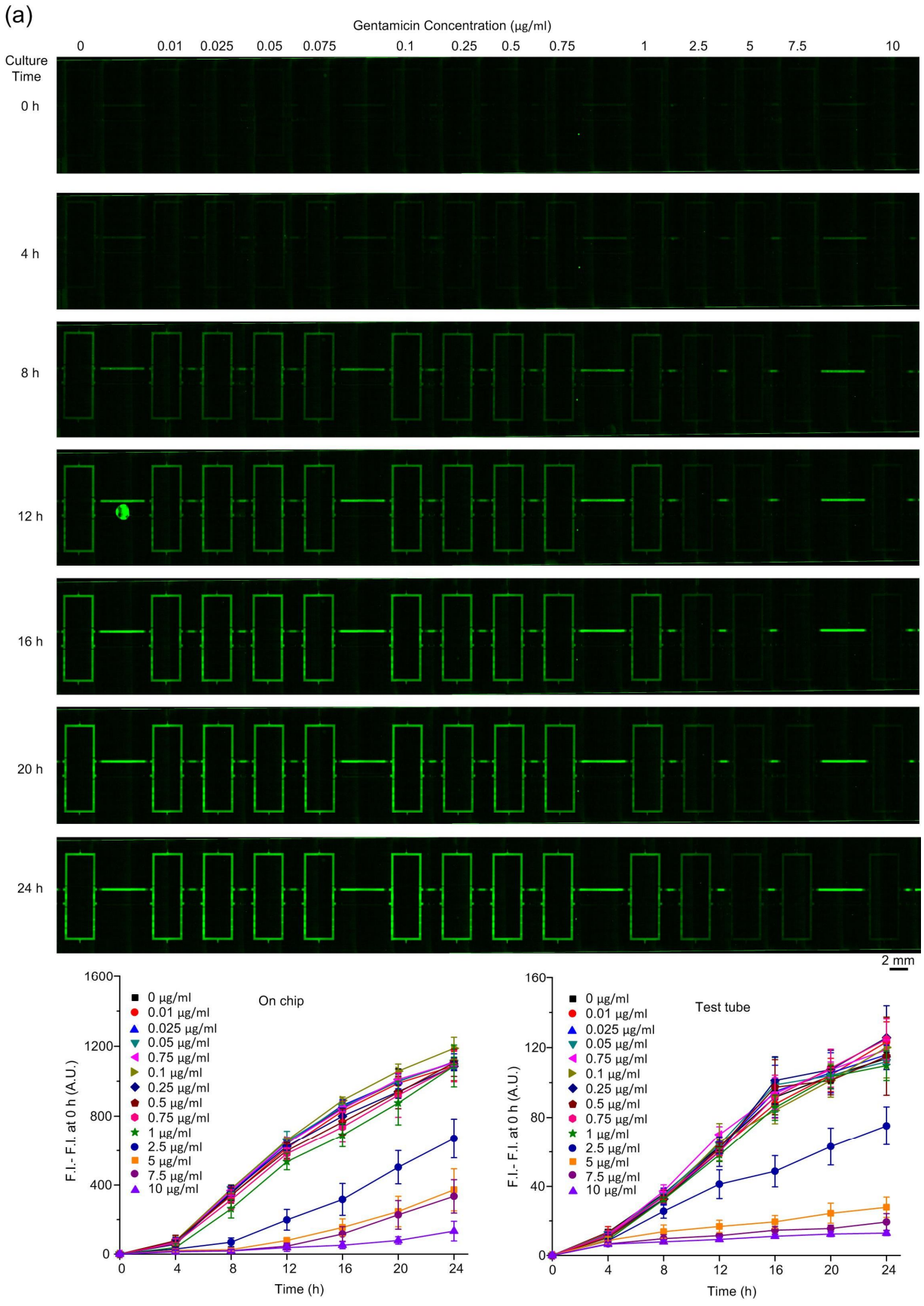
(a)
Gentamicin Concentration (μg/ml)
0
0.01
0.025
0.05
0.075
0.1
0.25
0.5
0.75
1
2.5
5
7.5
10
Culture Time
0 h
4 h
8 h
12 h
16 h
20 h
24 h
2 mm
On chip
Test tube
F.I.- F.I. at 0 h (A.U.)
Time (h)
0 μg/ml
0.01 μg/ml
0.025 μg/ml
0.05 μg/ml
0.75 μg/ml
0.1 μg/ml
0.25 μg/ml
0.5 μg/ml
0.75 μg/ml
1 μg/ml
2.5 μg/ml
5 μg/ml
7.5 μg/ml
10 μg/ml

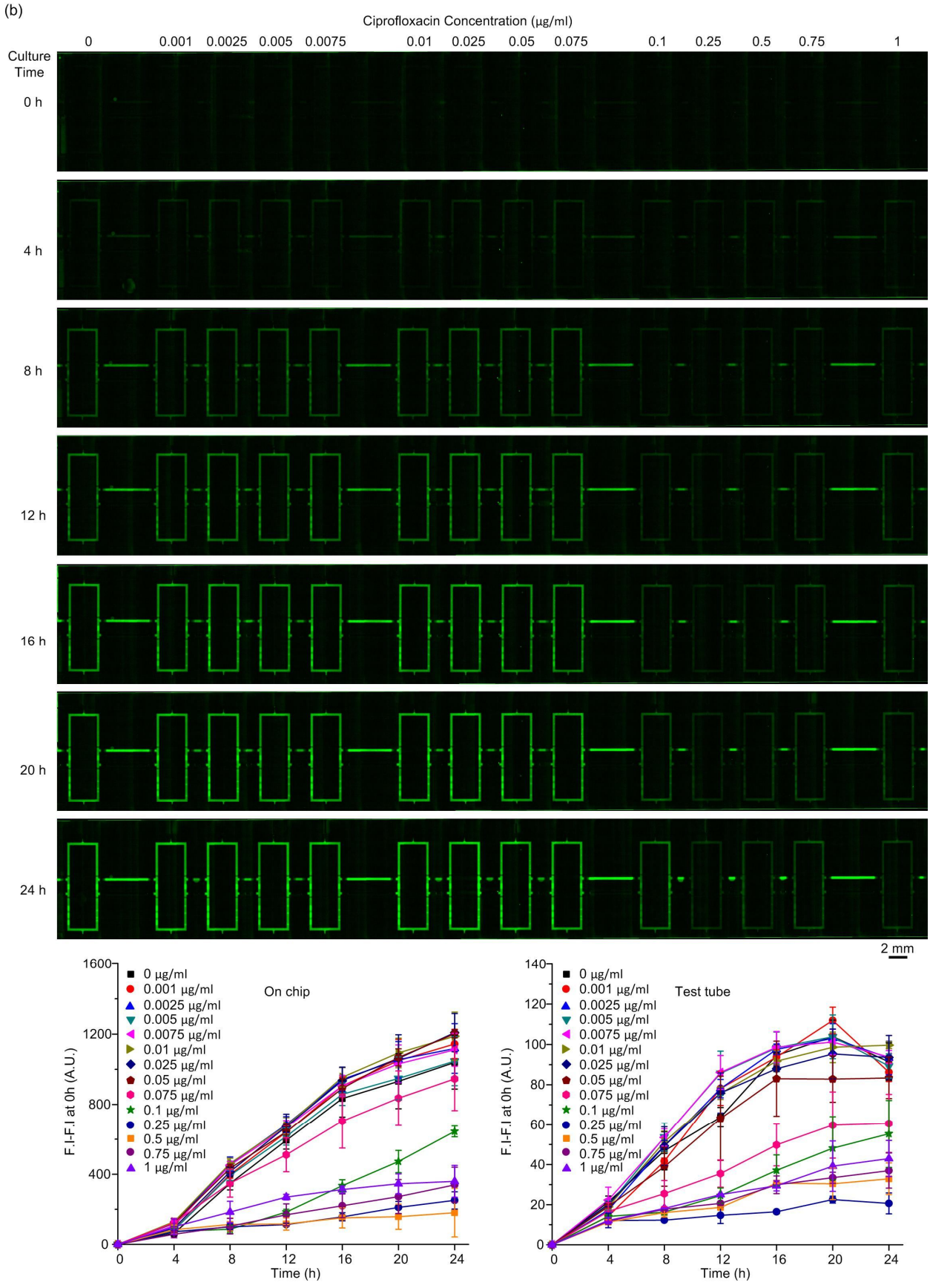
(b)
Ciprofloxacin Concentration (μg/ml)
0
0.001
0.0025
0.005
0.0075
0.01
0.025
0.05
0.075
0.1
0.25
0.5
0.75
1
Culture Time
0 h
4 h
8 h
12 h
16 h
20 h
24 h
2 mm
On chip
Test tube
F.I-F.I at 0h (A.U.)
Time (h)
0 μg/ml
0.001 μg/ml
0.0025 μg/ml
0.005 μg/ml
0.0075 μg/ml
0.01 μg/ml
0.025 μg/ml
0.05 μg/ml
0.075 μg/ml
0.1 μg/ml
0.25 μg/ml
0.5 μg/ml
0.75 μg/ml
1 μg/ml

Figure B3. Time-lapse fluorescence images of 14 reactors and fluorescence intensity of PT5-EGFP under the inhibitory effects of two bactericidal antibiotics in reactors and test tubes. (a) Gentamicin and (b) Ciprofloxacin. Data are represented as means ± SD of three independent experiments.

Appendix C

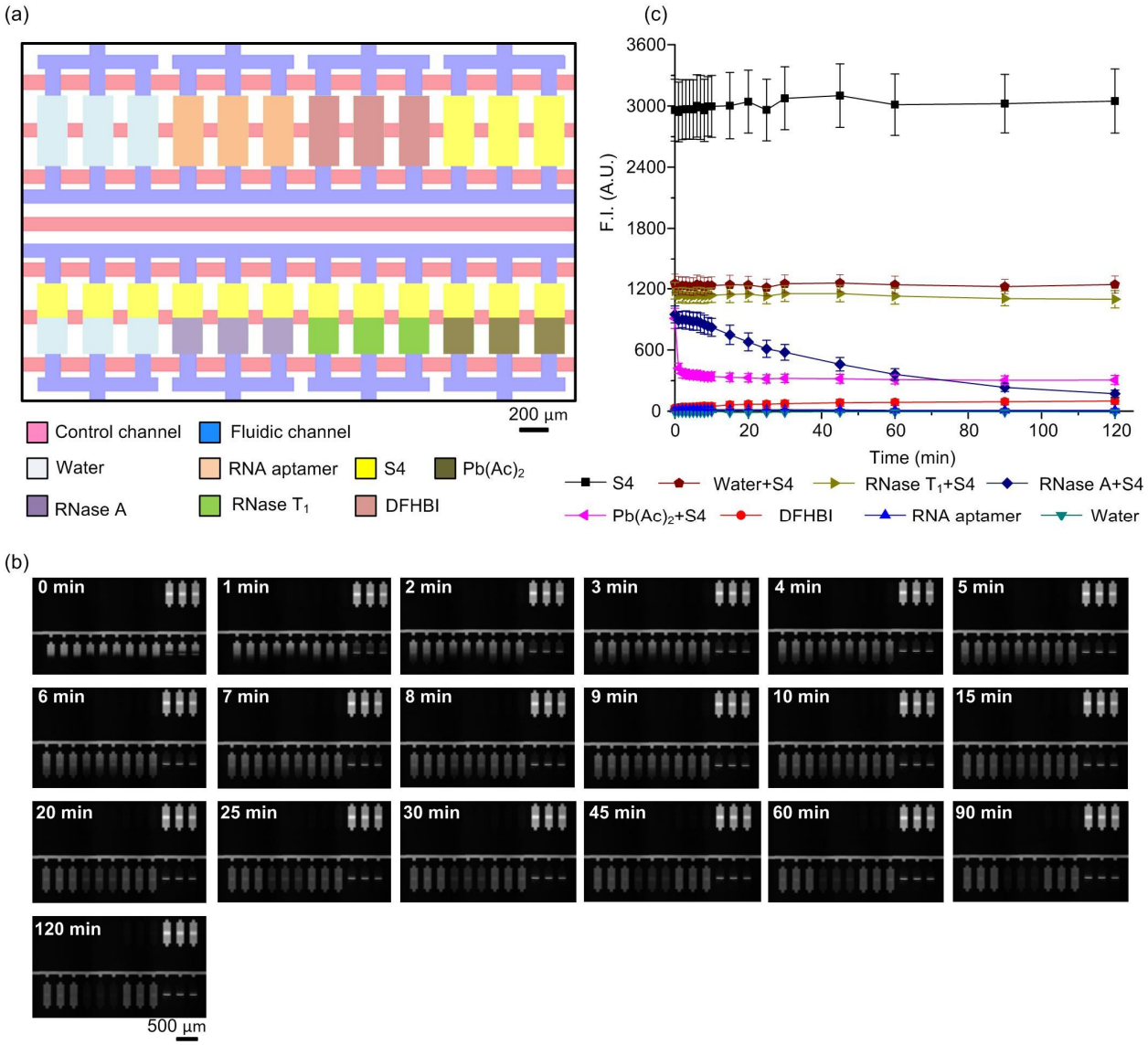

Figure C1. Time-course fluorescence intensity profiles of each reagent a microfluidic chip. (a) A multiplex microfluidic reactor chip. (b) Scanned images of reactors. (c) Time-course fluorescence intensity profiles of reagents in reactors. S4 ( ) represents biosensor (22.4 μM). Water+S4 ( ) represents biosensor (11.2 μM) which is 2-fold diluted with water. RNase T_1+S4 ( ) represents biosensor (11.2 μM) with RNase T_1 (3 U/μL). RNase A+S4 ( ) represents biosensor (11.2 μM) with RNase A (0.5 U/μL). $Pb(Ac)_2$+S4 represents biosensor (11.2 μM) with lead acetate (50 mM). Fluorescent molecule ( ) represents DFHBI (20 μM) which

is not conjugated with RNA aptamer. RNA ( ) represents RNA aptamer (22.4 μM). Water ( ) represents RNase free water. Data are represented as means ± SD of three replicate reactors.

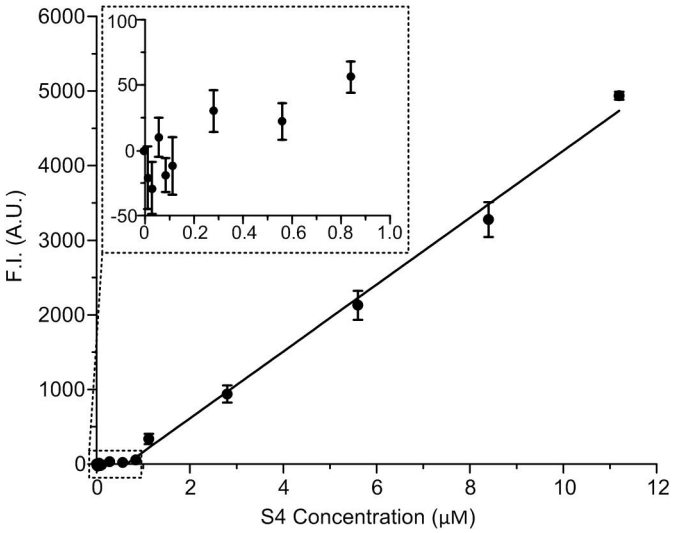

Figure C2. Fluorescence intensity of biosensor (S4) concentration gradient. A good linear relation between S4 concentration (0.84 μM~11.2 μM) and fluorescence intensity is obtained (R^2=0.994). Data are presented as means ± SD of three independent experiments.

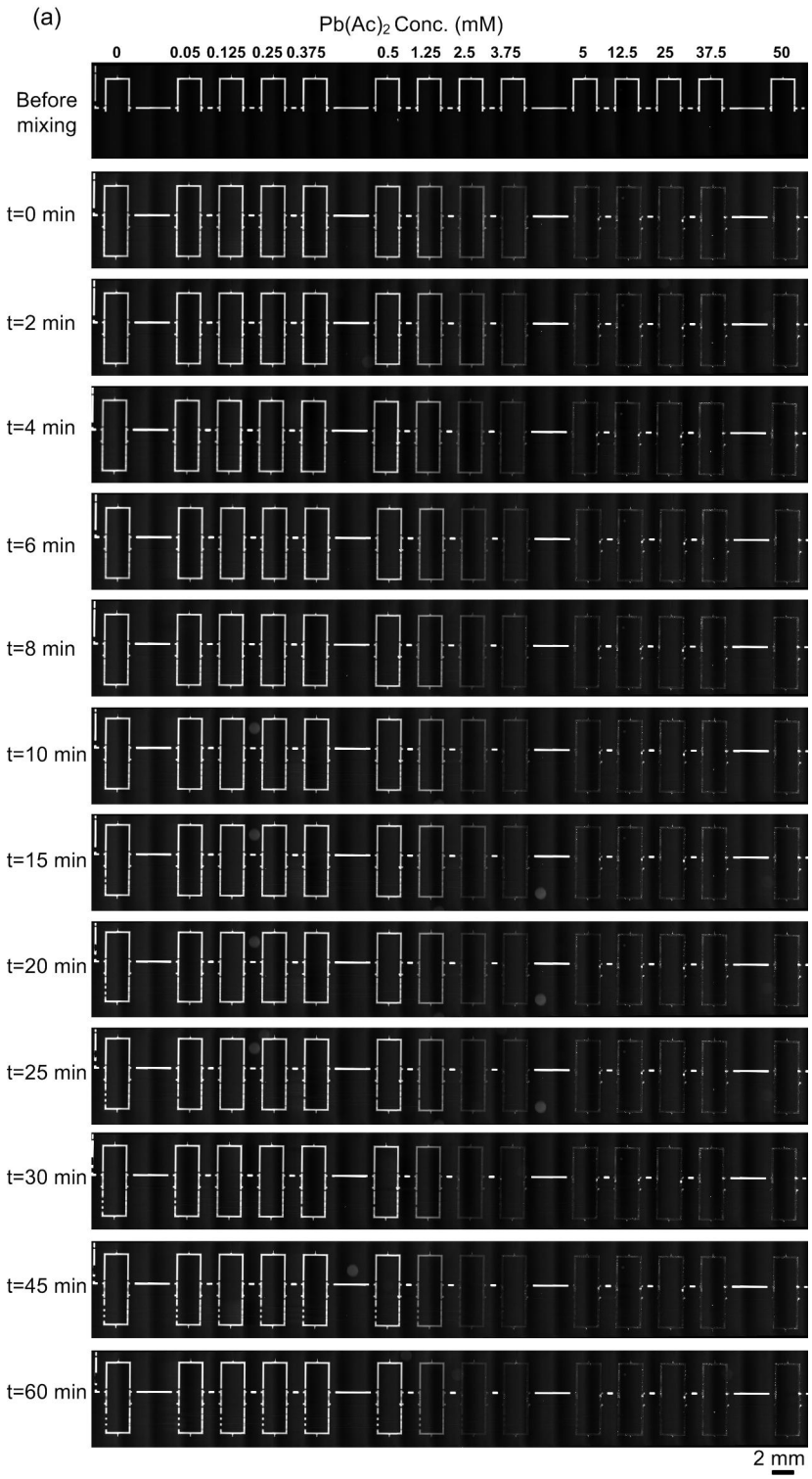
(a)
Pb(Ac)2 Conc. (mM)
0
0.05 0.125 0.25 0.375
0.5 1.25 2.5 3.75
5 12.5 25 37.5
50
Before mixing
t=0 min
t=2 min
t=4 min
t=6 min
t=8 min
t=10 min
t=15 min
t=20 min
t=25 min
t=30 min
t=45 min
t=60 min
2 mm

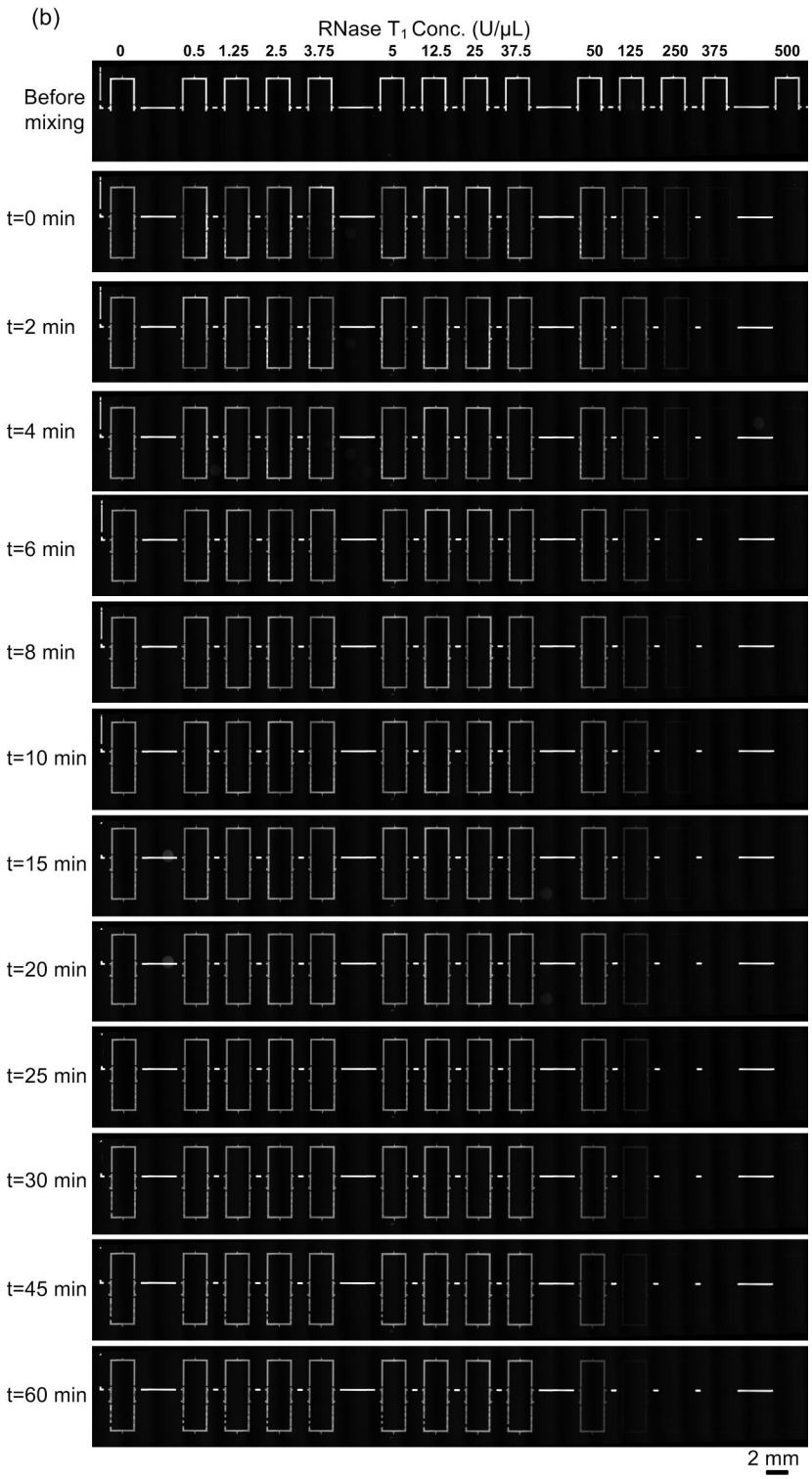
(b)
RNase T1 Conc. (U/μL)
0
0.5
1.25
2.5
3.75
5
12.5
25
37.5
50
125
250
375
500
Before mixing
t=0 min
t=2 min
t=4 min
t=6 min
t=8 min
t=10 min
t=15 min
t=20 min
t=25 min
t=30 min
t=45 min
t=60 min
2 mm

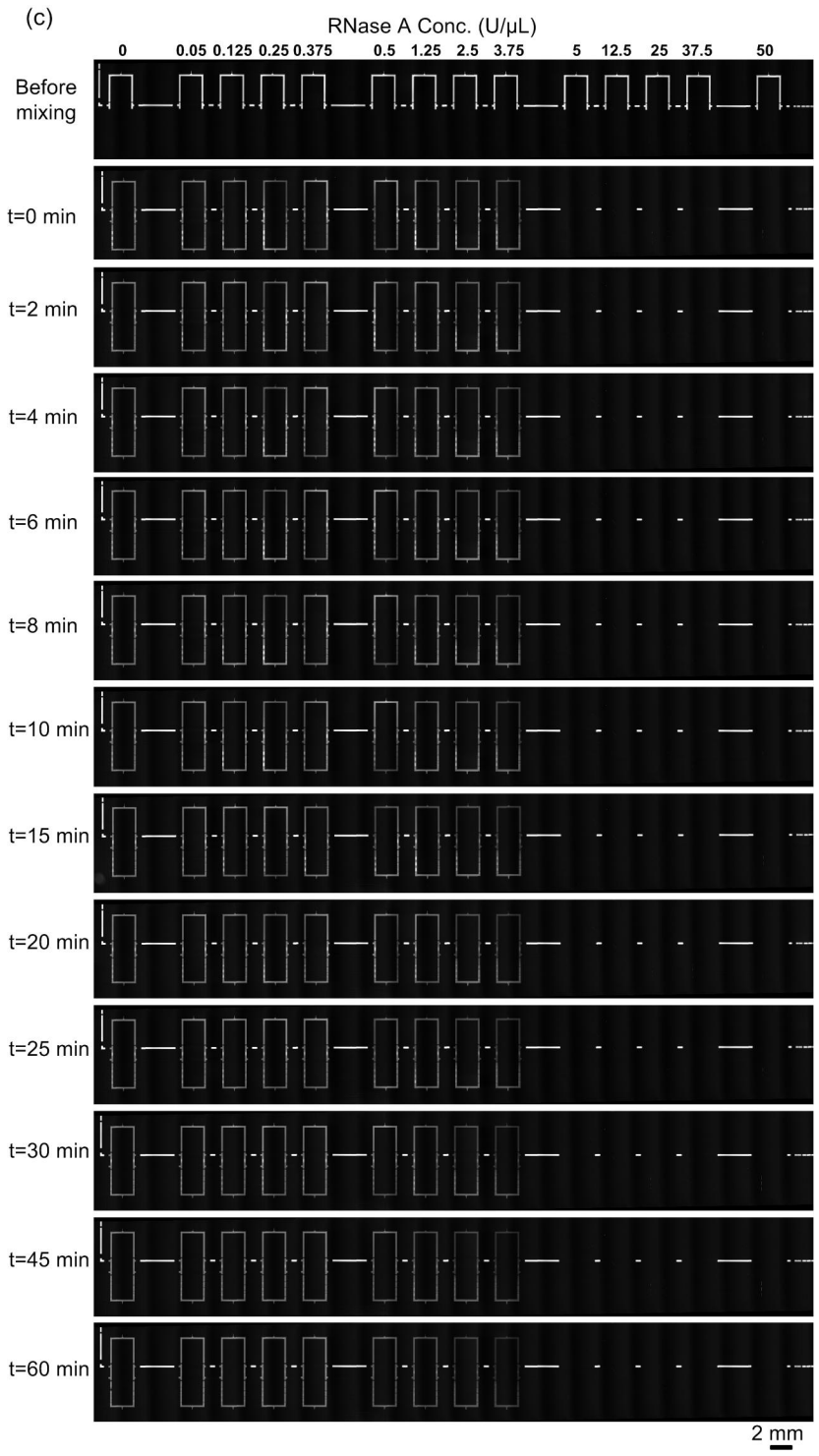

Figure C3. Time-lapse scanned images of reactors in which biosensor was degraded by (a) lead acetate, (b) RNase T_1, and (c) RNase A, respectively. Reaction time is from 0 min to 60 min.